Summer 8-14-2020

Multiquantal Glutamate Release from Rod Photoreceptors

Cassandra L. Hays
University of Nebraska Medical Center

MULTIVESICULAR GLUTAMATE RELEASE FROM ROD PHOTORECEPTORS

By

Cassandra L. Hays

A DISSERTATION

Presented to the Faculty of

the University of Nebraska Graduate College

in Partial Fulfillment of the Requirements

for the Degree of Doctor of Philosophy

Interdisciplinary Graduate Program in Biomedical Sciences
(Integrative Physiology & Molecular Medicine Doctoral Program)

Under the Supervision of Professor Wallace B. Thoreson

University of Nebraska Medical Center
Omaha, Nebraska

August 2020

Supervisory Committee:

Erika I. Boesen, Ph.D.	Pamela K. Carmines, Ph.D.
Scott Nawy, Ph.D.	Matthew Van Hook, Ph.D.

ACKNOWLEDGMENTS

I owe many folks, in and out of the UNMC community, my gratitude for support during the completion of my studies. First to my family at home, Bret and Lydia, who have fostered an environment that is a wonderful respite from the rigors of the laboratory. Bret has been particularly helpful in picking up extra household tasks in order to facilitate quiet writing time at home during a pandemic. Also deserving of thanks are my mom, brother, and in-laws who have been cheerleaders from my starting school again and throughout.

And, to the UNMC folks who have fostered an environment that is a wonderful respite from the rigors of mothering a toddler! Many in the Department of Cellular & Integrative Physiology have supported my studies including: the administrative staff, especially Kim Kavan; and graduate program director, Dr. Zimmerman, who has been a guide for meeting the requirements for graduation and also served on my examining committee for my comprehensive exam.

Fellow lab members are deserving of thanks as well. To Xiangyi Wen, for taking the time to teach me the nuances of his technique with dissection and patching; Justin Grassmeyer for thoughtful science discussions, answering my technical questions and unimportant but delightful social conversation. Thanks to Cody Barta for maintaining a steady supply of materials and mice, and for increased assistance when pregnancy restricted some of my abilities; Chris Mesnard for challenging me with questions and making me feel like I have something to teach; Asia Sladek for being the work friend, travel roommate, and happy hour companion that everyone needs.

My committee members have each mentored me in separate ways beyond simple discussion of my goals at biannual meetings. Dr. Carmines helped navigate my re-entry in the graduate program and has since served as a thoughtful and straightforward giver of career advice. Dr. Boesen has also been an approachable mentor for career aspirations and has afforded me

opportunities for teaching through tutoring. A special acknowledgment to Dr. Van Hook who brought fruitful ideas to discussion of my research project but also spent time personally teaching me electrophysiology. His enchantment with it was contagious. To Dr. Nawy, for teaching me to be a proper critic of the literature, and encouraging me to think harder before giving me answers to my questions.

Lastly, Dr. Thoreson, Wally, deserves the most recognition for supporting the work that went into this dissertation. From the inception of the project and its unexpected evolution, Wally has treated me collegially, keeping an open mind to my ideas. He has a special talent for never making me feel rushed in our conversations despite the constant demands on his time. He has also supported the learning that goes on during graduate school outside of research, including: establishing connections with other scientists, applying for funding, presenting at conferences, and allowing me to teach a semester at UNO. Non-science conversations, imparting life advice, vignettes about his kids, and music in the lab have made graduate school a much richer experience for me.

ABSTRACT

Neurons communicate via Ca^{2+}-dependent release of neurotransmitters packaged into vesicles (quanta). Some CNS neurons, especially sensory synapses, can release multiple vesicles at a time, increasing information transmission and overcoming the unreliability of a stochastic process. Ribbon-bearing neurons, including retinal photoreceptors, face the challenge of encoding sensory receptor potentials into an ever-changing train of vesicle release events. We studied release of glutamate using voltage clamp to measure anion currents activated during glutamate reuptake into presynaptic terminals ($I_{A(glu)}$) of salamander and mouse rods, finding that each employ distinct mechanisms for multiquantal release.

In amphibian rods, we found that 1/3 of the spontaneous $I_{A(glu)}$ fusion events involve synchronous fusion of multiple vesicles. By varying intracellular buffering to localize Ca^{2+}-dependent events, we found that multiquantal release occurs near Ca^{2+} sources. In photoreceptors, Ca^{2+} influx occurs just below synaptic ribbons. Vesicles house SNARE machinery so we hypothesized that vesicles on the ribbon undergo homotypic fusion prior to exocytosis. Destruction of ribbons and disruption of the SNARE-protein syntaxin3B prevented spontaneous multiquantal release, suggesting that salamander rods are capable of multivesicular release due to homotypic fusion of vesicles along ribbons.

In mouse rods, spontaneous release at −70 mV involved the stochastic fusion of single vesicles. With depolarization, glutamate release increased linearly with voltage-gated Ca^{2+} currents. As the membrane approached the resting potential in darkness of −40 mV, rods began to release glutamate in multivesicular bursts of 17±7 vesicles every 2801±598 ms. Release evoked by brief depolarizations and bursts both involved the same pool of ribbon-associated vesicles with fusion regulated by the vesicular Ca^{2+} sensor synaptotagmin-1. A second, slower component of release controlled by synaptotagmin-7 is also present in rods but not cones. We hypothesized a

role for coordinated bursts of release in transmitting single photon signals. The rate of bursting was responsive to small voltage changes of 1.0-3.5 mV and the voltage waveform that triggered bursts most effectively was similar to single photon responses. We propose that multiquantal bursts contribute to mechanisms that filter out small noisy events to improve reliable detection of single photons by the retina.

TABLE OF CONTENTS

LIST OF FIGURES

LIST OF TABLES

LIST OF ABBREVIATIONS

AMPA	α-amino-3-hydroxy-5-methyl-4-4isoazoleproprionic acid
BAPTA	1,2-bis(o-aminophenoxy)ethane-N, N, N', N'-tetraacetic acid
CaMKII	Calmodulin-dependent protein kinase II
cGMP	Cyclic guanosine monophosphate
CICR	Calcium-induced calcium release
CKO	Conditional knockout
C_m	Membrane capacitance
CNG	Cyclic nucleotide-gated channels
CV	Coefficient of Variance
EAAT	Excitatory amino acid transporter
EGTA	Ethylene glycol-bis(β-aminoethyl ether)- N, N, N', N'- tetraacetic acid
ER	Endoplasmic reticulum
ERG	Electroretinogram
ETA	Event-triggered average
FALI	Fluorophore-assisted laser inactivation
FITC	Fluorescein isothiocyanate
GABA	Gamma aminobutyric acid
GCL	Ganglion cell layer
G_t	Transducin

HC	Horizontal cell
$I_{A(glu)}$	Glutamate transporter current
I_{Ca}	Calcium current
$I_{Cl(Ca)}$	Calcium-activated chloride current
I_h	Hyperpolarization-activated current
I_{Kx}	Voltage-gated potassium current
ILM	Inner limiting membrane
INL	Inner nuclear layer
IPL	Inner plexiform layer
KA	Kainic acid (Kainate)
Kif3a	Kinesin family member 3A
LJP	Liquid junction potential
mEPSC	Miniature excitatory post-synaptic current
mGluR6	Metabotropic glutamate receptor 6
NBQX	2,3-dioxo-6-nitro-7-sulfamoylbenzo(f)quinoxaline
NFL	Nerve fiber layer
NMDA	N-methyl-D-aspartate
OLM	Outer limiting membrane
ON BC	ON type bipolar cell
ONL	Outer nuclear layer
OPL	Outer plexiform layer

PCR	Polymerase chain reaction
PDE	Phosphodiesterase
PL	Photoreceptor layer
Q_{10}	Temperature coefficient
RBC	Rod bipolar cell
R_m	Membrane resistance
RPE	Retinal pigment epithelium
RT	Room temperature
SOC	Store-operated channels
Syt	Synaptotagmin
TBOA	threo-β-benzyloxyaspartic acid
TIRFM	Total internal reflection microscopy
TRPM1	Transient receptor potential cation channel family M 1
V_{50}	Voltage at half-maximal activation
VAMP	Vesicle-associated membrane protein
VGCC	Voltage-gated calcium channel
V_m	Membrane voltage

CHAPTER 1: Introduction

Overview of Vision

Visual perception begins after photons of light have traveled through the front of the eye to reach a thin sheet of neural tissue at the back of the eye called the retina. Light is refracted by the cornea and lens to focus light on the retina. Focal length can be adjusted by the shape of the cornea and lens and aperture can be adjusted by changing pupil diameter. On its route to the retina, light passes through clear liquids in the anterior chamber between the cornea and lens and the vitreous cavity between the lens and retina. Aqueous humor in the anterior chamber bathes avascular tissues with nutrients and its circulation helps to maintain physiological intraocular pressure. The gelatinous vitreous humor contains mostly water with an ionic content similar to plasma along with a few phagocytes, hyaluronic acid, collagen, and other extracellular matrix proteins. Vitreous humor does not circulate like aqueous humor, but adheres to the retina and lens to support the shape of the globe and proper arrangement of ocular tissues.

Following photon absorption and transduction into electrical and chemical signals in the retina visual signals are transmitted to the brain along the optic nerve (cranial nerve II), which travels down the optic tract and across the optic chiasm to terminate in one of several brain areas (Murcia-Belmonte and Erskine, 2019). Conscious perception of images arises from signals traveling through the lateral geniculate nucleus of the thalamus to the primary visual cortex located in the occipital lobe. Pupillary light reflexes and circadian/diurnal rhythms do not depend on conscious perception and are instead mediated by projections to the optic pretectum (midbrain) and superchiasmatic nucleus (hypothalamus), respectively (Murcia-Belmonte and Erskine, 2019;Yoo and Mihaila, 2020). The superior colliculus of the midbrain (called the optic tectum in non-mammalian vertebrates) receives direct input from the retina in order to direct attention by fixation

or saccadic eye movements (Ito and Feldheim, 2018;Farrow et al., 2019). Retinal axons also project to the accessory optic system in the midbrain tegmentum.

Overview of Retinal Anatomy

The retina is a highly organized thin sheet of neural tissue that is embryologically derived from the neural ectoderm, forming an outcropping of the central nervous system. The retina is flanked by vitreous humor along the inner surface and the retinal pigment epithelium at the outer surface (Fig. 1). A rich vascular bed called the choroid lies just beyond the retinal pigment epithelium. Behind the choroid is the tough collagenous sclera that makes up the outermost layer of the posterior eye.

The retina contains five major types of neurons and one major glial cell organized into 7 layers. The most distal layer of the retina, the photoreceptor layer (PL), contains the outer and inner segments of photoreceptors. The next most proximal layer contains photoreceptor cell bodies that comprise the outer nuclear layer (ONL). The outer limiting membrane (OLM) separates inner segments from photoreceptor cell bodies and is formed from the apical processes of Müller glial cells. The outer plexiform layer (OPL) is the site of synaptic contact between photoreceptors and second order neurons, horizontal and bipolar cells. Cell bodies of bipolar, horizontal and amacrine cells make up the inner nuclear layer (INL). Synaptic contacts between bipolar, amacrine and ganglion cells occur in the inner plexiform layer (IPL). The ganglion cell layer (GCL) consists of ganglion cell bodies and some displaced amacrine cells. Ganglion cell axons that project toward the optic nerve head make up the nerve fiber layer (NFL) along the anterior surface of the retina. Müller glia are the principal glial cell of the retina and span the retina with apical processes forming the OLM and their endfeet forming the inner limiting membrane (ILM) that separates the vitreous humor from the nerve fiber layer.

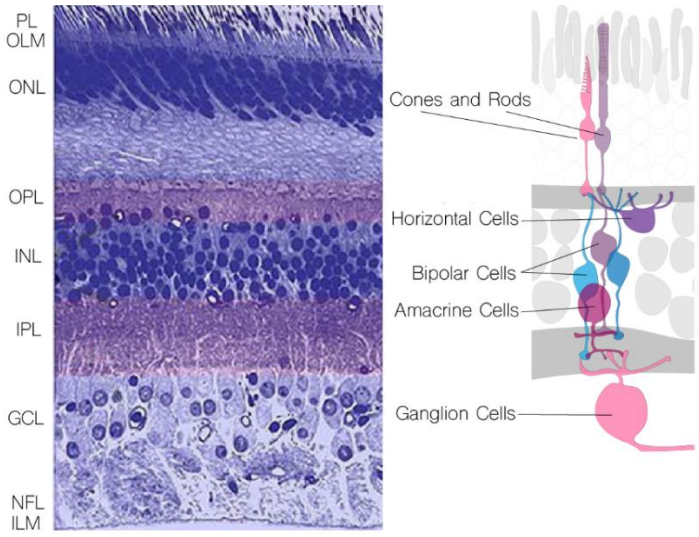

Figure 1 Vertical section of human retina. PL = Photoreceptor Layer (outer segments of rods and cones) ONL = Outer Nuclear Layer (nuclei of rods and cones) OPL= outer plexiform layer (photoreceptor synapses) INL = inner nuclear layer (bipolar cell somata) IPL= inner plexiform layer (bipolar cell synapses) GCL= ganglion cell layer (ganglion cell somata) and NFL= nerve fiber layer (axons of the ganglion cells). The right panel illustrates the basic circuitry of the retinal neurons.

Each of the five major neuronal cell types in the retina has various subtypes. Photoreceptors consist of rods and cones. Most species have a single type of rod and multiple types of cones that differ from one another in their spectral sensitivity (Thoreson and Dacey, 2019). Mammals typically have two types of horizontal cells although many non-mammalian species have as many as four and some rodents have only one (Thoreson and Mangel, 2012;Diamond, 2017). Most species have more than a dozen types of bipolar cells (Tsukamoto and Omi, 2017) and more than 25 types each of amacrine and ganglion cells have been described (Masland, 2011;Baden et al., 2016).

Photoreceptors

Rods and cones use similar phototransduction mechanisms to transduce light into membrane voltage changes although they differ in their sensitivity and kinetics. Rods are specialized to transmit signals in scotopic conditions and can generate detectable membrane voltage

changes in response to absorption of only a single photon. Cones operate at higher light levels to provide faster, high acuity signals. The presence of multiple cone subtypes with differing spectral sensitivities is also a substrate for color vision (Thoreson and Dacey, 2019).

Vision originates with the absorption of photons in the outer segments of rod or cone photoreceptor cells that lie adjacent to the retinal pigment epithelium (RPE). The outer segment is a modified cilium containing the phototransduction apparatus organized in layers of membranous disks studded with light-sensitive opsin molecules. In rods, these discs form separate organelles that are fully enclosed within the outer segment. In cones, discs are formed from repeated invaginations of the plasma membrane. Rods and cones receive their names because outer segments of rods are cylindrical whereas the outer segments of cones are more tapered.

Phototransduction

The process of converting photon capture to a membrane voltage change, phototransduction (Fig. 2), is initiated in the outer segments by absorption of a photon by a transmembrane G-protein-coupled receptor, opsin. The opsin in rods is called rhodopsin. The different types of cones have cone opsins that differ in spectral sensitivity from one another. Opsins are located in the disc membranes where they make up the vast majority of the protein content of outer segments. In its light-sensitive state, there is a covalent bond between opsin and its chromophore molecule, 11-cis-retinal (vitamin A aldehyde). Absorption of a photon by 11-cis-retinal causes it to isomerize to all trans-retinal, producing a conformational change in the opsin molecule. The conformational change in rhodopsin activates the associated G-protein, G_t (transducin), whose alpha subunit in turn activates cGMP-specific phosphodiesterase. The hydrolysis of cytosolic cGMP results in closure of cyclic nucleotide-gated cation (CNG) channels in the adjacent plasma membrane, thus hyperpolarizing the photoreceptor. PDE and G_t are rapidly inactivated so that the photoreceptor can respond to subsequent incoming photons. Because cGMP levels are higher in darkness than in light, many CNG channels are open in darkness leading to a

relatively depolarized membrane potential of −40 mV. By closing these CNG channels, light produces hyperpolarizing responses in the photoreceptor cell that increase in amplitude with increasing light intensity.

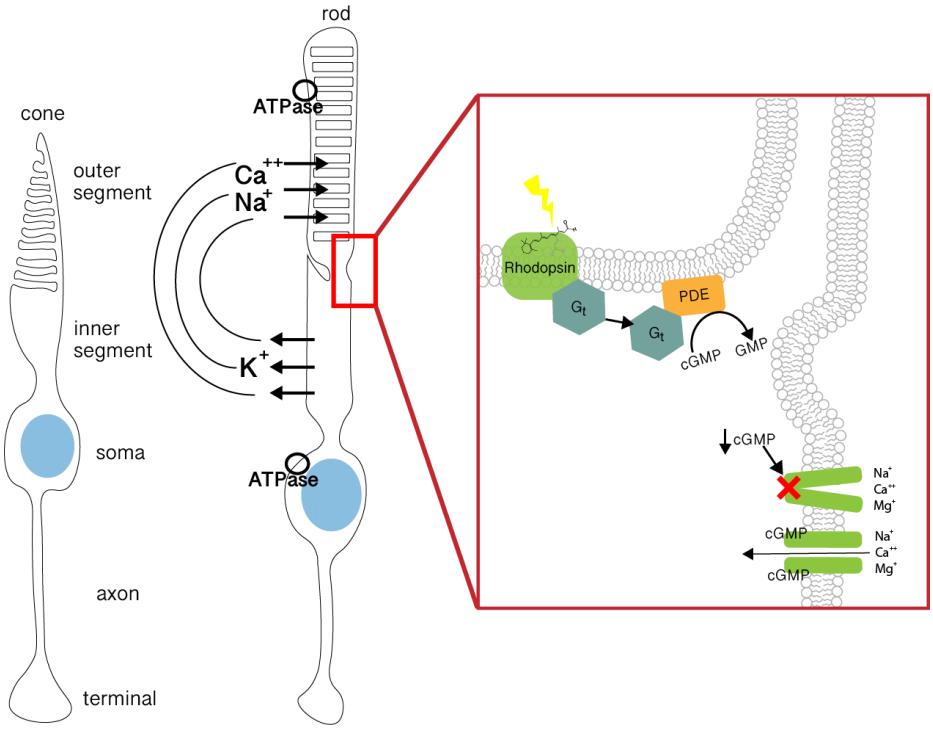

Figure 2 An illustration of anatomical features of rods and cones. The figure of the rod includes the various ion channel conductances that contribute to the membrane potential (V_m). In darkness, K^+ efflux from the inner segment is counteracted by cation influx through cyclic-nucleotide gated (CNG) channels in the outer segment maintaining a depolarized V_m (-40 mV). An Na^+/K^+-ATPase at the soma and $Na^+/K^+/Ca^{2+}$ exchanger in the outer segment maintain physiological concentration gradients. The general phototransduction cascade is illustrated in the red box. Light converts 11-cis retinal to all-trans retinal causing activation of rhodopsin-coupled G-protein transducin (G_t). Transducin activates phosphodiesterase (PDE) which degrades cGMP. When cGMP levels decline, CNG channels close, hyperpolarizing the photoreceptor.

The constant influx of Na^+ and Ca^{2+} ions through CNG channels in darkness requires continual extrusion of these ions. Ca^{2+} is extruded by Na^+/Ca^{2+} exchangers in the outer segment. Just beneath the outer segment, on the other side of the connecting cilium, is the inner segment. Na^+ is extruded by Na-/K^+-ATPase activity in the inner segment, requiring considerable amounts of ATP in darkness. The inner segment also houses an abundance of mitochondria, providing the

fuel needed to sustain these ATPases and phototransduction (Johnson et al., 2007). The adjacent choroidal vascular bed has among the highest unit blood flow in the body, but despite this rich supply, the constant activity of these mitochondria is sufficient to reduce the PO_2 at the level the inner segments to zero in darkness (Linsenmeier, 1986;Braun et al., 1995;Lau and Linsenmeier, 2012).

Photoreceptors express various ion channels that help to set the membrane potential, shape their responses to light, and regulate synaptic transmission. Rods and cones both possess inwardly rectifying cation currents that are activated by hyperpolarizing voltages (I_h), voltage-dependent K^+ currents activated by depolarization (I_{Kx}), L-type I_{Ca} and Ca^{2+}-activated Cl^- currents ($I_{Cl(Ca)}$)(Van Hook et al., 2019). Photoreceptors of some species also possess Ca^{2+}-activated K^+ currents but these appear to be absent from primate retina (Yagi and Macleish, 1994;Xu and Slaughter, 2005;Pelucchi et al., 2008;Ingram et al., 2020). Unlike most neurons, photoreceptors do not normally possess voltage-gated Na^+ channels (Van Hook et al., 2019). I_{Kx} is typically active at the resting potential in darkness of −40 mV. When CNG close in response to light, K^+ efflux through I_{Kx} channels provides the principal driving force to hyperpolarize the membrane. I_h is a cation channel that is 3 or 4 times more permeable to K^+ than Na^+, showing a reversal potential of −30-35 mV (Demontis et al., 1999;Demontis et al., 2002;Van Hook et al., 2019). The increase in I_h activity that accompanies light-evoked hyperpolarization provides a depolarizing influence that makes rod and cone light responses more transient.

As discussed in further detail below, the relatively depolarized membrane potential of rods and cones in darkness is sufficient to activate L-type Ca^{2+} channels that control synaptic transmission. Ca^{2+} channel activity diminishes when photoreceptors hyperpolarize to light and increases when they depolarize in darkness. Thus, Ca^{2+}-dependent release of glutamate-filled synaptic vesicles also diminishes in light and increases in darkness.

Photoreceptor Synapse

Synaptic vesicle release from rod and cone photoreceptors involves specialized plate-like protein structures known as synaptic ribbons. Synaptic ribbons are also present in other non-spiking sensory neurons including retinal bipolar cells and hair cells of the cochlea and vestibular apparatus (Schmitz, 2009). These cells share the capability for tonic graded release of neurotransmitter and ribbons are thought to be crucial for sustaining release. The main protein making up the synaptic ribbon is RIBEYE (Schmitz et al., 2000). This is a transcript variant of a more ubiquitously expressed transcriptional repressor protein CtBP2. RIBEYE differs from the more common CtBP2 variant in that it also contains an additional ribbon-specific A domain (Schmitz et al., 2000). Self-association among A-domains of adjoining RIBEYE molecules is thought to form the core of a ribbon. Ribbons are anchored close to the plasma membrane by interactions with the proteins, bassoon and piccolo (Schmitz, 2009;Moser et al., 2020). These proteins may make up part of the arciform density, a semilunar-shaped structure beneath each ribbon (Fig. 3).

Release from most neurons is regulated by activity of N- or P/Q-type Ca^{2+} channels, but photoreceptors and other ribbon-bearing neurons that show graded receptor potentials use L-type channels to maintain continuous Ca^{2+} influx necessary for continuous release (Waldner et al., 2018). The Ca^{2+} channels at photoreceptor ribbon synapses are constructed from $Ca_V1.4$ pore-forming alpha subunit associated with β_{2A} and $\alpha_2\delta_4$ accessory subunits (Doering et al., 2007;Waldner et al., 2018). $Ca_V1.4$ activity produces a relatively sustained current exhibiting hardly any inactivation by voltage or Ca^{2+} which makes it well suited for maintaining the continuous release of glutamate in times of darkness (Doering et al., 2007). The voltage at which $Ca_V1.4$ channels achieve half-maximal activation is close to the dark resting potential of rods and cones (Barnes and Kelly, 2002;Babai and Thoreson, 2009). Thus, Ca^{2+} channel activity is very sensitive to small changes in membrane voltage produced by changes in illumination, with activity

decreasing when photoreceptors hyperpolarize to light and increasing when they depolarize at light offset. $Ca_v1.4$ channels are clustered below synaptic ribbons (Nachman-Clewner et al., 1999;Morgans, 2001;tom Dieck et al., 2005a;Mercer and Thoreson, 2011;Dolphin and Lee, 2020) and remain there through a relationship with the ribbon-associated protein, Bassoon(tom Dieck et al., 2005b).

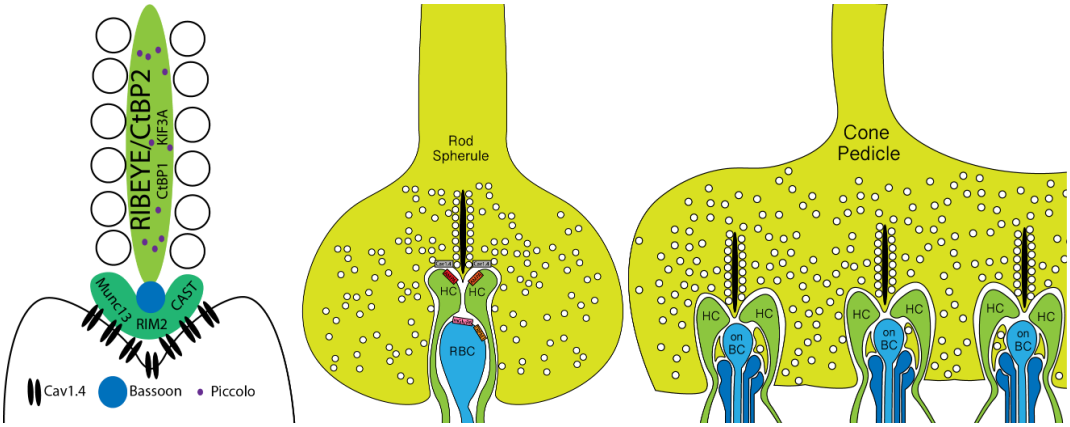

Figure 3 The left panel illustrates the arrangement of major protein components of the synaptic ribbon in rods and cones. The right panels show the overall organization of rod and cone synapses. Cones have multiple ribbons (10-50) whereas mammalian rods have only a single ribbon. RBC, rod bipolar cell; on BC, ON-type bipolar cell; HC, horizontal cell

Photoreceptor ribbons are adorned with vesicles in a roughly hexagonal array (Thoreson et al., 2004). The surrounding cytoplasm contains many highly mobile vesicles that provide a reservoir for replenishing ribbons (Rea et al., 2004). After attaching to a ribbon, it appears that vesicles depart the ribbon only by fusion with the plasma membrane at synaptic release sites along the base of the ribbon (Vaithianathan et al., 2016;Wen et al., 2017). Each vesicle is associated with the ribbon by a handful of fine tethers (Usukura and Yamada, 1987) but it appears that each individual tether provides a relatively weak attachment force, allowing vesicles to move freely along the plane of the ribbon (Graydon et al., 2014). With flash photolytic uncaging of Ca^{2+} in bipolar cells, all vesicles fuse within 2 ms suggesting a rate of >100 µm/s if all of the vesicles that are released must descend down the ribbon (Heidelberger et al., 1994;Parsons and Sterling, 2003).

This is considerably faster than the 800 nm/s rate of vesicle approach measured directly by visualizing vesicles using total internal reflectance microscopy (TIRFM) in bipolar cells (Zenisek et al., 2000) and rods (Parsons and Sterling, 2003;Chen et al., 2014) It has been suggested that the travel of vesicles down the ribbon may be aided by the ribbon-associated kinesin molecule Kif3a (Muresan et al., 1999). However, if so, the actions of Kif3A do not depend on molecular motors driven by ATP hydrolysis, because release of vesicles from bipolar cell ribbons can occur in the absence of usable ATP (Heidelberger et al., 2002;Matthews and Sterling, 2008). Also, there is no evidence for other molecular motor components other than Kif3A (Muresan et al., 1999). Finally, a speed of 100 μm/s is faster than known molecular motors can manage (Kolomeisky, 2013).

While it is generally thought that ribbons may increase the capacity for continuous release of vesicles, computational models suggest that cytoplasmic vesicles can arrive by simple diffusion at release sites rapidly enough to sustain tonic release rates in photoreceptors and bipolar cells without a ribbon (Graydon et al., 2014). Thus, ribbons may serve other functions besides delivery to release sites. For example, ribbons also play a role in priming of vesicles for release (Snellman et al., 2011). Another function suggested by experiments described in chapters 2 and 3 is that the ribbon situates vesicles near enough to one another to facilitate homotypic and sequential multivesicular fusion (Parsons and Sterling, 2003;Matthews and Sterling, 2008).

Rods possess larger ribbons than cones, averaging about 1 μm along their base and extending about 1 μm into the cytoplasm (Sterling and Matthews, 2005). Mammalian rods typically have a single ribbon (Carter-Dawson and LaVail, 1979;Sterling and Matthews, 2005;Zampighi et al., 2011) but amphibian rods possess 4-5 ribbons per terminal and up to 3 terminals per rod, yielding an average of 7 ribbons per rod (Townes-Anderson et al., 1985a). These 7 ribbons can accommodate over 3500 vesicles or about 500 vesicles apiece (Thoreson et al., 2004). This is similar to the number of vesicles tethered by a ribbon in mammalian rods (~600 vesicles) (Sterling and Matthews, 2005). We took advantage of the fact that mammalian rods have only a

single ribbon to study the statistics of release at individual rod ribbons in experiments described in Chapter 3.

Mammalian and amphibian cones contain smaller but more numerous synaptic ribbons than rods. Amphibian cones contain an average of 13 ribbons each able to tether 110 vesicles apiece (Bartoletti et al., 2010). The number of ribbons in mammalian cones ranges from 10 to 50, increasing as one moves further toward the retinal periphery (Haverkamp et al., 2001). Cones in mouse retina have 6-14 ribbons apiece (Johnson et al., 2007).

Second and Third Order Neurons

The light responses encoded by changes in glutamate release act on second-order bipolar and horizontal cells. Horizontal cells are lateral inhibitory neurons that act on photoreceptors and bipolar cells to shape the light responses of bipolar cells. Bipolar cells then contact retinal ganglion cells and amacrine cells. Amacrine cells are also lateral inhibitory neurons that further shape light responses. The axons of ganglion cells form the optic nerve that carries signals to other parts of the CNS. Like photoreceptors, horizontal cells and bipolar cells respond to changes in illumination with graded changes in membrane potential that are proportional to the stimulus whereas amacrine and retinal ganglion cells begin to encode information using sodium-driven action potentials, like other CNS neurons.

Bipolar cells are found in many special sensory systems and are named for having only two poles: a dendritic extension and an axon. The cell bodies of retinal bipolar cells lie in the INL and project short axons into the IPL where they release glutamate onto amacrine and ganglion cells. Like photoreceptors, bipolar cells respond to glutamate with graded membrane changes and are suited for continuous release of vesicles by also having synaptic ribbons. Bipolar cells can be classified as “ON” or “OFF” depending on whether they depolarize at light onset or offset. ON and OFF bipolar cells excite ON and OFF amacrine and ganglion cells, respectively. Recall that

photoreceptors hyperpolarize to light by decelerating glutamate release. Bipolar cells in the OFF-pathway respond to glutamate in a sign-conserving manner and so the decline in glutamate release from the photoreceptor that accompanies its hyperpolarizing light response causes OFF bipolar cells to hyperpolarize. By contrast, ON bipolar cells participate in a *sign-inverting* synapse whereby their membrane voltage change opposes that of the photoreceptor. In this case, the hyperpolarizing response of a photoreceptor to light produces a depolarization of the ON bipolar cell. The opposing responses to glutamate by ON and OFF bipolar cells result from their expression of different glutamate receptors (Saito and Kaneko, 1983;Masu et al., 1995).

Like most excitatory neurons in the CNS, OFF bipolar cells express ionotropic AMPA- or KA-type glutamate receptors in which glutamate binding triggers the opening of non-selective cation channels (Puller et al., 2007;Ichinose and Hellmer, 2016;Vielma and Schmachtenberg, 2016). Thus, the response of OFF bipolar cells to glutamate mirrors that of the photoreceptor in response to light: hyperpolarizing when photoreceptors hyperpolarize at light onset and depolarizing when photoreceptors depolarize at light offset.

ON bipolar cells appear to be unique among glutamatergic neurons in that glutamatergic inputs to this neuron are not transduced by ionotropic glutamate receptors but instead by a G-protein coupled metabotropic receptor. The ON bipolar cell glutamate receptor, mGluR6, responds to glutamate by initiating an intracellular signaling cascade that culminates in the closure of a nearby TRPM1 cation channels (Fig. 4)(Koike et al., 2010b). mGluR6 does not form an ion channel itself but is coupled to G_O whose alpha and beta/gamma subunits both participate in closure of the constitutively open TRPM1 (Xu et al., 2016). The mechanism by which this occurs remains unclear. Applying activated $G\alpha_O$ subunit closed TRPM1 channels expressed in CHO cells (Koike et al., 2010a) but dialysis of active $G_\beta\gamma_O$ subunit also reduced Ca^{2+} influx in transfected HEK cells and human melanocytes (Shen et al., 2012). More recently, there is evidence that both the $G\alpha$ and $\beta\gamma$ subunits act in a cooperative manner to close TRPM1 (Xu et al., 2016). In darkness, while rods

are continuously releasing glutamate, mGluR6 are saturated, maintaining the closed state of nearly every TRPM1 cation channel at that dendrite causing the bipolar cell to be hyperpolarized (Sampath and Rieke, 2004). After photon absorption and the slowing of glutamate release, mGluR6 are de-saturated and TRPM1 channels open to depolarize the cell in a "sign-inverting" manner.

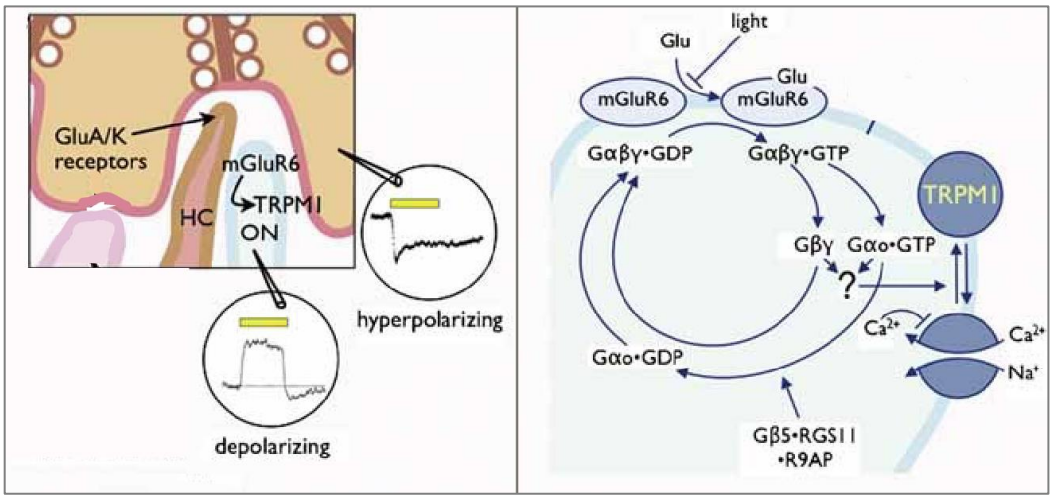

Figure 4 Photoreceptors communicate with ON-bipolar cells by releasing glutamate. With light stimuli, the photoreceptor hyperpolarizes, causing depolarization of the ON bipolar cell. The mGluR6 signaling cascade (right) is responsible for this sign inversion. With light, when glutamate is reduced in the cleft, cessation of mGluR6 stimulation leads to opening of TRPM1 cation channels. Modified from Morgans et al. 2010.(Morgans et al., 2010)

In mammalian retina, the dendrites of ON bipolar cells contact rods and cones by entering invaginations within the photoreceptor synaptic terminal. At both rod and cone synapses, one or two ON bipolar cell dendrites occupy the central position in the invagination, flanked by two horizontal cell dendrites. At cone synapses, a number of cone-driven OFF bipolar cell dendrites also make flat contacts with the cone membrane just outside of the invagination, close enough to sense glutamate released at ribbons within the invagination (Hack et al., 1999;Tsukamoto et al., 2001). Few OFF bipolar cells make contact with rods (Tsukamoto and Omi, 2014).

As light responses are transmitted from photoreceptors to bipolar cells and then to ganglion cells, they are modified by circuits involving inhibitory horizontal cells and amacrine cells (Diamond, 2017). With cell bodies residing within the inner nuclear layer and dendritic extensions

in the outer plexiform layer, horizontal cells make contact with rod and cone terminals and bipolar cell dendrites at invaginating photoreceptor ribbon synapses. Horizontal cells primarily express AMPA receptors and depolarize in response to glutamate released from photoreceptor terminals, thereby hyperpolarizing to light (Copenhagen et al., 1983;Connaughton, 1995;Kramer and Davenport, 2015). They provide feedback inhibition to presynaptic rods and cones and also appear to provide feedforward inhibition to at least some bipolar cells (Thoreson and Mangel, 2012), in part by the actions of GABA.

Non-mammalian vertebrates have up to four types of horizontal cells whereas most mammals have two types (Thoreson and Mangel, 2012). Mouse and some other rodents have only a single type of horizontal cell (Peichl and Gonzalez-Soriano, 1994). The chief contribution of horizontal cells in vision is to provide lateral inhibitory feedback to rod and cone photoreceptors establishing center-surround receptive fields in the retina. Center-surround receptive fields are important for color vision and enhancing spatial resolution and edge detection (Thoreson and Mangel, 2012). During feedback inhibition, when a cone hyperpolarizes to light, the post-synaptic horizontal cell also hyperpolarizes which reduces the inhibitory signals that it sends to neighboring cones. This in turn enhances membrane depolarization and I_{Ca} activity in photoreceptors surrounding the light-stimulated cone (Verweij et al., 1996). Three candidate feedback mechanisms have been proposed to explain how horizontal cell hyperpolarization may activate calcium channels in cone terminals (Thoreson and Mangel, 2012;Diamond, 2017).

The first is simply GABAergic disinhibition. Horizontal cells in most species contain GABA and appropriate machinery for GABA synthesis and transport (Yang et al., 1999;Deniz et al., 2011). In this scenario, in light when cone glutamate release is reduced, horizontal cells are also hyperpolarized reducing the release of GABA (Lam et al., 1978). This causes a disinhibition and depolarization at the cone terminal. However, GABA antagonists failed to block depolarizing responses recorded in cones evoked by light stimulation from neighboring horizontal cells,

indicating that this is not the principal mechanism mediating inhibitory feedback to cones (Thoreson and Burkhardt, 1990;Verweij et al., 2003).

Byzov et al. proposed an ephaptic feedback mechanism where horizontal cell hyperpolarization causes a voltage drop in the synaptic cleft that depolarizes the adjacent cone terminal membrane (Byzov and Trifonov Yu, 1981). However, this mechanism should operate instantaneously, and feedback develops rather slowly, suggesting it is also unlikely to be the principal mechanism of feedback (Warren et al., 2016b).

Lastly, it is hypothesized that when horizontal cells hyperpolarize to light, this relieves proton-mediated inhibition of cone Ca^{2+} currents. Consistent with this, strongly buffering pH blocks feedback from horizontal cells to cones (Cadetti and Thoreson, 2006;Hirasawa et al., 2012;Grove et al., 2019) and predicted pH changes have been directly measured in the synaptic cleft by attaching a pH sensor (phluorin) to the extracellular surface of presynaptic calcium channels in cones (Wang et al., 2014;Beckwith-Cohen et al., 2019). The mechanism by which pH changes occur in the synaptic cleft remain unclear. Evidence suggests that the ongoing extrusion of protons by Na^+/H^+ exchangers is essential to cleft acidification in darkness and that alkalization of the cleft upon the light-evoked hyperpolarization of horizontal cells arises from increased extracellular buffering involving bicarbonate efflux through horizontal cell GABA receptors (Warren et al., 2016a;Grove et al., 2019).

In addition to negative feedback, horizontal cells can also provide positive feedback to photoreceptors (Jackman et al., 2011). This mechanism involves activation of Ca^{2+}-dependent AMPA receptors and operates on a spatially local scale. By opposing negative feedback, this positive feedback mechanism may help to ensure ongoing synaptic activity of cones. Finally, there is also evidence for feedforward synaptic inhibition from horizontal cells to bipolar cells (Yang and Wu, 1991;Puller et al., 2014).

Amacrine cells are anaxonic but spiking neurons with cell bodies residing primarily in the IPL of the retina, along with a few displaced amacrine cells that have cell bodies in the GCL (Diamond, 2017). Their dendrites arborize in the IPL to contact bipolar cells, ganglion cells, and other amacrine cells. Over 30 types of amacrine cells have been classified by physiological, neurochemical and anatomical properties (Diamond, 2017). Physiological properties include whether they are sustained or transient, and whether they show ON, OFF or ON/OFF responses. Anatomical properties include their size, shape and termination of dendrites in specific sublaminae of the IPL. Most amacrine cells are inhibitory neurons containing GABA and/or glycine, but the different subtypes can also contain many other neurotransmitters and neuromodulators (Masland, 2012).

The output cells of the retina, retinal ganglion cells, receive synaptic input from bipolar and amacrine cells in the IPL. Ganglion cells express NMDA and AMPA ionotropic glutamate receptors and are thus excited by glutamate released from bipolar cells (Stafford et al., 2014). Ganglion cells can be classified into almost 30 types (Sanes and Masland, 2015) by their preference for certain stimuli (Kim et al., 2008;Vlasits et al., 2019), receptive field size (Wienbar and Schwartz, 2018) and characteristics of their post-synaptic currents (Awatramani and Slaughter, 2000). These include ON and ON-OFF direction-selective ganglion cells involved in controlling reflex eye movements (Liu, 1995), bistratified ganglion cells involved in blue/yellow color vision (Field et al., 2007), and 4 types of intrinsically photosensitive retinal ganglion cells that contain the photopigment melanopsin (Moore et al., 1995;Freedman et al., 1999). In the primate retina, the most common types are magnocellular (M) and parvocellular (P) ganglion cells. M-cells have a large receptive field and generally signify motion or luminance changes while P-cells have small receptive fields allowing for detailed image formation (Felten et al., 2016). M and P-cells project to different layers of the lateral geniculate nucleus (Felten et al., 2016). Ganglion cells transform the graded light responses of photoreceptors and bipolar cells into a spike code, encoding

information in trains of sodium driven action potentials that can be transmitted up the optic nerve to higher visual centers. Thus, ganglion cells behave more like other neurons in the CNS and PNS.

The physiology of the retina is supported by the RPE and Muller glial cells. The RPE is a single sheet of epithelium that lies behind the retina with microvilli that surround photoreceptor outer segments. Like other epithelia, RPE cells adhere to one another by tight junctions. The sheet of RPE cells separates the choroidal vasculature from the neurosensory retina and thus makes up part of the blood/retinal barrier in the retina that helps to confer some immune privilege to the retina (Naylor et al., 2019). Due to deep pigmentation by melanin granules, RPE cells also aid in the absorption of stray photons to prevent oxidative damage caused by the concentration of light focused on the retina (Cai et al., 2000). Additionally, RPE cells phagocytose outer segment discs shed by photoreceptors on a daily basis (Naylor et al., 2019). The RPE has a special relationship with rods where after photoconversion of cis-retinal to all-trans-retinal, the bleached chromophore is transported to the RPE for reconversion to its 11-cis configuration by retinol isomerase and 11-cis-retinol dehydrogenase (Saari, 2016;Kanow et al., 2017).

As in other nervous tissue, the retina has accessory glial cells to sustain healthy extracellular space and support neuronal processes. The predominant glial cells in the retina are the Muller glia with cell bodies in the inner nuclear layer and processes that span the retina radially. The terminations of these processes define the outer and inner limiting membranes (Ramirez et al., 1996). Functionally, they serve numerous roles in metabolism and homeostasis including: glucose provision for neurons, metabolic waste removal, neurotransmitter clearance, and regulation of extracellular K^+ concentrations throughout the retina (Reichenbach and Bringmann, 2019). They also recycle bleached all-trans retinal into photosensitive 11-cis-retinal for cones (Sato and Kefalov, 2016), serving a similar role as the RPE for rods.

Astrocytes can be found in the nerve fiber layer and oligodendrocytes sheathe axons with myelin as they enter the optic nerve (Reichenbach and Bringmann, 2019). Although the retina

exhibits some immune privilege, it also contains microglia that provide some immune response capabilities (Li et al., 2015).

Mechanisms of Synaptic Release

The central fusion apparatus in Ca^{2+}-dependent exocytosis of synaptic vesicles is a complex of proteins known as SNARE proteins. The minimum molecular machinery needed for fusogenicity is one vesicle-associated membrane protein (VAMP or synaptobrevin) and two plasma membrane proteins (SNAP25 and syntaxin) (Fig. 5) (Kavalali, 2002).

One of the hallmarks of the SNARE complex participation in synaptic exocytosis is its ability to be tightly regulated and coordinated by $[Ca^{2+}]_i$. The three SNARE proteins intertwine with one another to form a "SNARE complex" that is intrinsically fusogenic (Risselada and Grubmuller, 2012). In order to regulate and coordinate exocytosis with Ca^{2+} entry, the machinery must also include a Ca^{2+} sensor (Brose et al., 1992;Geppert et al., 1994;Xu et al., 2009;Bello et al., 2018). Synaptotagmins are the most commonly used exocytotic Ca^{2+} sensors in neurons, although hair cells use otoferlin (Johnson and Chapman, 2010;Michalski et al., 2017). Synaptotagmins couple elevated $[Ca^{2+}]_i$ to release by binding Ca^{2+} to their C2A and C2B domains which promotes insertion of the n-terminus into phosphatidyl serine-rich areas of target membrane (Fernandez et al., 2001;Ubach et al., 2001;Fernandez-Chacon et al., 2002). This insertion brings the vesicle closer to the target membrane and promotes the opening of a fusion pore that is stabilized by components of the SNARE complex. Neurons also express complexins that associate with SNARE proteins to inhibit and facilitate exocytosis. Complexins 3 and 4 are expressed in photoreceptors and suppress tonic release, but promote fast evoked exocytosis (Babai et al., 2016). Photoreceptors express synaptobrevin 2 and SNAP-25, common SNARE molecules used at most conventional synapses (Rizo and Sudhof, 2002;Ramakrishnan et al., 2012). However, rather than expressing the more common syntaxin 1, photoreceptors contain syntaxin 3 (Curtis et al., 2008;Curtis et al., 2010). In

Chapter 2, we describe the capabilities of this particular molecule to promote synchronous fusion of multiple vesicles and speculate on its impact on signaling from rods.

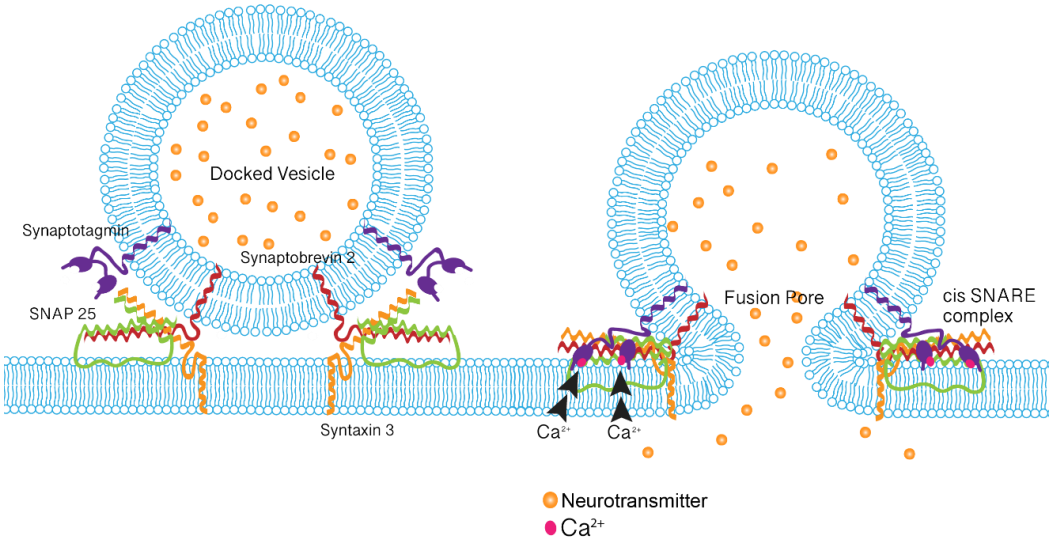

Figure 5 A SNARE complex is formed by the association of vesicular SNARE (synaptobrevin 2) with t-SNAREs syntaxin 3 and SNAP25. Vesicle-associated synaptotagmin binds Ca^{2+} molecules causing interactions with target membrane phospholipids which physically brings vesicle closer to target membrane, promoting fusion.

Synchronous, Asynchronous, and Spontaneous Release

Neurotransmitter release is often categorized into three kinetic groups: 1) evoked synchronous, 2) evoked asynchronous, and 3) spontaneous (Kaeser and Regehr, 2014;Kavalali, 2015) (Fig. 6). Evoked release requires a depolarizing stimulus and a subsequent rise in $[Ca^{2+}]_i$ to be coupled to the release mechanism while spontaneous release occurs at hyperpolarized potentials. It is commonly thought that differences in these three modes of release may reflect release at different active zones and/or release of functionally distinct pools of vesicles using different combinations of SNARE and SNARE-associated molecules (Crawford and Kavalali, 2015b).

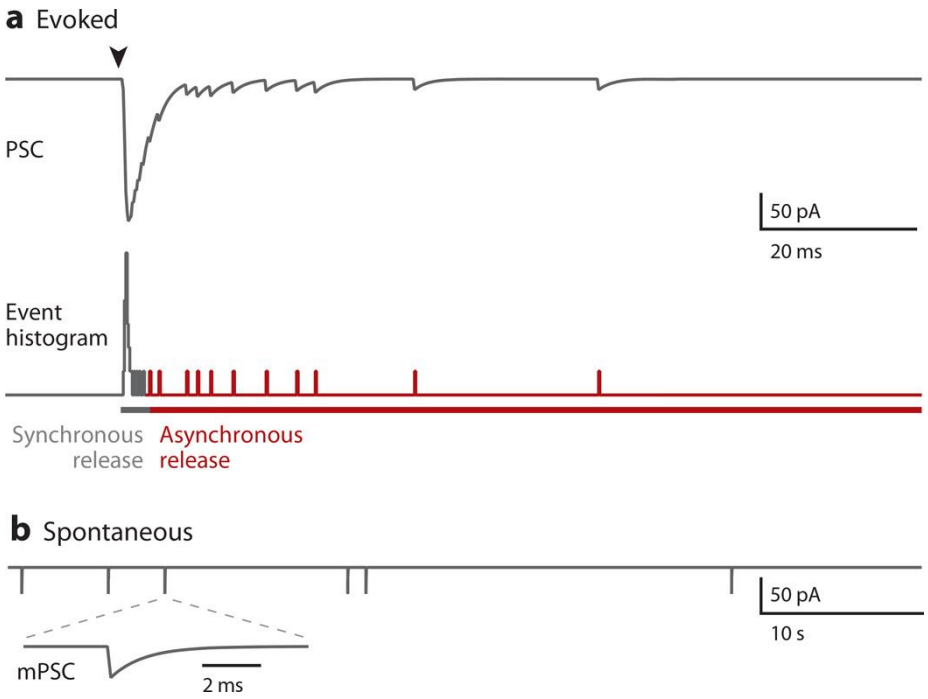

Figure 6 A. Illustration of synchronous release of many vesicles evoked by a depolarizing stimulus, followed by staggered release of single vesicles due to residual intraterminal Ca^{2+}. B. Spontaneous release of single vesicles occurs in the absence of a voltage stimulus. Adapted from Kaeser and Regehr, Ann Rev Physiol, 2014.

At many synapses, synchronous, asynchronous, and spontaneous release utilize different Ca^{2+} sensors. There are fourteen synaptotagmin (Syt) isoforms but only eight of these can bind Ca^{2+} ions (Sudhof, 2002). Syts 1, 2, and 9 show relatively low Ca^{2+} affinity and have been identified as sensors for fast synchronous release from neurons (Sudhof, 2014). The higher affinity sensor, Syt7, and another sensor, Doc2, have been proposed as sensors for slower asynchronous release that is not tightly coupled to Ca^{2+} channel openings (Chung et al., 2010;Yao et al., 2011;Bacaj et al., 2013;Luo and Sudhof, 2017). Doc2 has also been proposed as a sensor for spontaneous release driven by resting Ca^{2+} levels (Pang et al., 2011;Ramirez et al., 2017). The high affinity of Syt7 for phosphatidyl serine and Ca^{2+} molecules (EC_{50} = 1-2 µM) (Sugita et al., 2002) allows it to promote release with low residual [Ca^{2+}] achieved at more distant release sites by diffusion of Ca^{2+} from VGCCs (Bacaj et al., 2013;Luo et al., 2015;Chanaday and Kavalali, 2018). Although there is evidence that Syt7 exhibits slower fusion pore expansion kinetics than Syt1 (Hui et al., 2005), the

rate of Ca^{2+}-dependent exocytosis appears to be limited by Ca^{2+} diffusion, not the speed of sensor molecule conformational change (Bendahmane et al., 2018).

Spontaneous release can be Ca^{2+}-dependent or independent. Both types can occur at photoreceptor synapses (Cork et al., 2016). In many neurons, including photoreceptors and cochlear hair cells, a fraction of spontaneous release events remain even in the presence of strong Ca^{2+} buffering or Cd^{2+} blockade of VGCCs (Cork et al., 2016;Williams and Smith, 2018). The mechanism for Ca^{2+} independent release may involve spontaneous interactions between lipid molecules and Ca^{2+} sensor molecules that can arise in the absence of Ca^{2+} due to thermal fluctuations (Rickman and Davletov, 2003;Pang et al.).

Ca^{2+}-dependent spontaneous release relies on stochastic opening of membrane Ca^{2+} channels or release of Ca^{2+} from internal stores to stimulate fusion of already docked and primed vesicles. L-type Ca^{2+} channels, such as those found in photoreceptor cell terminals, can occasionally open even at hyperpolarized membrane potentials (e.g., −60 to −70 mV) (Kavalali and Plummer, 1996;Magee et al., 1996), but the propensity for spontaneous channel openings to drive Ca^{2+}-dependent spontaneous release appears to be predominantly a characteristic of inhibitory neurons (Goswami et al., 2012;Williams and Smith, 2018). As with evoked release, Ca^{2+}-dependent spontaneous release requires a Ca^{2+} sensor. There is evidence that the high affinity Ca^{2+} sensors Doc2a and Doc2b can mediate spontaneous release, with Doc2a operating primarily at glutamatergic synapses and Doc2b operating at inhibitory synapses (Courtney et al., 2018). There is evidence for segregation between the different vesicle pools that drive evoked and spontaneous release (Bal et al., 2013;Crawford and Kavalali, 2015a). For example, the SNARE protein VAMP7 appears to be expressed more strongly in vesicles that participate in spontaneous release than evoked release (Chanaday and Kavalali, 2018).

Compared with release from conventional neurons that has an immensely steep dependence on $[Ca^{2+}]_i$ (Schneggenburger and Neher, 2005), photoreceptors have an unusually shallow Ca^{2+}

dependence. Conventional neurons require the binding of 4-5 Ca^{2+} molecules to trigger release, defining a "cooperativity" that is illustrated as a slope of 4-5 when presynaptic Ca^{2+} and post-synaptic responses are related on a log-log plot (Heidelberger et al., 1994;Schneggenburger and Neher, 2000;Sun et al., 2007). For photoreceptors, this cooperativity is ≤ 3 (Rieke and Schwartz, 1996;Thoreson et al., 2004;Duncan et al., 2010). The Ca^{2+} dependence, cooperativity and sensitivity of release is conferred by the population of vesicular Ca^{2+} sensors at a particular synapse (Crawford and Kavalali, 2015a).

Synaptotagmin 1 (Syt1) is the Ca^{2+} sensor coupling Ca^{2+} influx to fast, evoked exocytosis at most synapses. While photoreceptors of non-mammalian retina do not possess Syt1 (Heidelberger et al., 2003), it is present in terminals of mammalian rods and cones (Berntson and Morgans, 2003;Fox and Sanes, 2007). Our recent studies showed that genetic deletion of Syt1 from rod and cone photoreceptors abolished fast, synchronous glutamate release evoked by a strong depolarizing step (Grassmeyer et al., 2019). Syt1 deletion entirely eliminated release from cones and reduced release from rods, but spared a slower release component from rods that is not as tightly synchronized to Ca^{2+} channel activation evoked by longer depolarizing steps. We hypothesize that Syt7 may be the sensor that mediates the residual asynchronous release from rods that persists after loss of Syt1. Syt1 deletion also did not diminish spontaneous release of vesicles by rods and cones that occurs in the absence of depolarizing stimulation, so we also tested whether the Doc2b isoform that is present in rods participates in spontaneous release from photoreceptors. We describe experiments studying the impact of deleting Syt1, Doc2b and Syt7 on release in Chapter 3 of this dissertation.

In photoreceptors, kinetically distinguishable vesicle pools can also be physically defined by whether or not they are tethered to the ribbon and would undergo ribbon-mediated release or release from ectopic sites. Vesicles tethered to the base of the ribbon that are also in contact with the plasma membrane appear to make up a readily releasable pool that can be released almost immediately

upon the depolarization-evoked opening of Ca^{2+} channels (Mennerick and Matthews, 1996;von Gersdorff et al., 1996;Datta et al., 2017). With maintained depolarization, a second slower component of release can be observed that matches the number of vesicles tethered to the remainder of the ribbon (Mennerick and Matthews, 1996). After depleting these two components, release can be maintained at a still slower rate that is thought to reflect replenishment of vesicles from the cytoplasmic reserve pool to the ribbon (Babai et al., 2010a). Conventional neurons have reserve pools of vesicles linked together by synapsins and vesicles must be liberated by Ca^{2+} signaling to become releasable (Humeau et al., 2001;Vasileva et al., 2012). This contrasts with photoreceptor terminals that have thousands of cytoplasmic vesicles lacking synapsin, allowing them to be extremely mobile and facilitating rapid replenishment of releasable pools (Heidelberger, 2007;Innocenti and Heidelberger, 2008). In amphibian cones, release originates entirely from the ribbon (Snellman et al., 2011). This also appears to be the case in mammalian cones (Mehta et al., 2013). Fast release from rods also occurs at ribbons, but rods can also release additional vesicles at more distant, non-ribbon sites. Release from these ectopic, non-ribbon sites is promoted by strong and sustained Ca^{2+} signaling from voltage-gated Ca^{2+} channels as well as by release of Ca^{2+} from intracellular stores in a process called Ca^{2+}-induced Ca^{2+} release (CICR) (Suryanarayanan and Slaughter, 2006;Chen et al., 2014). In CICR, Ca^{2+} sequestered in the endoplasmic reticulum (ER) is liberated by the activation of ryanodine receptors on the ER membrane. This mechanism is present in both mammalian and non-mammalian rods where it contributes to promoting slow asynchronous release of vesicles.

The physical separation between different pools of vesicles in rod and cone terminals allows for the spatiotemporal heterogeneity of terminal $[Ca^{2+}]_i$ to govern release from distinct pools and help to shape the kinetics of release. Ca^{2+} influx at photoreceptor terminals reaches vesicles located within nanometers of channels at the base of the ribbon, contributing to the fast, synchronous component of exocytosis. Remaining Ca^{2+} that diffuses farther from the ribbon can enlist the help

of CICR to initiate release from rods of vesicles from non-ribbon sites. The contributions of different vesicle populations can often be resolved by the effects of diffusible Ca^{2+} buffers. BAPTA has a similar affinity for free Ca^{2+} as EGTA, but chelates nearly 40 times as rapidly so inclusion of these buffers in intracellular solutions allows for spatial discrimination of Ca^{2+}-dependent events (Fig. 7)(Neher, 1998).

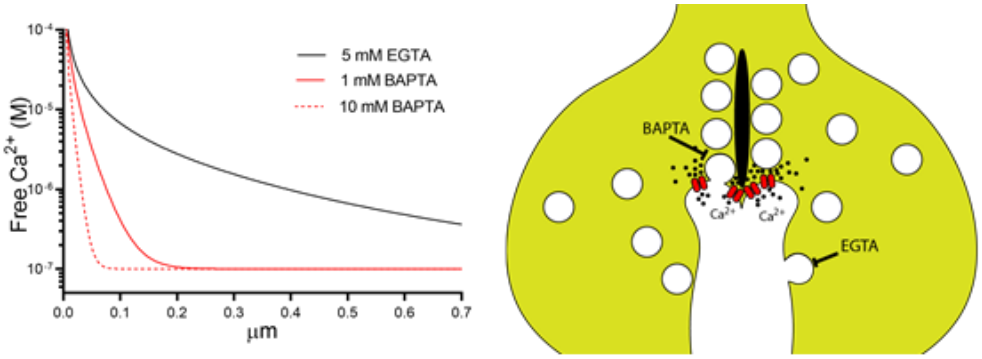

Figure 7 Strong buffering by BAPTA chelates free Ca^{2+} faster than EGTA, constraining Ca^{2+} −dependent events to within nanodomains of channels. In the rod terminal, EGTA prevents non-ribbon Ca^{2+}-dependent release events. Graphical model made with an Excel-based macro from Ward and Kenyon, 2000.

Millimolar levels of intracellular BAPTA limits Ca^{2+}-dependent events to nanodomains within 100 nm or less of Ca^{2+} sources, while EGTA allows further diffusion of Ca^{2+} molecules into microdomains to initiate more distant signaling events (Ward and Kenyon, 2000). In chapters 2 and 3, we use these buffers to probe the properties of release from rods in salamander and mouse retina.

Quantal Theory of Neurotransmission

Current understanding of chemical synaptic transmission is rooted in observations made by Bernard Katz of spontaneous end-plate potentials at the frog neuromuscular junction. Katz and colleagues noticed that many of these spontaneous miniature end-plate potentials (mEPPs) were roughly the same amplitude and that after lowering Ca^{2+} to reduce release probability, end plate potentials evoked by a depolarizing stimulus were integer multiples of these mEPPs (Fatt and Katz,

1952;Del Castillo and Katz, 1954). Later visualization of synaptic vesicles by electron microscopy (De Robertis and Bennett, 1955) led to the hypothesis that neurotransmitters are released from nerve terminals in discrete "quanta" and that each vesicle contains approximately the same number of neurotransmitter molecules, corresponding to a single "quantum" (Del Castillo and Katz, 1954).

Quantal neurotransmission is commonly assessed by creating frequency distributions of post-synaptic potentials or currents (Byrne et al.;Liley, 1956). Typically, the smallest amplitude events are defined as "uniquantal events" (release of one vesicle) with the mean amplitude of the first peak in the amplitude distribution defined as the "fundamental amplitude." Succeeding amplitudes that are frequently achieved are integer multiples (corresponding to the number of vesicles/quanta released) of the "fundamental amplitude." Many describe the release of multiple quanta by expressing quantal content (*m*) which reflects an average number of quanta released if all release events were equal (Byrne, 2014). To understand how quantal content is calculated and its significance, we assume that release of a vesicle is probabilistic and can be predicted by Poisson statistics. Each synaptic terminal contains docked and primed vesicles (*n*) with a small chance of fusing (*p*) with the terminal membrane. The mean number of quanta (quantal content = *m*) released after repetitive stimulation will be:

$$m = n \cdot p$$

Suppose a terminal contains 5 docked vesicles ($n = 5$) at any time and the probability of fusion is small ($p = 0.1$). With stimulation, occasionally none will fuse (failure) and more often one vesicle will fuse. However, it is possible that up to 5 vesicles may fuse simultaneously. Thus, the quantal content or mean number of quanta released (*m*) will fall somewhere between 0 and 5. On average, a stimulus would evoke the release of 0.5 quanta (0.5 = 5*0.1). If there was a way to accurately estimate *n* or *p*, the binomial distribution could be used to estimate the likely occurrence of release of 0, 1, 2, or more quanta. However, because *n* and *p* are typically not experimentally accessible,

the Poisson model is often used for this estimation and is appropriate given the small probability of release at most synapses.

$$P/x = \frac{m^x e^{-m}}{x!}$$

The above equation (Equation 2) describes the fraction of occasions on which the evoked response has a quantal content of *x*. *P* represents the probability that you would observe a quantal content (*x*), when the mean quantal content over many trials (*m*) is known. The variability of amplitudes predicted by the Poisson distribution can then be compared to those obtained experimentally and plotted as an amplitude frequency distribution. The mean and variance of each peak predicted by Poisson statistics is a unit multiple of the first peak, made up of uniquantal release events.

Although most neurons release neurotransmitters from vesicles in discrete packets, there are a number of sources for variability in quantal size that can complicate quantal analysis (Pulido and Marty, 2017). Non-linear summation of synaptic potentials or currents can obscure quantal analysis. Synaptic potentials that arise in different compartments with different active and passive membrane properties will differ in amplitude and kinetics. If there is poor voltage clamp of dendrites, synaptic currents arising in distant dendrites will be smaller and slower than those arising close to the soma.

Variability can also reflect genuine differences in quantal amplitude and kinetics. These can arise from the presence of different inputs from multiple converging neurons. At individual synapses, differences in the size of the post-synaptic density and the number of post-synaptic receptors can also contribute to heterogeneity in quantal size (Byrne, 2014). The pre-synaptic methods used to measure quantal release in experiments described in later chapters avoid post-synaptic contributions to quantal heterogeneity by measuring glutamate released directly from a single presynaptic neuron.

Presynaptic factors can also alter quantal amplitude. Single vesicles often do not release enough glutamate to saturate post-synaptic receptors, so heterogeneity of quantal size can arise from variations in vesicle size, neurotransmitter concentration, kinetics of fusion pore closure (e.g., kiss-and-run exocytosis vs. full-collapse fusion), and the distance that neurotransmitter molecules must travel to reach post-synaptic receptors (Byrne et al.;Ishikawa et al., 2002;Takamori, 2016). At central glutamatergic synapses, evidence supports the hypothesis that vesicular glutamate concentration is the major source of quantal size variation. Overexpression of vesicular transporters and increased cytosolic glutamate concentrations both led to an increase in quantal size whereas vesicular size (measured by capacitance jumps) was not correlated with quantal size (Song et al., 1997;Ishikawa et al., 2002;Wu et al., 2007;Bartoletti and Thoreson, 2011). On the other hand, the heterogeneity of excitatory post synaptic current amplitudes arising from inner hair cell glutamate release is thought to arise mostly from heterogeneity of vesicle size as measured by capacitance jumps (Grabner and Moser, 2018).

Spontaneous and asynchronous release of vesicles is generally thought to occur randomly (Chapman, 2008). Ca^{2+} channel openings also occur randomly (Williams and Smith, 2018). Thus, Poisson statistics can often be used to describe the random timing of vesicle release events. To apply Poisson statistics, a number of assumptions must be made: the events must be clearly defined and able to be counted only once, the average rate (λ) doesn't change over time, and each event occurs independently of other events. If vesicle release events occur stochastically, then the number of release events counted in a given time interval will vary. The average number of release events per interval (λ) can be calculated from the observation of many intervals over a long period of time. If events occur randomly, plotting the frequency of release events counted during each time interval will yield a slightly skewed bell curve. This curve can be defined by Equation 3 the Poisson Model, where P is the probability that x number of events will be observed in a defined interval given λ,

the average number of events per interval. This is the same probability distribution described for assessing quantal content (Equation 2), but applied to the number of events in a given time period.

$$P(x) = \frac{\lambda^x \cdot e^{-\lambda}}{x!}$$

One derivation of the Poisson distribution is that a frequency distribution of interevent intervals can be fit a single exponential decay function (Motulsky, 2010). As we consider further below and in chapters 3 and 4 our evidence suggests that the ribbon may help to coordinate release in a way that makes release more regular and less dictated by Poisson statistics.

Multivesicular Release

For many years, it was accepted that at most CNS synapses, an incoming action potential resulted in release of at most only one vesicle. However, more recent evidence has shown that even small central synapses containing only a few dozen vesicles can release more than one vesicle per action potential, thus regulating the concentration of neurotransmitter in the synaptic cleft (Rudolph et al., 2015). Multivesicular release is common in cells of other secretory systems(Blank, 2011;Zhu et al., 2013;Messenger et al., 2014;Sanchez et al., 2018;Vakilian et al., 2019), but amongst neurons, those with ribbons such as cochlear hair cells and retinal bipolar and photoreceptor cells seem particularly adept at coordinating and synchronizing the release of multiple vesicles (Singer et al., 2004;Graydon et al., 2011;Li et al., 2014). This greatly increases the bits of information a neuron can pass to another, effectively creating an analog code where the cell can continually vary synaptic output.

Multiquantal release increases the capability of a synapse for modulating information transmission. At calyceal synapses, release of multiple quanta desensitize scarce post-synaptic AMPA receptors to promote synaptic depression (Trussell et al., 1993). An obvious advantage of multivesicular release is that increased cleft neurotransmitter improves the reliability of presynaptic release to elicit an action potential in the post-synaptic cell. Such is the case with somatosensory

cortical cells, where multiquantal release is promoted by additional active zones, thereby strengthening synaptic connections and decreasing response variability (Loebel et al., 2009). This property of multiquantal release is also necessary for phase-locking precision of inner hair cells, allowing for reliable spiking of post-synaptic spiral ganglion neurons in synchrony with sound waves (Li et al., 2014). Recently in zebrafish retina, James et al. showed that variation in the amplitude of multivesicular release events from bipolar cells helps them to encode contrast (James et al., 2019). Chapter 2 describes experiments addressing the ability of rod photoreceptors to release multiple quanta in response to depolarization and discusses how this might enhance detection of light offset or heighten horizontal cell inhibition to surrounding cells to boost contrast sensitivity (James et al., 2019).

Multiquantal release can occur in a number of ways. The first mechanism is synchronous release of multiple individual vesicles at adjacent release sites, temporally coordinated by a Ca^{2+} signal (Fig. 8). The second and third mechanisms involve homotypic fusion of synaptic vesicles with one another. In sequential compound fusion, a Ca^{2+} signal causes release of contents from a docked vesicle and then the spread of Ca^{2+} triggers neighboring vesicles to fuse with the first vesicle which acts as a conduit to the extracellular space. In synchronous compound fusion, multiple vesicles that have fused with one another prior to Ca^{2+} entry may be released simultaneously.

All three of these mechanisms may be used at ribbon synapses. The multiple release-ready vesicles in the readily releasable pool tethered at the base of the ribbon can be released quickly at neighboring release sites by the opening of multiple Ca^{2+} channels beneath the ribbon (Singer et al., 2004;Bartoletti et al., 2011;Van Hook and Thoreson, 2015) Simultaneous release of two or three close vesicles within a single Ca^{2+} nanodomains could potentially be synchronized by opening of a single nearby Ca^{2+} channel (Eggermann et al., 2011;Graydon et al., 2011) Experiments

described in Chapter 2 show evidence that simultaneous compound fusion may also arise from prior homotypic fusion of adjacent vesicles along ribbon.

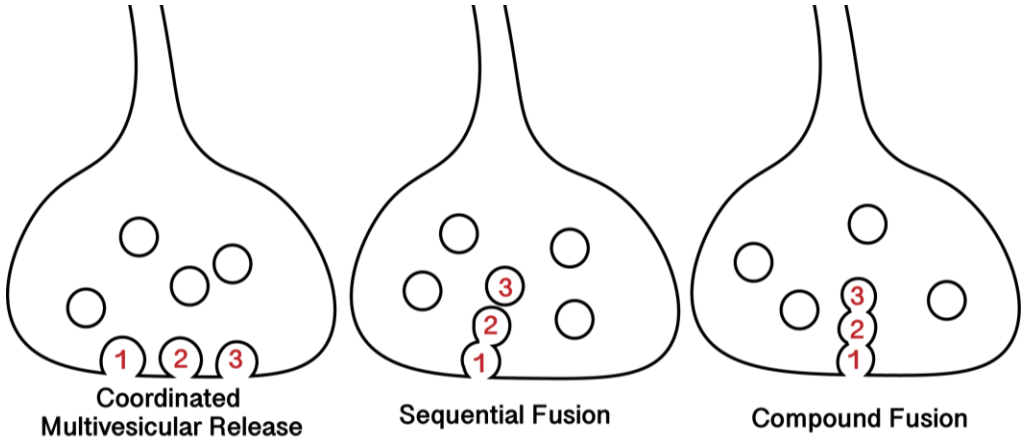

Figure 8 Illustration of mechanisms for multiquantal release. All of the examples show release of 3 quanta. Coordinated multivesicular release involves many individual vesicles fusing with the terminal membrane simultaneously, coordinated by Ca2+ signals. In sequential fusion, a vesicle fuses with the terminal membrane and as Ca2+ diffuses farther, deeper vesicles fuse with the previously exocytosed vesicle. This mechanism may lead to slight asynchrony. In compound fusion, there is homotypic fusion of vesicles prior to fusion with the terminal membrane and multiple quanta leave a single fusion pore, enhancing synchrony.

The structure of the ribbon may promote synchronous and sequential release of multiple vesicles by positioning vesicles next to one another along the face of the ribbon. The capability for simultaneous multivesicular fusion can also result from the presence of multiple release sites next to one another along the ribbon base. The structure of the ribbon may promote the spread of Ca^{2+} beneath its base, saturating local buffers and coordinating release of multiple nearby vesicles within Ca^{2+} nanodomains in hair cells (Glowatzki and Fuchs, 2002;Graydon et al., 2011) and photoreceptors (Mercer and Thoreson, 2011). The size of the multiquantal EPSCs matches closely to the readily releasable pool at the base of the ribbon in hair cells suggesting fusion within Ca^{2+} nanodomains (Graydon et al., 2011). Graydon et al. argue that because multivesicular release was not diminished by strong Ca^{2+} buffering, Ca^{2+}-dependent compound fusion of vesicles up the ribbon is unlikely and that Ca^{2+}-dependent events are thus limited to bottom-dwelling vesicles (Graydon

et al., 2011). Others have argued that the heterogenous amplitudes of EPSCs in hair cells are due to single vesicles with “flickering fusion pores” that release differing amounts of glutamate (Chapochnikov et al., 2014;Grabner and Moser, 2018).

In retina, coordinated multivesicular release from bipolar cells has been described by Singer et al. who discovered that the quanta released from bipolar cells exceeded the number of active zones marked by kinesin labeling (Singer et al., 2004). In bipolar cells, not only are evoked events comprised of multiple vesicles and lack the temporal jitter associated with multivesicular release at other synapses, but spontaneous mEPSCs are also variable in amplitude. Their results suggest that the ribbon coordinates highly synchronous release of several individual vesicles due to high release probability of multiple vesicles within a single active zone. They argue against homotypic fusion, claiming that pre-fused vesicles would contain more fusion proteins, thereby enhancing release probability and diverging from the binomial statistics that multivesicular release appears to adhere to at the bipolar cell terminal. Singer et al. go on to note that evoked glutamate release from bipolar cells does not saturate AMPA receptors at AII amacrine cells which suggest that they are able to encode multivesicular release events. Recently, James et al. also verified multivesicular release from zebrafish using a fluorescent glutamate reporter (James et al., 2019) They go on to show that, functionally, bipolar cells are then able to encode contrast sensitivity with an amplitude code, effectively increasing the amount of information that can be transmitted above that which can be obtained using a traditional rate code.

In contrast, Gary Matthews proposed compound fusion as a mechanism for synchronous multiquantal release from bipolar cells (Matthews and Sterling, 2008). Matthews proposed that vesicles close to one another on the ribbon undergo homotypic vesicle-vesicle fusion prior to exocytosis at the membrane (Parsons and Sterling, 2003;Matthews and Sterling, 2008). Homotypic fusion is known to occur in other secretory systems such as mast cells and pancreatic beta cells (Blank, 2011;Zhu et al., 2013;Sanchez et al., 2018;Vakilian et al., 2019). Ribbon-tethered vesicles

express the minimum fusogenic machinery (Walch-Solimena et al., 1995a) and, consistent with homotypic fusion, electron micrographs show large irregularly shaped ribbon-bound vesicles following stimulation and rapid fixing (Matthews and Sterling, 2008). Large cisternae have also been observed near the ribbon after stimulation of inner hair cells (Lenzi et al., 2002) and rods(Rao-Mirotznik et al., 1995). This mechanism would provide a means for multiple quanta to be released through the same fusion pore, enhancing synchrony. Chapter 2 presents evidence that homotypic compound fusion of vesicles on the ribbon may contribute to release in salamander rods.

Glutamate Transporters at the Rod Synapse

After glutamate is released from photoreceptors and other neurons, it is typically retrieved by Excitatory Amino Acid Transporters (EAAT) (Hasegawa et al., 2006). EAATs are found on both neurons and glia and are responsible for the rapid removal of glutamate from the synaptic cleft. The presynaptic terminals of rods and cones contain an abundance of EAATs. There are five known isoforms (EAATs1-5) that function to transport glutamate but can also act as anion channels (Jensen et al., 2015). EAAT1 and EAAT2 are typically expressed in CNS glia while EAATs 3 and 4 are primarily expressed in neurons of the cerebellum, striatum, and hippocampus (Jensen et al., 2015;Magi et al., 2019). Splice variants of EAAT2 are also found in the non-mammalian vertebrate retina with an isoform present in Muller glia and cone photoreceptor terminals (Schneider et al., 2014). In mammalian retina, Muller glia express EAAT1 (Magi et al., 2019). EAAT5 appears to be retina specific, expressed in the synaptic terminals of photoreceptors and bipolar cells (Schneider et al., 2014;Magi et al., 2019).

Removal of one glutamate molecule from the synaptic cleft by EAATs into presynaptic terminals or glial cells involves the simultaneous inward transport of 3 Na^+ ions, 1 H^+, with counter-transport of 1 K^+ (Fahlke et al., 2016). Glutamate transport is electrogenic in nature, but the current is slow and of negligible scale. However, nearly 3 decades ago, a glutamate transport-

associated anion current was discovered in salamander photoreceptors (Eliasof and Werblin, 1993;Picaud et al., 1995). This Cl^- current is gated by the glutamate transport process, is highly selective for anion, and shows unitary conductances that fall in the ranges of other standalone ion channels (Fahlke et al., 2016). Glutamate transporter anion currents ($I_{A(glu)}$) are activated during glutamate transport but are thermodynamically uncoupled from the transport process (Machtens et al., 2015). The Cl^- currents associated with transport are thought to be more functionally important than glutamate uptake for many EAATs, by modulating excitability and other cellular processes. In fact, EAAT4 and EAAT5 are now often called "glutamate-gated ion channels." This contrasts with EAATs1-3, which have evolved solely for glutamate handling.

$I_{A(glu)}$ is linearly related to glutamate in the cleft, so it can be used to measure glutamate release (Otis and Jahr, 1998). There are several properties of the retinal isoform EAAT 5 that should be considered when measuring $I_{A(glu)}$ in photoreceptors. The first is the large single channel conductance of EAAT5 that is estimated to be 0.7- 13.3 pS compared to sub-fS levels for EAAT1 (Picaud et al., 1995;Palmer et al., 2003;Magi et al., 2019). The activation of Ca^{2+}-activated Cl^- currents with depolarizing steps longer than a few milliseconds should likewise be given attention (Palmer et al., 2003).

Further consideration should be given to the ionic composition of intracellular solutions for electrophysiological measurements. Including Cl^- as the principal ion produces a measurable current; however, the current is enhanced when Cl^- is replaced with the chaotropic anions NO_3^- or SCN^-, with the latter being the most permeant (Wadiche et al., 1995;Palmer et al., 2003). Current density is almost doubled when including NO_3^- over Cl^- with no effects on channel kinetics. EAAT5 $I_{A(glu)}$ is sensitive to the common transporter blocker threo-β-benzyloxyaspartate (TBOA) (Palmer et al., 2003). An EAAT2-specific blocker, dihydrokainic acid (DHK), does not diminish retinal EAAT5 currents (Palmer et al., 2003). EAATs need sufficient transport substrate in order to function. For some EAATs, including

the transport substrate K^+ in the intracellular solution is necessary to measure anion currents, however substituting K^+ for Cs^+ does not diminish anion currents in EAAT5-expressing cells (Palmer et al., 2003). On the other hand, increasing extracellular pH buffering reduces $I_{A(glu)}$, suggesting that EAAT5 is more sensitive to the availability of H^+ in the synaptic cleft (Palmer et al., 2003). Because transport depends primarily on the immense transmembrane Na^+ gradient, Na^+ should be included in the extracellular solution at physiological concentrations (Grewer et al., 2008).

The magnitude of anion currents associated with EAAT transport has led to the hypothesis that a current leak and anion flux contribute to photoreceptor signaling. For example, EAAT5 contributes enough to the depolarizing light response of cone ON-BCs in mice to be detected as a component of ERG b-waves (Tse et al., 2014). The following chapters exploit the glutamate "sensing" ability of the EAAT5 transporter to examine release from rods.

Reliable Single Photon Responses

Humans can perceive light at very low intensities, and signals gleaned from photoisomerization of a single rhodopsin molecule (Rh*) are able to reach an ON ganglion cell (Ala-Laurila and Rieke, 2014;Field and Sampath, 2017;Takeshita et al., 2017). This impressive capability was first evaluated in dark-adapted human subjects by Hecht et al. in 1942 when they determined that the threshold energy required for reliable detection of a flash was roughly equivalent to 50-150 photons (Hecht et al., 1942). Because these few dozen photons would be scattered across the entire retina, this meant that individual rods must be capable of responding to single photons. For perspective, approximately 0.1 photons/μm^2/s strike the retina in starlight, considerably less than 1 photon per rod (Sterling et al., 1987). Several later psychophysical experiments presenting humans with a ~500 nm (peak wavelength sensitivity of rhodopsin) stimulus replicated the photon requirement of ~50-150 for generating reliable signals (Sharpe et

al., 1993;Koenig and Hofer, 2011;Tinsley et al., 2016). The ability of rods to respond to absorption of a single photon was shown directly by recordings from individual rod (Baylor et al., 1979). Rods are thus capable of achieving the absolute limit of visual sensitivity, since a single photon is the irreducible quantity of light energy (Pugh, 2018)! Naarendorp et al. completed a behavioral study in mouse demonstrating similar absolute sensitivity (Naarendorp et. al. 2010). This finding provides a necessary basis for using mouse to model mechanisms of single photon detection.

The requirements for reliable single photon detection are 1) high gain of phototransduction, 2) enhanced signal-to-noise ratio at the rod-to-rod bipolar cell (RBC) synapse, and 3) optimal signal processing in the post-rod retinal circuitry. While the remarkable sensitivity of rods to respond to individual photons is well established (Lamb and Pugh, 1992;Pugh and Lamb, 1993;Leskov et al., 2000), the mechanisms that allow reliable transmission of small single photon responses through the retina remain unclear. A substantial portion of this section is devoted to mechanisms that increase reliability at the rod-RBC synapse and the experiments described in Chapters 3 and 4 address pre-synaptic processes that contribute to this capability.

The ability of rods to produce a detectable voltage change in response to absorption of a single photon originates with high efficiency for the absorption of single photons and amplification within the enzymatic phototransduction cascade (Lamb and Pugh, 1992;Pugh, 2018) Photons within the visible light spectrum very reliably (50-60%) activate rhodopsin in mouse and human due to its high concentration (3 mM) in outer segment disks (Rieke and Baylor, 1998;Nickell et al., 2007;Reingruber et al., 2015). Efficient absorption is also promoted by arrangement of rod outer segments with hundreds of disks, each packed with rhodopsin, stacked on top of one another. Thus a photon that enters a rod has many opportunities to be captured by a rhodopsin molecule. When a photon is captured, rhodopsin is able to activate nearly 300 transducin molecules per second(Krispel et al., 2006) (Krispel et al., 2006). Transducin activates PDE in a 1:1 ratio but the prodigious enzymatic efficiency of PDE lends itself to further signal amplification (Krispel et al.,

2006;Reingruber et al., 2015). The gain provided by activation of many G_t molecules and a high rate of catalysis by PDE makes rods exquisitely sensitive to single photons. The membrane voltage change resulting from single photon absorption (photovoltage) ranges from 1 mV in macaque (Schneeweis and Schnapf, 1995;Hornstein et al., 2005) to 3.44 ± 1.37 mV (mean ± SD) in mouse retina (Cangiano et al., 2012). Even this larger value for mouse rods presents a substantial challenge for generating a sufficiently large reduction in glutamate release to be detected post-synaptically by a RBC, given the stochastic processes that underlie synaptic transmission discussed earlier.

A membrane voltage change of 3.4 mV is not far outside the range of physiological voltage noise in mouse rods (S.D. = 0.4-0.8 mV) (Jin et al., 2015). This physiological voltage noise in rods contributes to variation in release rate and quantal noise. If release at the membrane potential in darkness is stochastic, the rate of tonic release must be so frequent that the interval between release events is not mistaken for a pause in release caused by photon absorption. Rao et al. calculated a release rate of $\geq$ 40 quanta/s is needed to ensure reliability for detecting only true photon absorption events and rejecting false positives (Rao et al., 1994). The ability to maintain a high tonic release rate is served by the rod having a synaptic ribbon. It is not only necessary to have a sufficiently high rate of release to avoid false positives, but there must also be a sufficiently large reduction in release produced by a single photon voltage change to accurately and reproducibly signal the change in release. Fortunately, release rate in rods is proportional to I_{Ca} and the dark potential lies at an optimal position in the I_{Ca} Boltzmann function such that a 3.4 mV hyperpolarization caused by the absorption of one photon should reduce glutamate release rate by ~20% (Schein and Ahmad, 2005). If the release rate exhibits Poisson statistics, then the range of instantaneous rates observed after absorption of a single photon will greatly overlap with instantaneous release rates in total darkness. Thus, the change in release caused by absorption of a single photon will be barely detectable. To achieve less overlap between the release rate in darkness and that produced by a small hyperpolarization, the variance of release rates can be decreased, thus increasing the

likelihood of accurate discrimination by the bipolar cell. To reduce variance in release rates, Schein and Ahmad proposed the "clockwork hypothesis" which postulated that release at rod ribbon synapses in darkness may not be purely stochastic, showing Poisson statistics, but instead may be more regular (Schein and Ahmad, 2005). Reducing variability in the rate of release has two benefits. One, making release more regular smooths out glutamate changes in the synaptic cleft, thereby reducing RBC membrane voltage changes and improving the signal-to-noise for detecting authentic changes. Making release more regular tightens deviations in number of quanta counted by the RBC dendrite in a sampling interval, thus reducing the number of false positives. This concept is illustrated in Fig. 9.

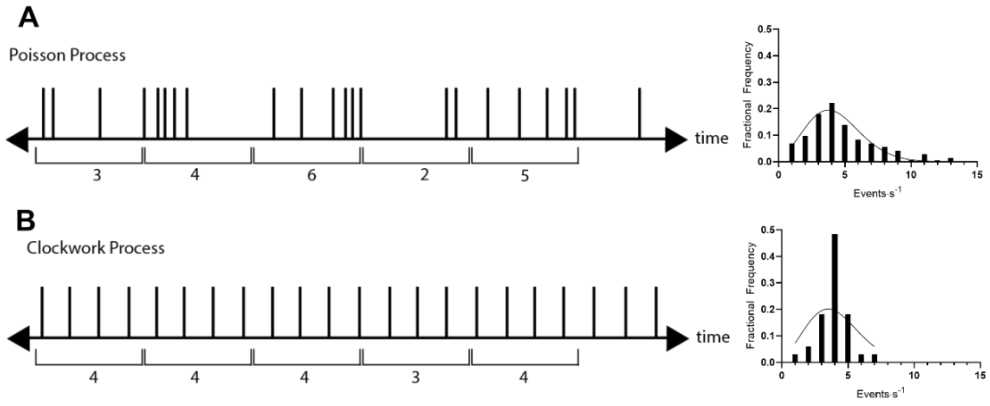

Figure 9 Illustration of stochastic and clockwork processes. A. Shows events distributed randomly in time. Counts of events in each sampling interval range from 2-6, average (λ) = 4. Their distribution can be fit with the Poisson model when $\lambda = 4$, $R^2 = 0.91$ (right). B. When events occur more regularly in time, the variance of the count in each sampling interval is reduced. This example has the same mean number of events $\lambda = 4$ in each interval but is not approximated by the Poisson model, $R^2 = 0.39$ (right).

Rods transmit single photon responses using a specialized scotopic circuit (Fig. 10) (Kolb and Famiglietti, 1974;Dacheux and Raviola, 1986). Rods and cones utilize different circuits in the retina and so the mammalian retina is sometimes considered to be a "duplex" retina. Cones contact ON and OFF cone-driven bipolar cells, which then transmit signals to ON and OFF ganglion cells. However, rods signal ganglion cells using a more indirect circuit. First, almost all of the contacts

made by rods are with a single ON-type RBC. Direct contacts between rods and OFF bipolar cells are quite sparse (Soucy et al., 1998;Li et al., 2004;Tsukamoto and Omi, 2014). Furthermore, rod bipolar cells do not synapse directly onto ganglion cells but rather contact AII amacrine cells in the inner plexiform layer. AII amacrine cells then communicate the response via gap junctions to ON cone bipolar cells and glycinergic synapses onto OFF cone bipolar cells. Cone bipolar cells then send glutamatergic signals to ganglion cells. This circuit operates primarily under scotopic conditions in mouse. As luminance increases, rods can also communicate with the cone circuit by sending signals through electrical synapses and direct contacts with OFF bipolar cells.(Grimes et al., 2015;Tsukamoto and Omi, 2015;Grimes et al., 2018)

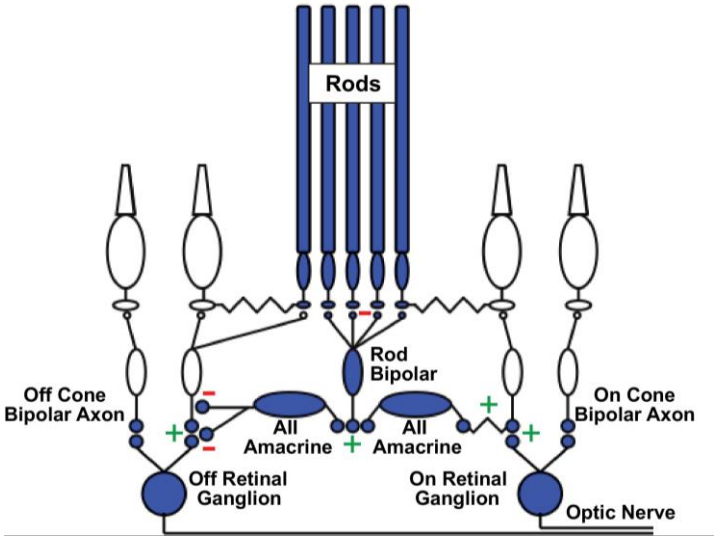

Figure 10 Illustration of the scotopic circuit in the mouse. Rods transmit glutamatergic signals to rod bipolar cells (ON-type) which signal AII amacrine cells. AII amacrine cells signal ON-cone bipolar via gap junctions that transmit glutamatergic signals to ON-ganglion cells. AII amacrine cells also make glycinergic, sign-inverting synapses onto OFF-cone bipolar cells that transmit their signals to OFF-ganglion cells. Image from Grimes et al. 2018 under Creative Commons License type CC-BY.

Non-Linear Thresholding

Reliable signal transfer of single photon responses of rods is served by postsynaptic filtering and gain modification in the rod bipolar cell dendrite. Twenty-to-thirty rods converge onto each rod bipolar cell and each rod contacts two rod bipolar cell dendrites (Gray and Pease,

1971;Rao-Mirotznik et al., 1995;Berntson et al., 2004b). The invaginating synapse allows for physical separation of dendrites, so it is assumed that only one rod communicates with each dendrite. If receptor potentials are summed linearly, then the noise from all of these rods also gets summed. This could obscure the small hyperpolarizing signal (1-3 mV) from a single photon lasting ~300 ms (Baylor et al., 1984;Taylor and Smith, 2004). Indeed, when measuring photovoltage triggered by a train of fixed-strength flashes, the amplitudes of light responses fall within the amplitudes of basal cellular noise; thus, true single photon responses cannot effectively be separated from failures.(Field and Rieke, 2002) One way to avoid transmitting noisy voltage changes that are unrelated to photon absorption is to threshold the signal at the bipolar cell dendrite, transmitting only large responses to the soma and excluding small responses that are more likely to be due to noise (Baylor et al., 1984;Berntson et al., 2004b;Sampath and Rieke, 2004).

The presence of such a thresholding non-linearity was shown by Field and Rieke who compared photocurrents of rods, which scale linearly with flash strength, to rod bipolar cells which responded in a supralinear fashion(Field and Rieke, 2002) (Field and Rieke, 2002). Furthermore, when presenting the bipolar cell with a slow train of fixed-intensity flashes, the fluctuations in responses were larger than would be expected if they varied linearly with rod responses (Field and Rieke, 2002). This non-linear increase in rod bipolar cell responses proportional to light intensity provides a means for thresholding the signal. The non-linearity appears to be intrinsic to the rod-RBC synapse as pharmacologically inhibiting amacrine cell input and voltage-activated conductances did not eliminate the relationship (Field and Rieke, 2002). Their data showed that rod bipolar cells ignore smaller single photon signals and only respond to larger signals, discarding 25% of the true single photon responses of presynaptic rods. Similar findings have been reported by other groups although the percentage of discarded responses varies from 50 to 90% (Berntson et al., 2004b;Schein and Ahmad, 2006;Trexler et al., 2011). By discounting small fluctuations in

membrane voltage, this non-linearity allows for transfer of multiphoton or large single photon responses while avoiding false positives that might arise from noise.

There are two hypotheses that consider how non-linearity and thresholding increase the reliability of detecting true responses. The first hypothesis is that signals are thresholded in each dendrite, filtering out false responses and noise before they are summed linearly at the soma. To model this, rod responses were passed through a non-linearity (cumulative Gaussian) before the resulting signals were summed. The model for threshold-like nonlinearity at the dendrite only worked if the midpoint of the cumulative gaussian was large, meaning that the bipolar cell rejected a substantial amount of true single photon responses.

The second hypothesis, which the data in Chapter 3 favor, is that the nonlinearity arises after pooling signals at the soma. This hypothesis is only feasible if the non-linearity has a particularly small standard deviation that allows for the discretization of signals that mirrors the measured responses.

What pre- and post-synaptic mechanisms might contribute to supralinear signal transfer at the rod-RBC synapse? Pre-synaptically, amphibian rods vary glutamate release rate non-linearly with membrane voltage (Schmitz and Witkovsky, 1997;Witkovsky et al., 1997). We also find that while rod release rate is linearly related to I_{Ca} (Thoreson et al., 2004), the current-voltage relationship reflects a nonlinearity thresholded by the VGCC activation potential. This relationship leads to large changes in release rate with relatively small voltage changes within a range of voltages and is further discussed in Chapter 3. Alternatively, post-synaptic non-linearity may arise from the saturation of one of several components of the mGluR6 signaling cascade (van Rossum and Smith, 1998). Saturation fixes TRPM1 cation channels closed in darkness and unperturbed by small fluctuations in rod release while reductions in release that pass a particular threshold cause supralinear changes in voltage (Sampath and Rieke, 2004). The remarkable sensitivity and efficiency of phototransduction of single photon absorption would be wasted if not for reliable

signal transfer from the rod to RBC, thus making these mechanisms absolutely vital to visual sensitivity. The pre-synaptic mechanisms of release that exist and may contribute to minute signal fidelity in darkness are explored in Chapter 3.

CHAPTER 2: Simultaneous Release of Multiple Vesicles from Rod Photoreceptors Involves Ribbons and Syntaxin 3B [1]

Abstract

First proposed as a specialized mode of release at sensory neurons possessing ribbon synapses, multivesicular release has since been described throughout the CNS. Many aspects of multivesicular release remain poorly understood. We explored mechanisms underlying simultaneous multivesicular release at ribbon synapses in salamander retinal rod photoreceptors. We assessed spontaneous release presynaptically by recording glutamate transporter anion currents ($I_{A(glu)}$) in rods. Spontaneous $I_{A(glu)}$ events were correlated in amplitude and kinetics with simultaneously measured miniature excitatory post-synaptic currents (mEPSCs) in horizontal cells. Both measures indicated that a significant fraction of events is multiquantal, with analysis of $I_{A(glu)}$ revealing that multivesicular release constitutes ~30% of spontaneous release events. $I_{A(glu)}$ charge transfer increased linearly with event amplitude showing that larger events involve greater glutamate release. The kinetics of large and small $I_{A(glu)}$ events were identical as were rise times of large and small mEPSCs, indicating that release of multiple vesicles during large events is highly synchronized. Effects of exogenous Ca^{2+} buffers suggested that multiquantal, but not uniquantal, release occurs preferentially near Ca^{2+} channels clustered beneath synaptic ribbons. Photo-inactivation of ribbons reduced the frequency of spontaneous multiquantal events without affecting uniquantal release frequency, showing that spontaneous multiquantal release requires functional ribbons. While both occur at ribbon-style active zones, the absence of cross-depletion indicates that evoked and spontaneous multiquantal release from ribbons involve different vesicle pools. Introducing an inhibitory peptide into rods to interfere with the SNARE protein, syntaxin 3B, selectively reduced multiquantal event frequency. These results support the hypothesis that

[1]The content of this Chapter has been published previously:
Hays CL, Grassmeyer JJ, Wen X, Janz R, Heidelberger R, Thoreson (2020). Simultaneous release of multiple vesicles from rods involves synaptic ribbons and syntaxin 3B. Biophys J **118**(4): 967-979. https://www.sciencedirect.com/science/article/pii/S0006349519308537

simultaneous multiquantal release from rods arises from homotypic fusion among neighboring vesicles on ribbons and involves syntaxin 3B.

Statement of Significance

It is now recognized that many neurons and non-neuronal secretory cells can release multiple vesicles in response to stimulation. Among other properties, multivesicular release can improve the ability to encode timing of events at neuronal synapses. Synaptic ribbons are protein structures in sensory neurons that tether vesicles near release sites and support multivesicular release. We studied mechanisms underlying spontaneous multiquantal release at large ribbon synapses of rod photoreceptor cells in salamander retina. Recording release events presynaptically in rods using glutamate transporter-associated anion currents, we found that multiquantal release involves homotypic fusion among vesicles on synaptic ribbons and believe it shows a novel role for the SNARE protein, syntaxin 3B in promoting multiquantal release separate from its role in exocytosis.

Introduction

Early studies suggested that an action potential triggered fusion of only a single vesicle at most synapses, but there is increasing recognition that many synapses can release multiple vesicles (Rudolph et al., 2015). Synaptic ribbons in sensory neurons—protein structures that tether numerous vesicles near release sites—are specialized to support multivesicular release (Li et al., 2009;Rudolph et al., 2015). Ribbon-bearing hair cells, retinal bipolar cells and photoreceptor cells respond to sensory stimulation with graded changes in membrane potential that regulate the rate of ongoing vesicle release. While also maintaining release almost indefinitely, ribbons synapses must be able to adjust release rapidly in response to changes in membrane potential. Release of a vesicle at synaptic ribbons in a number of different cell types, including rods, requires opening of only a few nearby Ca^{2+} channels (Brandt et al., 2005;Jarsky et al., 2010;Bartoletti et al., 2011;Van Hook

and Thoreson, 2015). Stimulating the opening of multiple Ca^{2+} channels with a rapid, strong depolarizing stimulus can thus trigger rapid fusion of multiple vesicles from the readily releasable pool docked at the base of a ribbon (Mennerick and Matthews, 1996;Brandt et al., 2005;Cadetti et al., 2005). However, even when Ca^{2+} channel openings are few and far between, one can observe spontaneous post-synaptic events that vary widely in amplitude. While the amplitude of vesicle release events may also be shaped by the kinetics of vesicle pore opening (Chapochnikov et al., 2014;Wen et al., 2017), this suggests that even individual spontaneous events may involve release of multiple vesicles (Singer et al., 2004;Cadetti et al., 2005;Grant et al., 2010;Cork et al., 2016). Multivesicular release may help ribbon synapses encode sensory information by regulating event amplitude as well as frequency (James et al., 2019).

A number of mechanisms have been proposed to account for multivesicular release. One is coincident fusion of individual vesicles located at different release sites along the base of the ribbon (Singer et al., 2004). One way this might occur is if Ca^{2+} ions entering Ca^{2+} channels beneath the ribbon spread far enough to trigger the fusion of multiple ribbon-associated vesicles (Graydon et al., 2011;Mehta et al., 2013). It has also been suggested that amplification of Ca^{2+} influx by Ca^{2+}-induced Ca^{2+} release from intracellular stores may promote multivesicular fusion in rods (Suryanarayanan and Slaughter, 2006). Another potential mechanism for multivesicular release is homotypic fusion, where neighboring vesicles fuse with one another either before or after fusion with the plasma membrane (Parsons and Sterling, 2003;Blank, 2011;Messenger et al., 2014;Datta et al., 2017;Vakilian et al., 2019). Homotypic fusion of exocytotic vesicles is prominent in parotid and pancreatic acinar cells (Messenger et al., 2014), immune cells (Alvarez de Toledo and Fernandez, 1990;Lollike et al., 2002;Blank, 2011;Eckly et al., 2016;Sanchez et al., 2018), and pancreatic beta cells (Zhu et al., 2013;Messenger et al., 2014;Vakilian et al., 2019). Vesicle-vesicle fusion has also been shown to increase quantal size at conventional neuronal synapses (He et al.,

2009) and may occur at ribbon synapses in the retina(Matthews and Sterling, 2008;Vaithianathan et al., 2016;Datta et al., 2017).

Homotypic fusion among secretory vesicles depends on several SNARE and SNARE-associated proteins including munc18-2 (Lam et al., 2013;Gutierrez et al., 2018), munc13-4 (Woo et al., 2017;Rodarte et al., 2018), SNAP23 (Klein et al., 2017), and VAMP8 (Behrendorff et al., 2011;Thorn and Gaisano, 2012). In many secretory cells, vesicle-vesicle fusion involves syntaxin 3 (Hansen et al., 1999;Zhu et al., 2013;Sanchez et al., 2018). Similarly, retinal ribbon synapses of bipolar and photoreceptor cells use syntaxin 3B rather than the syntaxin 1 isoform used by most neurons (Curtis et al., 2008;Curtis et al., 2010). While syntaxin is principally expressed on target membranes, it can also be found on vesicular membranes (Walch-Solimena et al., 1995b;Borisovska, 2018;Yin et al., 2018), including those of ribbon synapses (Liu et al., 2014). The close proximity of vesicles tethered next to one another on a synaptic ribbon (Thoreson et al., 2004) could potentially facilitate vesicle-vesicle fusion. It has therefore been hypothesized that syntaxin 3B might promote formation of intervesicular SNARE complexes and homotypic fusion among neighboring vesicles on a ribbon (Datta et al., 2017).

We studied the frequency and mechanisms of simultaneous multiquantal release at ribbon synapses in rod photoreceptor cells of salamander retina. We measured release presynaptically by recording glutamate transporter anion currents ($I_{A(glu)}$) from rods. Excitatory amino acid transporters (EAATs) can be found in neurons and glial cells where they retrieve glutamate for terminating synaptic transmission and re-use (Arriza et al., 1997;Eliasof et al., 1998a;Eliasof et al., 1998b). EAATs are electrogenic antiporters, exchanging glutamate, 3 Na^+, and 1 H^+ for 1 K^+ molecule, however most of the EAAT current measured by whole cell voltage clamp is due to an uncoupled anion conductance (Eliasof et al., 1998b). Although not directly coupled to glutamate transport, the EAAT anion current is linearly proportional to the number of glutamate ions released (Otis and Jahr, 1998;Koch et al., 2007). The principal glutamate transporters in salamander rods

are sEAAT2 and 5A; the latter exhibits a particularly large anion conductance (Eliasof et al., 1998a;Eliasof et al., 1998b). Measuring release presynaptically eliminates synapse-to-synapse variation in the number of glutamate receptors or differences in electrotonic distance among synapses that can contribute to quantal variability in post-synaptic measurement (Pulido and Marty, 2017).

Our results show that ~30% of spontaneous release events in rods involve the simultaneous fusion of multiple vesicles. We found that simultaneous multiquantal fusion involves vesicles situated close to Ca^{2+} channels, is impaired by damage to ribbons, and is selectively reduced by interfering with syntaxin 3B. These results support the hypothesis that simultaneous multiquantal release at rod photoreceptor synapses is largely due to homotypic fusion of vesicles promoted by syntaxin 3B at synaptic ribbons.

Methods

Retinal Slices

Vertical slices were prepared from the retinae of aquatic tiger salamanders (*Ambystoma tigrinum*) as previously described (Van Hook and Thoreson, 2013). Animal husbandry and experimental procedures were approved by the University of Nebraska Medical Center's Institutional Animal Care and Use Committee. Salamanders of both sexes were housed in a water tank (4 deg C) on a 12:12 hour light-dark cycle. Experiments were typically conducted 1-3 h after the beginning of subjective night. Following brief submersion in 0.25 g/L MS222, salamanders were sacrificed by decapitation. After enucleating the eye, the cornea and iris were removed and the resultant eyecup cut into two or three pieces. One piece was then placed vitreal side down onto a nitrocellulose membrane. Under cold amphibian Ringer's solution, the retina was carefully isolated by removing the sclera, choroid and pigment epithelium. A razor blade tissue slicer (Stoelting Co., Wood Dale, IL) was used to cut the retina into 125 μm slices. The thin slices of

filter paper with attached retina were rotated 90° and anchored in the recording chamber by two strips of vacuum grease. Dissections were performed under cold amphibian Ringer's solution and room light. Retinal slices were visualized on an upright, fixed-stage microscope (Nikon E600FN, 60x 1.0 NA LWD objective) and continuously superfused (1 ml/min) with an oxygenated amphibian saline solution containing (in mM): 116 NaCl, 2.5 KCl, 1.8 $CaCl_2$, 0.5 $MgCl_2$, 5 Glucose, 10 HEPES (pH 7.8; room temperature).

Electrophysiology

Whole cell recordings were obtained from rods and horizontal cells in retinal slices. Patch-pipettes were crafted on a Narishige (Amityville, NY) PP-830 vertical puller from borosilicate glass (1.2 mm outer diameter, 0.9 mm inner diameter with internal filament; World Precision Instruments, Sarasota, FL). Each had tip diameters of 1-2 µm and resistances of 5-15 MΩ. Recordings of $I_{A(glu)}$ from rod photoreceptors were obtained with a pipette solution using SCN^- as the principal anion to enhance $I_{A(glu)}$ (in mM): 90 KSCN, 10 TEA-Cl, 3.5 NaCl, 1 $MgCl_2$, 10 HEPES, 10 ATP-Mg, 0.5 GTP-Na. Except for Ca^{2+} chelator experiments where we used 0.05 mM EGTA or 10 mM BAPTA, the solution also contained 5 mM EGTA. We did not correct for the liquid junction potential (LJP) calculated with PClamp (Axon Instruments) to be −4.5 mV. Recordings from horizontal cells used a pipette solution containing (in mM): 90 CsGluconate, 10 TEA-Cl, 3.5 NaCl, 1 $MgCl_2$, 10 HEPES, 5 EGTA, 10 ATP-Mg, 0.5 GTP-Na (18). The LJP for this solution was −12.2 mV. Rod recordings showed an average capacitance of 34.5 ± 3.0 pF, membrane resistance of 221.6 ± 24.8 MΩ, and series resistance of 26.5 ± 3.7 MΩ (n =16).

For fluorophore-assisted laser inactivation (FALI) experiments described below, we included 80 µM fluorescein isothiocyanate (FITC)-conjugated RIBEYE-binding peptide or a scrambled version of the same peptide in the KSCN pipette solution along with 3 mM reduced glutathione and 3 mM trolox as antioxidants (Zenisek et al., 2004). RIBEYE (or CtBP1) is a transcript variant of CtBP2 containing a ribbon-specific A domain and a B domain shared with

CtBP2 (Schmitz et al., 2000). The FITC-conjugated peptide (FITC-Ahx-EQTVPLDLSKRDR) binds to a PXDLS sequence in CtBP2 (Zenisek et al., 2004). As a control, we used a scrambled version of the same peptide (FITC-Ahx-RTSPDKLVLDERQ).

To test a role for syntaxin 3B, we introduced 250 μM syntaxin 3B inhibitory peptide (stx3pep; RHKDIMRLESSIKELHDMFVDVA) or a scrambled version of the same peptide (RIALKDDVIHMRESVDHKSFMEL) into the pipette solution along with 1 mM reduced glutathione and 1 mM trolox (Curtis et al., 2010).

Quantal Analysis

Spontaneous rod $I_{A(glu)}$ events were recorded while holding rods at −70 mV. Trials were typically 180 s in duration. Individual $I_{A(glu)}$ events in rods and miniature excitatory post-synaptic currents (mEPSCs) in horizontal cells were identified using the "event detection" function in Clampfit 10.4 with a template created from an average of 5-15 events from the same cell. During simultaneous recordings, rod $I_{A(glu)}$ and horizontal cell mEPSCs were considered to be coordinated if onset of an $I_{A(glu)}$ event occurred within 10 ms of the beginning of an mEPSC. Amplitude histograms were constructed and fit with a multiple Gaussian function. Events within one standard deviation of the mean of the first peak were considered "uniquantal" and remaining larger events were considered "multiquantal." Quantal content was calculated from weighted averages of the area under the curves from a multiple Gaussian fit (GraphPad Prism 4).

Fluorophore-Assisted Laser Inactivation

For FALI experiments, we introduced 80 μM FITC-conjugated RIBEYE-binding peptide or a scrambled version of the same peptide through the patch pipette into a rod. Immediately after rupture, we applied a 2-ms voltage step from −70 to −10 mV to evoke ribbon-mediated release, then recorded spontaneous events for 90 s while holding the rod at −70 mV. We followed this with a second 2-ms step and another 90-s measurement of spontaneous events. A 488 nm laser from the spinning disk confocal was then turned on for 60 s to bleach the FITC-conjugated peptide. After

bleaching, we applied a 2-ms step followed by 90 s of recording spontaneous events, and then a final 2-ms step. We analyzed trials with the RIBEYE-binding peptide in which discrete bright puncta were observed showing that the FITC-conjugated peptide had successfully bound to ribbons.

Results

Spontaneous Release Events in Rods

We studied vesicle fusion events in rods by recording presynaptic anion currents activated during glutamate uptake by EAATs in rod terminals. $I_{A(glu)}$ was enhanced by using the permeant SCN^- as the principal anion in the rod pipette solution. Although Cl^- ions are not directly involved in the process of glutamate transport, the amplitude of $I_{A(glu)}$ is linearly related to the number of glutamate molecules that are retrieved (Otis and Jahr, 1998;Koch et al., 2007). As illustrated in Fig. 11A, we observed occasional large spontaneous $I_{A(glu)}$ events interspersed among more numerous smaller events in recordings from rods held under voltage-clamp control at −70 mV. Spontaneous $I_{A(glu)}$ events could be blocked with a glutamate transport inhibitor, TBOA (Cork et al., 2016). Because light hyperpolarizes rods, voltage-clamping them at −70 mV is functionally equivalent to strong light adaptation. Baseline noise during recordings of $I_{A(glu)}$ from rods voltage-clamped at −70 mV could be further reduced by applying a bright background light to hyperpolarize neighboring rods and cones (data not shown). This suggests that glutamate released from photoreceptors in darkness can reach glutamate transporters of neighboring rods. To minimize the possible impact of release from neighbors, recordings were performed in strongly light-adapted preparations. The amplitude distributions of mEPSCs in horizontal cells did not differ significantly whether measured under scotopic or photopic conditions (Cadetti et al., 2005), suggesting that the relative frequency of multiquantal events is not significantly altered by light adaptation. Under these experimental conditions, the amplitude of spontaneous $I_{A(glu)}$ events in rods voltage-clamped at −70 mV averaged 15.5 ± 1.61pA (n = 16 rods, n = 49 to 1134 events/cell) with an average rise time of 13.8 ± 1.37 ms, half width of 9.65 ± 1.63 ms and decay time of 23.2 ± 2.18 ms.

Fig. 11B shows a representative amplitude histogram of spontaneous $I_{A(glu)}$ events. The inset shows a small section of the record from this cell illustrating both small and large events. Similar to amplitude histograms of mEPSCs (Cadetti et al., 2005;Pang et al., 2008b;Feigenspan and Babai, 2015), amplitude histograms of $I_{A(glu)}$ were skewed to the right (Fig. 11B). Similar to monophasic excitatory post-synaptic currents (EPSCs) at other synapses (Rossi et al., 1994;Chapochnikov et al., 2014), event amplitude and charge transfer of $I_{A(glu)}$ events increased linearly with one another indicating that larger amplitude events involve greater glutamate release (Fig. 11C).

Binomial statistics predict that the distribution of event amplitudes should be fit by a sum of Gaussian functions with peaks that are integer multiples of one another (Fig. 11B). The individual quantal amplitude obtained by fitting amplitude histograms with multiple Gaussians averaged 10.7 ± 2.02 pA compared to an overall mean amplitude of 15.5 ± 1.61 pA in the same cells. A multiple Gaussian function fit the amplitude frequency distributions better than a single Gaussian ($p < 0.001$ for 7/8 cells; $p = 0.051$ for 1 cell). Quantal content was calculated from a weighted average of areas under the curves for each peak in the multiple Gaussian. From these multiple Gaussians, quantal content was estimated to be 1.53 ± 0.11 ($n = 10$) from rod $I_{A(glu)}$. We found a similar quantal content of 1.42 ± 0.09 ($n = 8$) from the amplitude of horizontal cell mEPSCs. We defined events within one standard deviation of the mean of the first peak to be "uniquantal" and considered larger events to be "multiquantal." Multiquantal release events accounted for 34.1 ± 4% of all $I_{A(glu)}$ events ($n = 7$) and, because some events are quite large, made up an even larger fraction of the total spontaneous glutamate release from rods (42.7 ± 8%; $n = 7$).

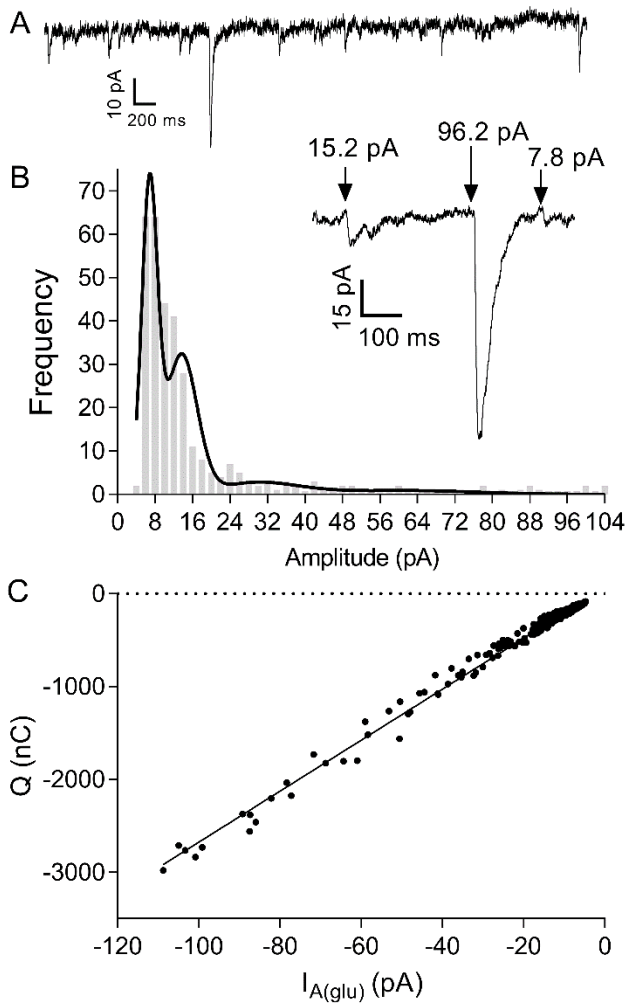

Figure 11 Amplitude characteristics of spontaneous $I_{A(glu)}$ events are consistent with multiquantal release. **A.** Spontaneous multiquantal events were observed amongst many uniquantal events in rods voltage clamped at −70 mV. **B.** Representative amplitude histogram of spontaneous rod $I_{A(glu)}$ events (n = 325) fit with a multiple Gaussian function. The inset shows a representative segment of the recording from which the histogram was derived. By assuming that the mean ± SD of the initial peak represents a single quantum, quantal content for this cell was calculated as a weighted average of the areas under the curve and found to be 1.69. **C.** Amplitude of $I_{A(glu)}$ events (n = 339) was strongly correlated with event charge transfer (R = 0.99) with non-zero slope (F-test, $p < 0.0001$).

We compared pre- and post-synaptic measurements of glutamate release at the same synapses by obtaining simultaneous whole cell recordings from rods and a postsynaptic horizontal cell. Both the rod and its post-synaptic partner horizontal cell were voltage clamped at hyperpolarized potentials: −70 (-75 mV after correcting for LJP) and −60 mV (-72 mV after LJP correction), respectively. We confirmed that these neurons were synaptically connected by

determining whether an EPSC could be evoked in the horizontal cell by a strong depolarizing step applied to the rod. We then recorded a long series of spontaneous $I_{A(glu)}$ events in the rod and mEPSCs in the horizontal cell (Fig. 12A). Spontaneous mEPSCs in horizontal cells were faster than $I_{A(glu)}$ events in rods (Fig. 12B). mEPSCs averaged 10.39 ± 0.79 pA (n = 8 cells, n = 451 to 1715 events/cell) in amplitude with an average rise time of 1.44 ± 0.21 ms, half width of 3.52 ± 0.71 ms and decay time of 4.30 ± 0.39 ms.

Occasionally, a pre-synaptic $I_{A(glu)}$ event occurred at the same time as an mEPSC in the horizontal cell. Most pre- and post-synaptic events were not correlated because: 1) Many mEPSCs in the horizontal cell arise from release by photoreceptors other than the voltage-clamped rod and 2) only a few of the roughly 7 ribbons per rod contact any individual horizontal cell (Townes-Anderson et al., 1985b;Van Hook and Thoreson, 2015). Despite the low frequency of correlated events, the cross-correlation between long segments of baseline currents recorded from synaptically-coupled rods and horizontal cells (R^2 = 0.32 ± 0.076, n = 8 pairs) was significantly greater than the cross-correlation observed after time-shifting the horizontal cell current record by 100 ms (R^2 = 0.08 $\underline{+}$ 0.017; p = 0.025, paired t-test).

We examined individual rod $I_{A(glu)}$ and horizontal cell mEPSCs in which the peak of the $I_{A(glu)}$ event occurred 10 ms or less after onset of an mEPSC. Among such coincident events, the amplitude of $I_{A(glu)}$ events and mEPSCs were linearly correlated (R^2 = 0.36, Table 1) and showed a significant non-zero slope in 6/8 pairs ($P < 0.05$, Table 1; Fig. 12C). Because of the high frequency of spontaneous mEPSCs, a few coincident events can occur by chance. However, the correlation of amplitudes between coincident pre- and post-synaptic events was abolished by time shifting the records (R^2 = 0.02) and 0/8 pairs showed slopes that were significantly non-zero.

Table 1 Descriptions of coincident pre- and post-synaptic events including the number of coincident events (*n*) from paired rod and horizontal cell recordings. Regression statistics are reported from amplitudes of coincident events plotted against one another. Events were considered coincident if the start of the rod event occurred within 10 ms of the peak of horizontal cell (HC) mEPSC. Six out of 8 pairs show a slope that deviated significantly from zero (F-test). Rod and HC quantal amplitudes (QA) are reported, along with a coefficient of variance (CV).

Pair	*n*	Slope	R^2	P (F-test)	Rod QA (pA)	Rod CV	HC QA (pA)	HC CV
1	39	0.47 ± 0.08	0.49	< 0.0001	5.5	0.09	8.6 ± 1.7	0.20
2	43	1.40 ± 0.35	0.28	0.0003	5.7	0.11	9.5 ± 2.1	0.22
3	34	2.10 ± 0.60	0.28	0.0014	6.9	0.12	7.6 ± 1.3	0.17
4	24	2.12 ± 0.90	0.19	0.03	7.8	0.09	15.2 ± 0.6	0.04
5	34	0.14 ± 0.16	0.02	0.39	6.3	0.10	3.6 ± 0.3	0.08
6	12	0.47 ± 0.21	0.33	0.05	7.8	0.04	15.7 ± 1.3	0.08
7	35	0.62 ± 0.13	0.4	< 0.0001	10.8	0.08	15.3 ± 0.5	0.03
8	11	0.66 ± 0.07	0.9	<0.0001	12.4	0.14	16.5 ± 0.9	0.05
mean	29	1.00	0.36	0.09	7.9	0.09	11.5	0.1
σ	12	0.77	0.26	0.17	2.5			

Glutamate molecules bind rapidly to EAAT glutamate transporters and this binding activates $I_{A(glu)}$. The cycle time for glutamate transporter is rather slow, ca. 70 ms (Wadiche et al., 1995), so the increase in $I_{A(glu)}$ during a pulse of glutamate effectively integrates presynaptic glutamate release (Szmajda and Devries, 2011). Differentiating the glutamate transporter current should therefore provide a measure of the rise in synaptic glutamate levels. Consistent with this, differentiating the glutamate transporter currents from individual large $I_{A(glu)}$ events yielded waveforms with kinetics that closely matched the kinetics of simultaneously recorded mEPSCs that reflect glutamate binding to AMPA receptors on horizontal cells (Fig. 12B). In these recordings, the latency to the peak of mEPSCs was attained at 3.13 $\pm$ 0.19 ms and the peak of the differentiated $I_{A(glu)}$ occurred 2.0 $\pm$ 0.38 ms later (n = 8 events). Assuming a diffusion coefficient for glutamate of 0.33 μm/s (Nielsen et al., 2004), a total latency of 5.1 ms places an upper limit to the average distance between release sites and glutamate transporters of 3.37 μm. The correlated amplitude

and kinetic properties of coincident pre- and post-synaptic events in paired recordings indicates that $I_{A(glu)}$ provides a dependable presynaptic measure of glutamate release.

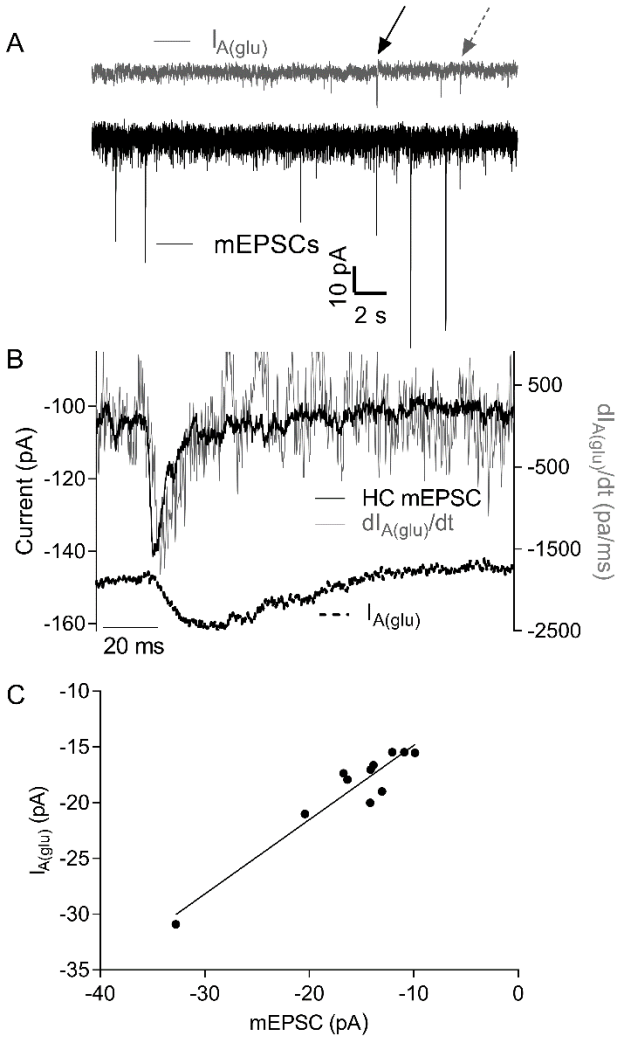

Figure 12 Simultaneous recordings of spontaneous $I_{A(glu)}$ events in a rod and miniature excitatory post-synaptic currents (mEPSCs) in a horizontal cell. **A.** During this record, two spontaneous pre-synaptic $I_{A(glu)}$ multiquantal events in rods (upper gray trace) occurred simultaneously (arrows) with post-synaptic mEPSCs (lower black trace). **B.** Coincident mEPSC (upper black trace) and presynaptic $I_{A(glu)}$ (lower black trace) events (panel A, dashed gray arrow). The noise gray trace shows the first derivative of $I_{A(glu)}$. The close match between the derivative of $I_{A(glu)}$ and mEPSC time course indicates that the increase in $I_{A(glu)}$ integrates glutamate release from the rod. **C.** The amplitudes of coincident pre- and post-synaptic events were linearly correlated ($n = 11$, $R^2 = 0.9$) with a slope that was significantly non-zero (F-test, $p < 0.001$), demonstrating that $I_{A(glu)}$ provides a pre-synaptic measure of glutamate release.

The kinetics of large, multiquantal $I_{A(glu)}$ events matched those of small events. Fig. 13A shows the average of small (n = 97) and large (n =20) $I_{A(glu)}$ events from a single rod (selected by a template with defined amplitude parameters). After scaling the average small uniquantal event to match the large multiquantal average, the time courses of the two closely matched one another (red trace, Fig. 13A). The 10-90% rise time did not differ significantly between uniquantal and multiquantal events ($p = 0.72$; Mann-Whitney test) and the rise time was not correlated with event amplitude (Fig. 3B). The variance among 10-90% rise times was greater for small events because baseline noise more often hindered accurate detection of start and stop times with smaller events. These data suggest that large and small events result from kinetically similar mechanisms.

We also compared the kinetics of large and small mEPSCs. Fig. 13C shows an example of average large and small mEPSCs from the same horizontal cell. After scaling the small event to match the amplitude of the large event (red trace, Fig. 3C), the rise times of the two waveforms closely matched one another. Uniquantal and multiquantal EPSC 10-90% rise times were 1.42 ± 0.01 vs 1.43 ± 0.03 ms, respectively and did not differ significantly ($p = 0.25$, n = 9 cells). In this example, the average large event decayed more slowly than the average uniquantal event, consistent with a greater persistence of glutamate in the cleft following release of multiple vesicles. However, because of variability among half-width measurements, the overall difference in half-widths between uniquantal and multiquantal mEPSCs was not statistically significant across the entire sample ($p = 0.18$, n = 9 cells). The similar rise times for large and small events suggests that large events arise from the closely synchronized release of multiple vesicles.

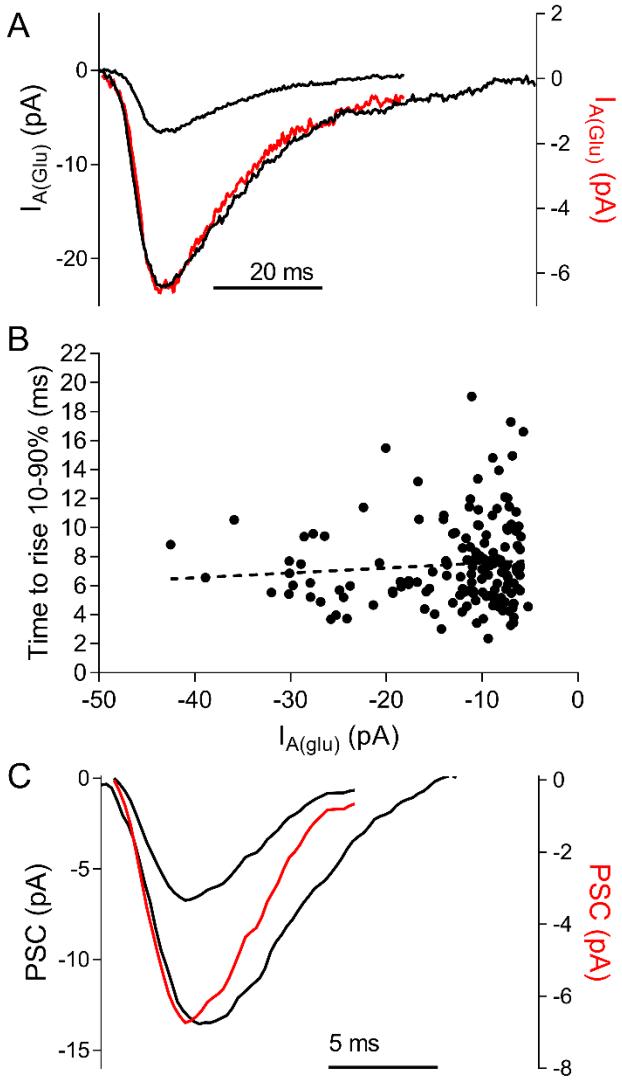

Figure 13 Large and small spontaneous release events show similar kinetics. **A**. Average uniquantal (small black trace; n = 97) and multiquantal $I_{A(glu)}$ events (large black trace; n = 20) from a single rod. There were no kinetic differences between the two after scaling the average uniquantal event (red trace, right axis) to match the amplitude of the average multiquantal event. B**.** Graph of individual $I_{A(glu)}$ event amplitudes plotted against 10-90% time to rise. The slope of the linear regression (dotted line) did not differ significantly from zero (F-test; p = 0.28). **C.** Average uniquantal mEPSC (small black trace, n = 38) and multiquantal mEPSC (n = 16) from a single horizontal cell. Scaling the uniquantal event (red trace, right axis) to match the amplitude of the larger event revealed that rise times of the two events were equivalent.

Comparing Evoked and Spontaneous Release

We compared the amplitude of spontaneous $I_{A(glu)}$ events to $I_{A(glu)}$ evoked by 2 ms depolarizing pulses to −25 mV. For these experiments, we alternated recordings of spontaneous and evoked events, waiting at least 45 s between test pulses for replenishment of the releasable pool of vesicles. Evoked release ran down during our recordings and so for this analysis, we only included recordings in which evoked release persisted long enough for us to measure at least 10 trials. We constructed amplitude histograms for both spontaneous and evoked events. The example in Fig. 14 shows a recording in which the evoked amplitude appears quantized. When fit with multiple Gaussians, the average fundamental amplitude did not differ between evoked and spontaneous events ($p = 0.29$; $n = 4$, paired t-test), consistent with the hypothesis that the first peak in the amplitude histogram reflects release of a single vesicle and subsequent peaks reflect release of multiple vesicles (Fig. 14B).

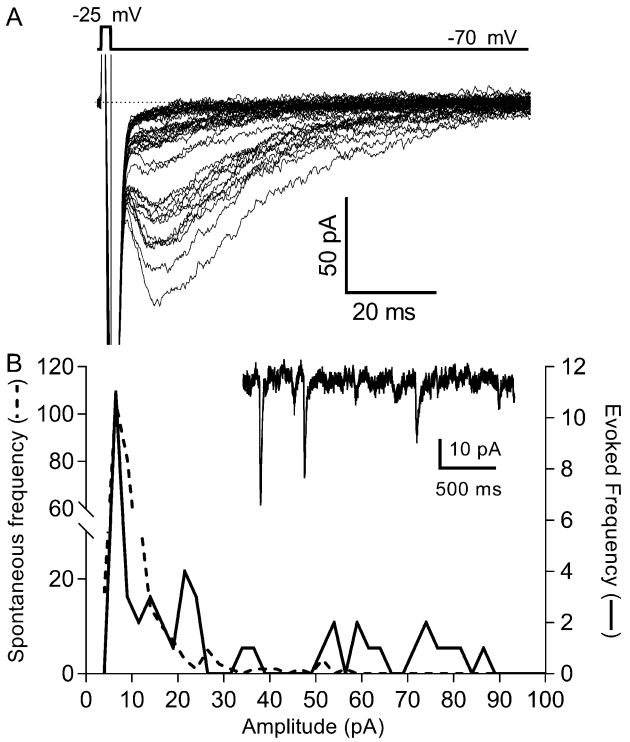

Figure 14 Comparisons of evoked and spontaneous $I_{A(glu)}$ events supports the interpretation that the first peak in the amplitude histogram of spontaneous release events reflects release of a single vesicle and subsequent peaks reflect release of multiple vesicles. **A.** A series of 41 overlaid $I_{A(glu)}$ responses evoked by 2-ms steps to −25 mV in a rod. Peak amplitudes of these evoked responses are plotted in the amplitude histogram in **B** (solid line). The amplitudes of spontaneous $I_{A(glu)}$ events from the same rod were also plotted in **B** (dashed

line), revealing a similar fundamental uniquantal amplitude (n = 289 events). The inset in B shows an example of spontaneous events from this same cell.

Spontaneous and evoked release appear to access different vesicle pools. In some trials, we tested release using a short, strong test pulse (2 ms, −70 to −10 mV) to maximally activate I_{Ca} but avoid stimulating Ca^{2+}-activated Cl^- currents. In these experiments, we alternated 3-min recordings of spontaneous activity with 2-ms test pulses to −10 mV. This depolarizing stimulus depletes a large fraction of the readily releasable pool of available vesicles. The readily releasable pool in rods averages 25 vesicles/ribbon, matching the number of vesicles that contact the plasma membrane at the base of a rod ribbon (Heidelberger et al., 2005), and there are an average of 7 ribbons per salamander rod (Townes-Anderson et al., 1985b;Pang et al., 2008b;Van Hook and Thoreson, 2015) suggesting a total readily releasable pool of ~175 vesicles/rod. Rod ribbons are typically separated from one another by 1 μm or more (Lasansky, 1978;Townes-Anderson et al., 1985b;Pang et al., 2008b), so it is unlikely that vesicles at neighboring ribbons would spontaneously fuse together. Although spontaneous events presumably arise from individual ribbons whereas evoked responses reflect release from all of the functional ribbons, spontaneous events often exceeded evoked responses in the same cell. In 12/18 rods, at least one spontaneous event exceeded the amplitude of the largest evoked response in that cell. An example of large spontaneous events recorded before and after a smaller evoked response are shown in Fig. 15A. The largest evoked response averaged 73.7 $\pm$ 12.3 pA (n = 18 rods) while the largest spontaneous event recorded in the same cells averaged 92.9 $\pm$ 13.2 pA. If the entire readily releasable pool of 25 vesicles/ribbon were available for release from all of the ribbons in a rod, then we should have seen much larger evoked responses. This suggests there was considerable rundown of the evoked response even before the first test pulse was applied (at least 3 min after patch rupture) but nevertheless rods remained capable of large spontaneous responses.

We saw no evidence for cross-depletion between spontaneous and evoked release. In Fig. 15B, we plot the ratio of the amplitude of spontaneous multiquantal events relative to the amplitude of the evoked response as a function of time before (open circles) or after (filled circles) a test pulse applied at time 0. For this analysis, we only included events in which both spontaneous and evoked events were at least 30 pA in amplitude. The amplitude of spontaneous events relative to evoked events did not vary in any systematic way with time of occurrence relative to the evoked response. Consistent with this, the slope of linear regressions fit to the data for spontaneous events occurring before or after the test pulse did not differ significantly from zero ($p = 0.58$ after test pulse; $p = 0.77$ before test pulse). These data suggest that the amplitude of a prior evoked response did not significantly influence the amplitude of a subsequent spontaneous event and vice versa (Fig. 5B).

For the analysis in Fig. 15B, we required that both evoked and spontaneous responses exceed 30 pA. However, as illustrated in Fig. 15C, we often saw cases in which the depolarizing test pulse failed to evoke any release whatsoever but a large spontaneous event was nevertheless observed in the same cell. By showing that spontaneous multiquantal release does not require that evoked release from ribbons remain intact, this illustrates an extreme case of the absence of cross-depletion. The rapid rundown of evoked release and absence of cross-depletion suggest that spontaneous multivesicular and evoked release involve different vesicle pools.

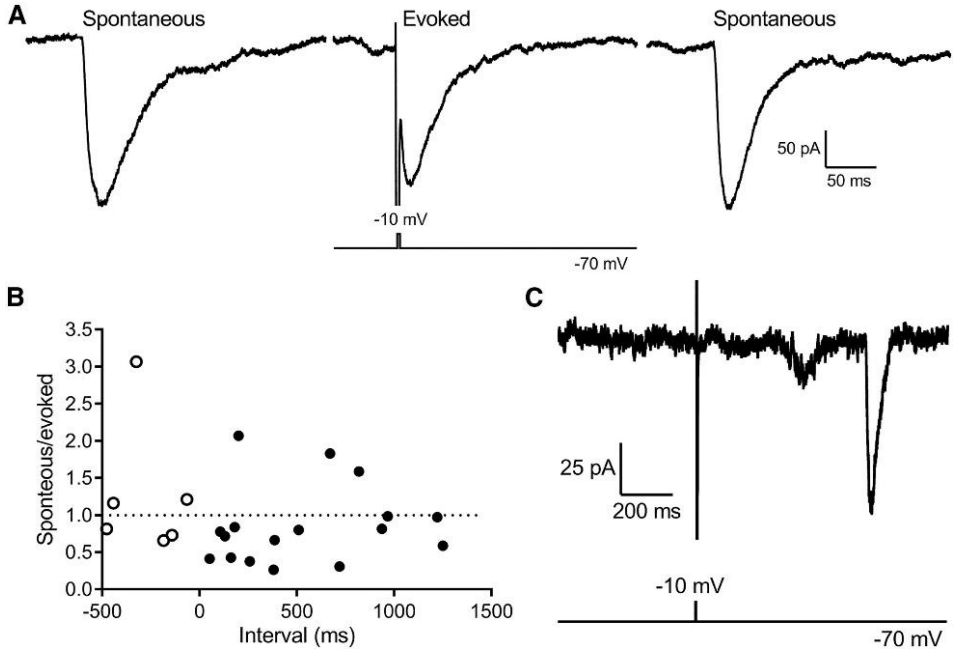

Figure 15 Large spontaneous events involve a different vesicle pool than evoked release. **A.** Examples of spontaneous events that occurred before and after a smaller event evoked by a depolarizing step to −10 mV (2 ms). **B.** Ratio of the amplitude of spontaneous multiquantal events relative to an evoked response in the same trial. These ratios are plotted as a function of the timing of the spontaneous event before (open circles) or after (filled circles) the test stimulus (2 ms, −10 mV) applied at time 0. Spontaneous and multiquantal events were included in this analysis only if both exceeded 30 pA. Data were from 1 s (n = 5) and 2 s (n = 18) trials. **C**. Example of a large spontaneous multiquantal event that occurred 650 ms after a depolarizing pulse (2 ms to −10 mV) failed to evoke release.

Multiquantal Release Involves Release Sites Close to Ca^{2+} Channels

To determine the dependence of multiquantal $I_{A(glu)}$ events on intracellular Ca^{2+}, we varied the Ca^{2+} buffering capacity of the intracellular solution introduced into rods through the whole cell recording pipette. To localize Ca^{2+} signaling events relative to the source of Ca^{2+}, we exploited differences in the kinetics with which EGTA and BAPTA chelate Ca^{2+}. While both chelators have the same affinity, the slower buffer EGTA will have less of an effect on Ca^{2+} levels near the source than the faster buffer BAPTA. The graph in Fig. 16A plots Ca^{2+} levels as a function of distance from an open Ca^{2+} channel as predicted by an Excel-based macro, "Pore" (Ward and Kenyon, 2000). The graph predicts that Ca^{2+} levels will decline to 100 nM within 100 nm of an open Ca^{2+} channel when the patch pipette solution is buffered with 10 mM BAPTA. With 5 mM EGTA, Ca^{2+}

levels are predicted to stay above 1 μM for 390 nm from a channel. Lowering Ca^{2+} buffering to 0.05 mM, which approximates endogenous buffering in salamander rods (Van Hook and Thoreson, 2015), allows Ca^{2+} to remain above 1 μM for almost 780 nm from an open channel.

The frequency of uniquantal events was reduced by limiting the spread of Ca^{2+} with 5 mM EGTA compared to 0.05 mM EGTA and further reduced by using 10 mM BAPTA as the chelator (Fig. 16B, $p < 0.0001$; 1-way ANOVA/ Tukey's multiple comparisons). This suggests that some uniquantal events occur well outside of Ca^{2+} nanodomains generated by Ca^{2+} sources, consistent with imaging results showing that many spontaneous release events in rods occur at non-ribbon release sites (Cork et al., 2016). By contrast, the frequency of multiquantal events did not differ between 5 and 0.05 mM EGTA and was only reduced by 10 mM BAPTA (Fig. 16C). This suggests that multiquantal release involves vesicles within a few hundred nanometers of Ca^{2+} channels that are just beneath ribbons (Nachman-Clewner et al., 1999;Morgans, 2001;tom Dieck et al., 2005a;Lv et al., 2012a).

A previous study suggested that activation of Ca^{2+}-induced Ca^{2+} release (CICR) in rods can increase coordinated vesicle release (Suryanarayanan and Slaughter, 2006). We tested contributions of CICR during spontaneous release by bath applying a ryanodine receptor inhibitor, dantrolene (10 μM), but did not see any significant change in the frequency of spontaneous multiquantal release when compared to vehicle control ($p = 0.98$; 2-way ANOVA).

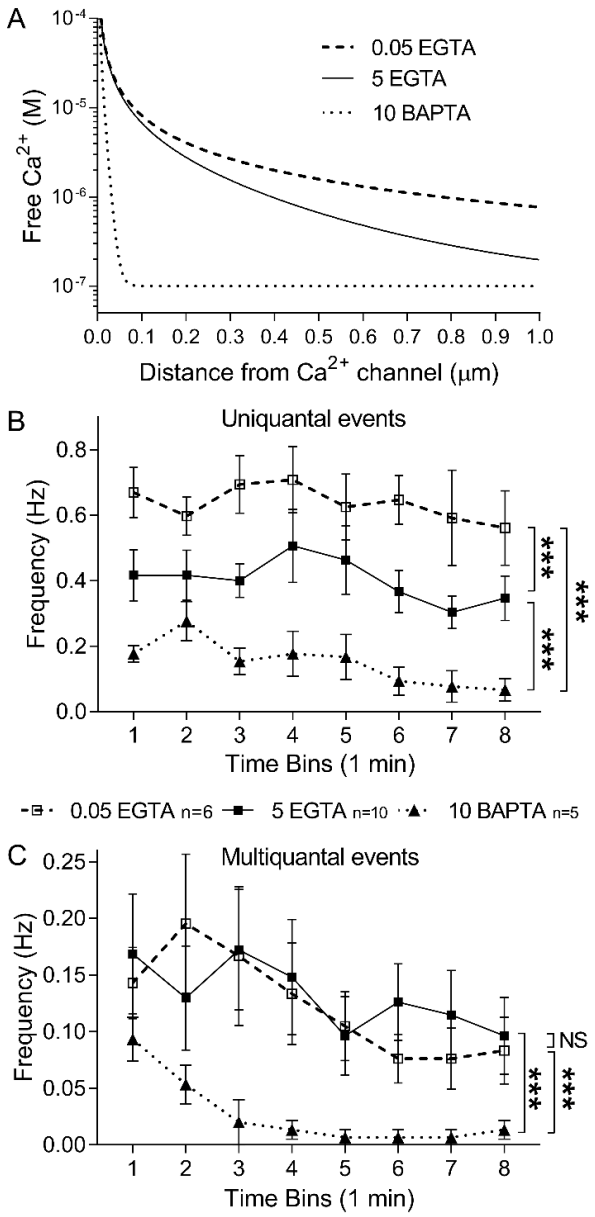

Figure 16 . Effects of Ca^{2+} chelators on spontaneous release indicate that multiquantal release involves vesicles situated close to intracellular Ca^{2+} sources. **A.** Graph of intracellular Ca^{2+} levels plotted as a function of distance from an open Ca^{2+} channel, predicted from an Excel-based macro "Pore" adapted from Ward and Kenyon, 2000. **B.** Frequencies of uniquantal events from rods plotted as a function of time after obtaining a whole cell recording from a rod with different Ca^{2+} buffers in the patch pipette solution. The frequency of uniquantal events was reduced significantly when buffering was raised from 0.05 (open squares, n = 7 rods) to 5 mM EGTA (filled squares, n = 10) and reduced further with 10 mM BAPTA (triangles, n = 5) as the chelator ($P < 0.0001$; 1-way ANOVA/ Tukey's multiple comparisons). **C.** Multiquantal event frequency did not differ between 0.05 and 5 mM EGTA but was reduced significantly by 10 mM BAPTA ($P < 0.0001$; 1-way ANOVA/ Tukey's multiple comparisons).

Multiquantal Events Originate on the Ribbon

The Ca^{2+} chelator results suggest that multiquantal release involves release sites close to Ca^{2+} channels beneath synaptic ribbons. As a more direct test of whether multiquantal release involves ribbon release sites, we damaged the ribbon by fluorophore-assisted laser inactivation (FALI) with a FITC-conjugated RIBEYE-binding peptide. As a control, we used a FITC-conjugated scrambled version of the same peptide. We introduced the peptides through a patch pipette. As illustrated in Fig. 17A, the FITC-conjugated RIBEYE-binding peptide binds selectively to ribbons, yielding bright spots (arrow) in the synaptic terminal when imaged with a confocal microscope. The pipette solutions included the antioxidants trolox (3 mM) and reduced glutathione (3 mM) to limit non-specific oxidative damage. We waited 5 min to allow time for the peptide to enter the cell and then turned on a 488 nm laser for 60 s to bleach the dye. Bleaching of FITC by FALI releases singlet oxygen that causes damage localized to within 50 Å of the FITC moiety (Hoffman-Kim et al., 2007).

Fast synchronous, evoked release from rods is largely ribbon-dependent (Chen et al., 2013;Chen et al., 2014;Van Hook and Thoreson, 2015) and so a short depolarizing step should evoke release almost exclusively from ribbon-associated vesicles. Consistent with this, $I_{A(glu)}$ evoked by a 2-ms depolarizing step to –10 mV was nearly abolished after damaging the ribbon by FALI (filled squares and insets, Fig. 17B). When using the scrambled peptide, evoked release ran down over time but was not abolished acutely by the laser (open squares, Fig. 17B). Laser inactivation with FITC-conjugated RIBEYE-binding peptide also reduced the frequency of spontaneous multiquantal events (filled squares, Fig. 17C) compared to control (open squares, $p = 0.03$) but did not significantly affect the frequency of uniquantal events (Fig. 17D, $p = 0.97$). The few multiquantal events that remain after FALI may reflect incomplete damage to the ribbon as found earlier with this same peptide concentration (Snellman et al., 2011). These results extend

those seen with Ca^{2+} buffering by revealing that multiquantal release depends on the presence of functional synaptic ribbons.

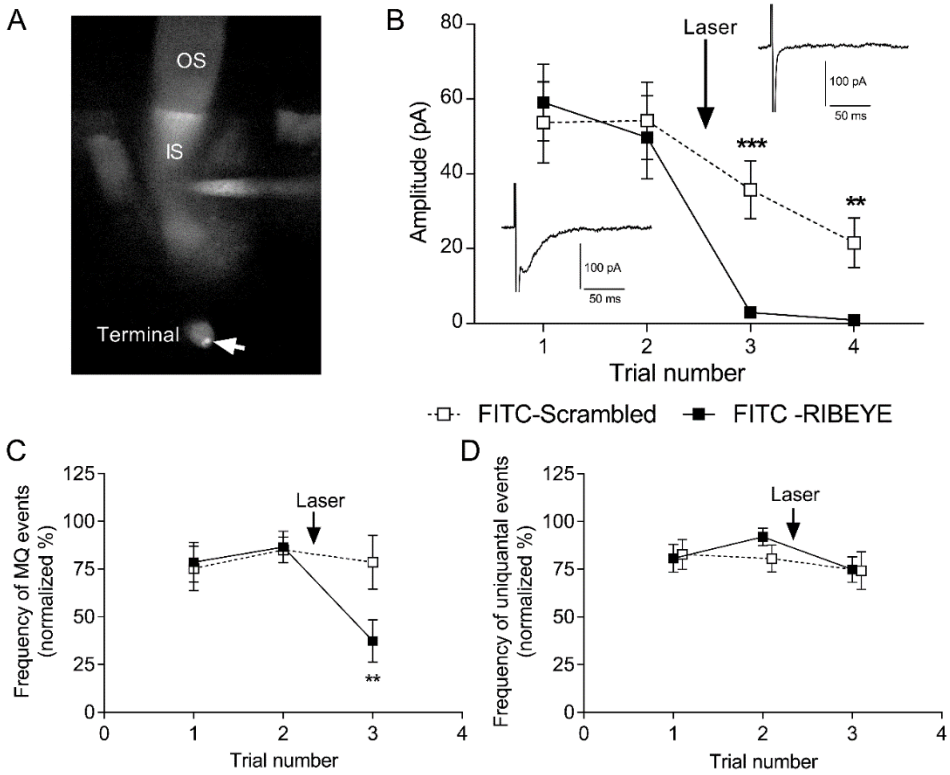

Figure 17 Fluorophore assisted laser inactivation (FALI) of ribbons with a FITC-conjugated RIBEYE-binding peptide indicates that multiquantal release occurs preferentially at ribbon release sites. A. Confocal z-stack image of a rod after introducing the peptide through a patch pipette. Weak fluorescence from cytoplasmic dye is visible in the outer (OS) and inner segment (IS). Two small bright spots in the terminal (arrow) show dye bound to ribbons prior to laser bleaching. B. Damaging ribbons by FALI reduced evoked $I_{A(glu)}$ events evoked by a brief depolarizing stimulus (2 ms, −25 mV). The insets show examples of responses evoked in a rod before and after 60 s bleach with 488 nm laser light. C. FALI with the RIBEYE-binding peptide significantly reduced the frequency of multiquantal events (n = 7 rods; p = 0.0127; 2-way ANOVA/Tukey's multiple comparisons), but FALI with a scrambled control peptide did not (n = 7, p = 0.91; 2-way ANOVA/Tukey's multiple comparisons). D. FALI did not reduce the frequency of uniquantal events with either the RIBEYE-binding (p = 0.3; 2-way ANOVA/Tukey's multiple comparisons) or scrambled control peptide (p = 0.84; 2-way ANOVA/Tukey's multiple comparisons).

Multiquantal Release Involves Syntaxin 3B

Studies at ribbon synapses and in non-neuronal secretory cells have both suggested a role for syntaxin 3 in supporting intervesicular SNARE complexes and vesicle-vesicle fusion (Zhu et al., 2013;Eckly et al., 2016). To test whether syntaxin 3B is involved in multiquantal release from

rods, we introduced a short peptide based upon the N-terminal region of the SNARE domain of syntaxin 3B (stx3pep) or a scrambled version of this peptide (control) into rods through a patch pipette. Stx3pep has been shown to inhibit the formation of SNARE complexes in retinal ribbon synapses (Datta et al., 2017). The frequency of all events, tallied in 3-min bins, ran down over time during recordings with both peptides, but the stx3pep inhibitory peptide caused a significantly greater reduction in the frequency of multiquantal events over time compared to the control peptide (Fig. 18, $p < 0.007$, 2-way ANOVA). By contrast, there was no change in the frequency of uniquantal events with stx3pep compared to the scrambled control peptide after 15 min (Fig. 18, $p = 0.94$, unpaired t-test). These results suggest that multiquantal events are SNARE-mediated and preferentially affected by acute perturbation of syntaxin 3B function.

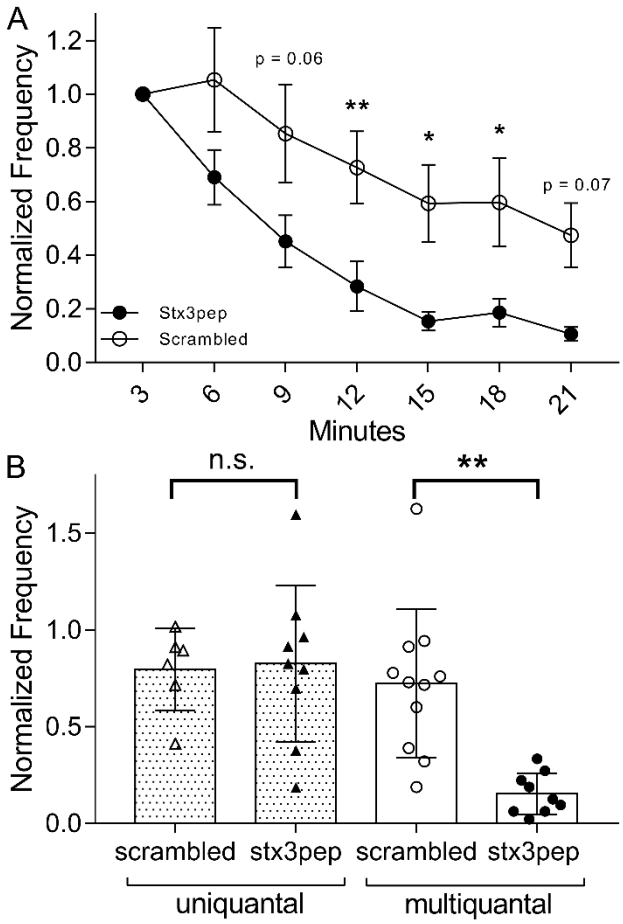

Figure 18 . Inhibiting the SNARE protein syntaxin 3B by introducing an inhibitory peptide (stx3pep) into a rod through the patch pipette selectively reduced multiquantal but not uniquantal release. **A.** Spontaneous multiquantal event frequency measured in 3-min bins after beginning whole cell recording was reduced by stx3pep (n = 12) compared to a scrambled control peptide (n = 9, p = 0.002; 2-way ANOVA). **B.** Comparison of uniquantal and multiquantal event frequency measured 15 min after patch rupture. The frequency of uniquantal events did not differ between stx3pep (filled triangles) and scrambled control peptide (open triangles), but the frequency of multiquantal events was reduced significantly by stx3pep (filled circles) relative to the scrambled control peptide (open circles, $P < 0.003$; 1-way ANOVA, Tukey's multiple comparisons).

Discussion

Our results show that multiquantal release occurs frequently in rods, constituting ~30% of spontaneous release events and 40% of the total spontaneous glutamate release. The identical rise times for large vs. small $I_{A(glu)}$ events in rods and for large vs. small horizontal cell mEPSCs suggests

that spontaneous multiquantal release involves synchronous, not sequential, fusion of vesicles. Experiments with exogenous Ca^{2+} buffers showed that synchronous multiquantal release occurs at sites within a few hundred nanometers of Ca^{2+} channels that are in turn close to ribbons in rod terminals. Selectively damaging ribbons by FALI and interfering with syntaxin 3B by use of an inhibitory peptide both reduced multiquantal but not uniquantal events. Together, these results are consistent with the hypothesis that simultaneous multiquantal release from rods arises from homotypic fusion among neighboring vesicles on a ribbon and involves the SNARE protein, syntaxin 3B (Datta et al., 2017). We consider this hypothesis further below.

In hair cells, there is evidence that the spread of Ca^{2+} entering the cell via Ca^{2+} channels beneath the ribbon can reach multiple vesicles and thereby facilitate simultaneous multivesicular release (Graydon et al., 2011). By contrast, measurements of release from rods found that a single Ca^{2+} channel opening triggers an average of only 0.17 ± 0.12 (S.D.) vesicle fusion events — far fewer than needed to account for the frequency of spontaneous multiquantal events observed in rods (Van Hook and Thoreson, 2015) . In rods, it has also been suggested that amplification of Ca^{2+} influx by Ca^{2+}-induced Ca^{2+} release might facilitate coordinated multivesicular release (Suryanarayanan and Slaughter, 2006). We did not observe a significant effect of the CICR blocker dantrolene on spontaneous multiquantal release, although CICR may play a bigger role in amplifying release during evoked release at more depolarized potentials (Suryanarayanan and Slaughter, 2006). Still, consistent with an earlier study on spontaneous release from rods (Cork et al., 2016), our results with BAPTA show that the frequency of multiquantal events depends strongly on available $[Ca^{2+}]_i$. This is similar to the finding at ribbon synapses of bullfrog hair cells that 10 mM BAPTA almost completely abolishes release events (Li et al., 2009). The most likely source for Ca^{2+} ions to support spontaneous release is the stochastic opening of L-type Ca^{2+} channels clustered beneath ribbons. Consistent with this, deletion of RIM1/2 or RIM-binding proteins from ribbon synapses caused a reduction in Ca^{2+} influx through L-type Ca^{2+} channels along with a

reduction in spontaneous release (Grabner et al., 2015;Luo and Sudhof, 2017). By contrast to the apparent Ca^{2+}-dependence of spontaneous release at ribbon synapses, spontaneous release at many conventional excitatory synapses depends less on Ca^{2+} entry from voltage-gated channels than does spontaneous release at inhibitory synapses (Scanziani et al., 1992;Llano and Gerschenfeld, 1993;Druzin et al., 2002;Tsintsadze et al., 2017;Liu et al., 2018;Williams and Smith, 2018). It is hypothesized that these differences in spontaneous release at conventional excitatory and inhibitory synapses arise from differences in the protein isoforms used by those synapses (Tsintsadze et al., 2017). Similarly, the greater dependence of spontaneous glutamate release on voltage-gated Ca^{2+} channels at ribbon synapses may reflect a reliance on particular protein isoforms. For example, as we consider below, the Ca^{2+}-dependence in multiquantal release might involve actions of Ca^{2+} or Ca^{2+}/calmodulin-dependent protein kinase II (CaMKII) on syntaxin 3B, a t-SNARE protein specific to retinal ribbon synapses, that occur prior to final fusion.

Could the heterogeneous amplitudes of $I_{A(glu)}$ be due to variable dilation of fusion pores rather than multiquantal release, as proposed for inner hair cells (Chapochnikov et al., 2014)? We found that large and small events showed matching kinetics, as found in bullfrog hair cells (Li et al., 2009), and rarely saw multiphasic events that are commonly seen in inner hair cells from rats. Multiphasic events at rat hair cell synapses are thought to reflect fusion pore flickering and thus show similar charge transfer for both large and small events (Chapochnikov et al., 2014). However, we found that event amplitude and charge transfer increased in parallel with one another indicating that larger events result from greater release of glutamate (Rossi et al., 1994;Chapochnikov et al., 2014). This suggests that the variability in amplitude of release events in rods is unlikely to arise from flickering openings of the fusion pore.

Our results show a role for both ribbons and syntaxin 3B in facilitating synchronous multiquantal release. Consistent with these results, genetic deletion of syntaxin 3 reduced multiquantal but not uniquantal release frequency in peritoneal mast cells (Sanchez et al., 2018).

One way in which syntaxin 3B might facilitate multivesicular release would be to promote homotypic fusion among vesicles. Consistent with the ability of vesicles to fuse with one another on the ribbon, repetitive stimulation led to an enlargement of ribbon-attached cisternae in retinal bipolar cells (Matthews and Sterling, 2008). While most syntaxin 3B is located on the plasma membrane, it can also be found on vesicular membranes at ribbon synapses, where it could potentially form SNARE complexes with v-SNAREs on neighboring vesicles (Liu et al., 2014). The proximity of neighboring vesicles on the ribbon and their situation near Ca^{2+} channels would facilitate vesicle-vesicle interactions (Datta et al., 2017).

We observed that spontaneous multiquantal release could occur in rods that are no longer capable of evoked release due to rundown. The ability for spontaneous release to occur in the absence of evoked release is consistent with evidence from rods and other neurons that spontaneous and evoked pools show functional and molecular differences (Sara et al., 2005;Crawford and Kavalali, 2015a;Cork et al., 2016). Although they involve different pools, FALI experiments showed that evoked and spontaneous multiquantal release both occur at ribbons. The differing capabilities for Ca^{2+}-dependent and -independent release may reflect differences in composition of the SNARE complexes among different ribbon-associated vesicles (Crawford and Kavalali, 2015a).

The rundown of evoked release is not due to rundown of I_{Ca}, which remains stable for long periods of recording from salamander rods (data not shown). Instead, the loss of evoked release is likely due to impairment of the Ca^{2+}-dependent fusion apparatus. This interpretation is in line with previous evidence indicating that the final fusion step for spontaneous multiquantal release in rods does not necessarily require Ca^{2+} (Cork et al., 2016) and thus, should be less affected, as observed. That spontaneous multivesicular release can occur without being triggered by stimulus-evoked Ca^{2+} entry also argues against the idea that the spontaneous release of multiple vesicles is coordinated by the spread of Ca^{2+} beneath the ribbon or by sequential Ca^{2+}-dependent fusion of vesicles further

up the ribbon. A more likely explanation for spontaneous multivesicular release is prior homotypic fusion among vesicles.

While the final fusion step during spontaneous multiquantal release can occur in a Ca^{2+}-independent manner, our results also showed a dependence of multiquantal release on Ca^{2+} levels near the ribbon. This may reflect actions of Ca^{2+} during the delivery and priming of vesicles on the ribbon. CaMKII is located on ribbons (Uthaiah and Hudspeth, 2010;Kantardzhieva et al., 2012) and activation of this enzyme facilitates the open configuration of syntaxin 3B, enhancing its interactions with SNAP-25 (Liu et al., 2014). Prior elevation of cytoplasmic [Ca^{2+}] and subsequent activation of CaMKII localized to ribbons could thus promote homotypic fusion of neighboring vesicles on the ribbon, explaining the preferential reduction of ribbon-mediated multiquantal fusion events by the inhibitory peptide, stx3pep.

The functional role of multiquantal release at this synapse is not entirely clear. While variability in the amplitude of spontaneous release events might be expected to impair detection of small light-evoked changes in release, the ability to coordinate fusion of multiple vesicles during evoked release could improve the coding for contrast changes, especially when photoreceptors depolarize in response to light decrements. Multiquantal release might provide a thresholding mechanism at the rod synapse for selectively transmitting large events. Such a mechanism can reduce the impact of noise, although in salamander retina this type of non-linearity is thought to be more prominent at bipolar cell synapses (Chichilnisky and Rieke, 2005). A recent study concluded that multivesicular release at bipolar cell ribbon synapses improves temporal precision for detecting contrast changes and showed that a single vesicle provides more information about the preceding stimulus change during multivesicular release than during univesicular release (James et al., 2019).

CHAPTER 3: Voltage dependent release properties in mammalian rods

Abstract

The vertebrate visual system can detect and transmit signals from single photons. To understand how single photon responses are signaled by rods, we characterized voltage-dependent properties of glutamate release in mouse rods by making presynaptic measurements of their glutamate transporter currents ($I_{A(glu)}$). Release rates increased in parallel with voltage-dependent increases in rod Ca^{2+} currents (I_{Ca}). Ca^{2+} influx and release rate rose further with temperature attaining a rate of ~10 vesicles/s/ribbon at −40 mV (35 °C). Ca^{2+} buffering experiments showed that release evoked by brief depolarizing steps to −10 mV occurred at release sites within ribbon-associated Ca^{2+} channel nanodomains. Longer depolarizing steps (e.g., 500 ms) engaged release from more distant non-ribbon sites. Spontaneous release at hyperpolarized potentials (−60 to −70 mV) occurred at random intervals, but when rods were voltage-clamped at −40 mV for many seconds to simulate maintained darkness, release occurred in semiregular, coordinated bursts of 17 ± 7 quanta (n = 22). Like fast release evoked by short steps, these bursts involved vesicles in the readily releasable pool at the base of the ribbon and were triggered by opening of nearby Ca^{2+} channels. Lowering more distant Ca^{2+} levels lengthened interevent intervals between bursts, perhaps by influencing vesicle replenishment. Ribbon-associated fast release and bursts were both absent after genetic elimination of the Ca^{2+} sensor, synaptotagmin-1 (Syt1), from rods whereas slower release evoked by 500 ms steps was abolished by eliminating a different sensor, synaptotagmin-7 (Syt7). This study shows that, in darkness, rods release glutamate-filled vesicles at low rates that involve coordinated bursts of vesicles from the readily releasable pool at the base of synaptic ribbons. In Chapter 4, we discuss functional implications of these release properties for encoding single photon responses at the rod synapse.

Introduction

The exquisite visual sensitivity of vertebrates begins with the ability of rod photoreceptor cells in the retina to detect single photons. Absorption of a single photon produces small voltage changes of 1-3.4 mV in rods that must be transmitted across the synapse to second-order bipolar cells (Schneeweis and Schnapf, 1995;Cangiano et al., 2012). In darkness, rods have a resting membrane potential near −40 mV that is sufficiently depolarized to activate $Ca_V1.4$ L-type Ca^{2+} channels that control synaptic glutamate release from rods (Pangrsic et al., 2018). Unlike most voltage-gated Ca^{2+} channels, $Ca_V1.4$ channels show minimal voltage- and Ca^{2+}-dependent inactivation, allowing continued Ca^{2+} influx into rod terminals during maintained darkness.(Baumann et al., 2004;Waldner et al., 2018) Synaptic release from rods varies linearly with Ca^{2+} influx, faithfully translating light-evoked voltage responses into changes in the rate of glutamate release that act on second-order neurons. The sustained release of glutamate from a rod is also facilitated by the presence of a plate-like, presynaptic structure known as the synaptic ribbon (Heidelberger et al., 2005). Ribbons help to capture and tether vesicles along their planar surfaces and then deliver them to release sites at the base (Snellman et al., 2011;Vaithianathan et al., 2016). The stochastic release of synaptic vesicles introduces noise that must be overcome in the transmission of single-photon voltage responses at rod synapses. Two strategies have been proposed to distinguish genuine light-evoked changes in release rate from random changes: 1) maintain a sufficiently high rate of glutamate release for small changes in membrane voltage to cause a large enough reduction in release to be distinguished from basal rates (Rao et al., 1994;Rao-Mirotznik et al., 1998;van Rossum and Smith, 1998), or 2) make release more regular and predictable (Schein and Ahmad, 2005).

In this study, we measured voltage-dependent changes in rates of release in individual mouse rods that possess a single ribbon synapse. We took advantage of the fact that the glutamate transporters in rod terminals (largely EAAT5) are linked to an uncoupled anion conductance so that

when an anion channel is opened as glutamate is retrieved (Arriza et al., 1997;Schneider et al., 2014). Using this approach, release rates increased linearly with Ca^{2+} influx, but rose only to ~10 v/s/ribbon at −40 mV (35 °C). When rods were voltage-clamped at −70 mV, we observed spontaneous release of single vesicles at random intervals, but while rates remained low at −40 mV, release occurred in bursts of ~17 vesicles apiece at more regular intervals. We found that these bursts at −40 mV involved vesicles in the readily releasable pool of vesicles at the base of the ribbon and were triggered by opening of nearby Ca^{2+} channels. Lowering distant Ca^{2+} levels lengthened interevent intervals between bursts, perhaps by influencing ribbon replenishment rates. These results suggest that while the rate of release in darkness is too low to overcome noise in synaptic transmission, the replenishment and delivery of vesicles to release sites at the base of each ribbon may make release more regular. In Chapter 4, we explore whether this regularization of release facilitates transmission of single photon responses to downstream neurons.

Methods

Animals

Control and mutant mice of predominately or wholly C57/Bl6 backgrounds were kept on 12-hour dark-light cycles. Animal handling and experimental protocols were approved by the University of Nebraska Medical Center Institutional Animal Care and Use Committee. $Rod^{Syt1cko}$ mutants in which Syt1 was selectively eliminated from rods were bred by crossing *Rho-iCre* mice (RRID:ISMR_JAX:015850) with $Syt1^{flox}$ mice (Syt1: MGI: 99667)(Quadros et al., 2017). Similarly, $rod^{Syt7cko}$ mice selectively lacking Syt7 in rods were bred by crossing *Rho-iCre* mice with $Syt7^{flox}$ mice. $Syt7^{flox}$ mice were generated by the UNMC Mouse Genome Engineering Core by introducing loxP sites that flanked exon 7 using EasiCRISPR (Quadros, Miura et al. 2017). Mice of both sexes aged 4-12 weeks were euthanized in accordance with the AVMA Guidelines for the Euthanasia of Animals by CO_2 asphyxiation and cervical dislocation.

Electrophysiology

Rod cells were visualized in a flatmount preparation performed on an upright fixed-stage microscope (Nikon E600FN) under a 60x, 1.0 NA water-immersion objective. Rod inner segments and cell bodies were identified morphologically and targeted with positive pressure using recording electrodes mounted on Huxley-Wall micromanipulators (Sutter Instruments). Rod recordings were performed in whole-cell voltage clamp using an Axopatch 200B amplifier (Axon Instruments/Molecular Devices) and signals were digitized with DigiData 1550 (Axon Instruments/Molecular Devices). Data acquisition and analysis were performed using pClamp 10 Software (Molecular Devices). Voltages were not corrected for liquid junction potentials unless specifically noted (CsGluconate pipette solution: 12.3 mV, KSCN pipette solution: 3.9 mV).

Flatmount preparations were continuously superfused with room temperature Ames solution (US Biological) bubbled with 95%/5%CO2 at ~1 mL /minute unless otherwise noted. Intracellular pipette solutions for $I_{A(glu)}$ measurements contained (in mM): 120 KSCN, 10 TEA-Cl, 10 HEPES, 1 CaCl2, 1 MgCl2, 0.5 Na-GTP, 5 Mg-ATP, 5 phospho-Creatine, pH 7.3. Intracellular solution was buffered with 5 mM EGTA unless otherwise noted. For I_{Ca} measurements, CsGluconate replaced KSCN and buffering was reduced to 2 mM EGTA. Passive membrane properties measured with KSCN pipette solution were not different between control and mutant rods ($p = 0.9$) and averaged $C_m = 3.2 \pm 0.2$ pF and $R_m = 2.3 \pm 0.04$ GΩ (mean ± SD, n = 20).

$I_{A(glu)}$ event frequency, kinetics, and charge transfer were identified with the event finder function in pClamp directed by a template averaged from approximately 10 events. Statistical analysis was performed on GraphPad Prism 7 and all data are represented as mean ± SEM unless otherwise noted.

In some experiments we used an in-line heater to heat the bath superfusate to 35 °C. We calculated the Q_{10} for $I_{A(glu)}$ frequency, I_{Ca} amplitude and V_m using the following equation:

$$Q_{10} = \left(\frac{F_H}{F_L}\right)^{10/\Delta T}$$

Where F_H and F_L are the features of interest at high and low temperatures, respectively, and ΔT is the absolute value of the difference in temperature in °C.

Results

Voltage and Calcium Dependent Release Properties

$I_{A(glu)}$ can provide a reliable pre-synaptic measure of glutamate release from rods, reflecting the timing and magnitude of exocytotic events. In several experimental systems, including salamander rods as described in the previous chapter, the anionic charge transfer has been shown to be proportional to glutamate concentrations in the cleft and likewise proportional to EPSCs (Otis and Jahr, 1998;Koch et al., 2007;Hays et al., 2020). To measure glutamate release presynaptically, we obtained whole cell recordings from mouse rods with the permeant SCN^- as the principal anion in the patch pipette solution. When rods were voltage-clamped at −70 mV, we observed occasional spontaneous presynaptic currents averaging 5.5 ± 1.7 pA (Fig. 19A). As illustrated by the average in Fig. 19B, these events exhibited a waveform typical of quantal post-synaptic currents but with slow kinetics, showing a 10-90% rise time of 9.3 ± 0.1 ms and decay time constant of 42.3 ± 2.3 ms (n > 10 events in each of 12 rods). As shown in the previous chapter, the rising phase of $I_{A(glu)}$ integrates glutamate levels in the synaptic cleft. The slow rate of decline reflects the slow cycle time of glutamate transport (Palmer et al., 2003;Gameiro et al., 2011). Consistent with Grassmeyer et al., $I_{A(glu)}$ events in mouse rods were blocked by bath application of the glutamate transport blocker threo-β-benzyloxyaspartate (TBOA), confirming that they reflect glutamate transporter activity (Fig. 19C)(Grassmeyer et al., 2019). Event amplitude histograms assumed the shape of a

single Gaussian function, suggesting that the distribution consists primarily of single vesicle fusion events (Fig. 19D).

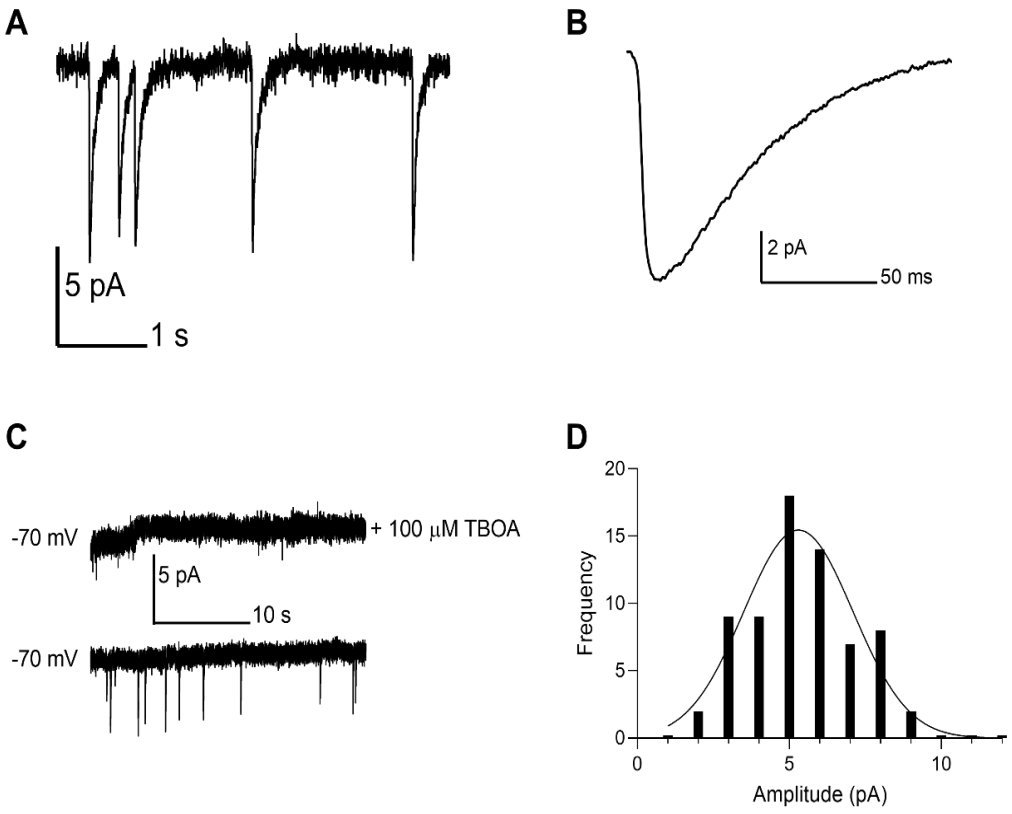

Figure 19. A. Example trace from a rod voltage clamped at −70 mV showing spontaneous $I_{A(glu)}$ release events. **B.** Waveform averaged from 45 $I_{A(glu)}$ events. **C.** Bath application of the glutamate transport inhibitor TBOA (0.3 mM) abolished spontaneous $I_{A(glu)}$ events. **D.** Amplitude frequency distributions of $I_{A(glu)}$ events measured in a rod at −70 mV were well fit by a single Gaussian suggesting single vesicle fusion events (4.9 ± 1.6 pA, mean ± SD, n = 12).

The glutamate taken up originated from the voltage- clamped cell and not neighboring cells. If glutamate release from neighboring rods reached transporters in the clamped rod, we would predict an increase in the number of smaller events when we depolarized surrounding rods with bath application of a solution containing 30 mM K^+; however, 30 mM K^+ did not increase event frequency at −70 mV (0.87 ± 0.5 vs 0.62 ± 0.1 quanta/s, p = 0.28, n = 3) or change the magnitude of unitary events (4.16 ± 1.82 vs 5.40 ± 2.00 pA, p = 0.47, n = 3). Likewise, hyperpolarizing

surrounding photoreceptors by application of a bright white light did not decrease baseline noise that would have been generated from extra-synaptic glutamate (SD = 0.50 ± 0.03 pA vs 0.52 ± 0.18 pA; p = 0.79, n = 5, t-test).

The rate at which vesicles were released increased gradually with membrane depolarization. The increase in release rate at various membrane potentials tracked voltage-dependent increases in I_{Ca} (Fig. 20C). I_{Ca} was measured in separate experiments using voltage ramps and CsGluconate rather than KSCN as the principal ions in the pipette solution. Fig. 20C plots the voltage-dependent changes in release on the same axis as the voltage-dependence of I_{Ca} after correcting for the different liquid junction potentials. Increasing temperature to 35 °C from room temperature (20 °C) nearly doubled Ca^{2+} influx and caused a proportional increase in release rate (Fig. 20C). The Q_{10} value for peak I_{Ca} was 2.09 ± 0.25 (n =10). Within cells, vesicle release rate Q_{10} at -40 mV was 1.58 ± 0.36 (n = 4) which agreed with Q_{10} calculated from the overall release rates of the unpaired cells (1.49). Temperature affects gating properties of many voltage gated channels, although in transfected HEK cells the window current for $Ca_V1.4$ was unchanged (Peloquin et al., 2008), and in our study, V_{50} was also not shifted by temperature (Q_{10} = 1.03 ± 0.02).

As illustrated in Fig. 20, the character of release changed dramatically as the membrane potential approached −40 mV. At −70 mV, nearly all of the spontaneous release events were uniquantal and roughly equal in amplitude. However, at −40 mV, rods consistently switched to a bursting behavior with release of many vesicles that showed an average duration (50% rise time to 50% decline) of 216 ± 69 ms (mean ± SD, n = 22). $I_{A(glu)}$ amplitude and variance initially increased as a function of membrane voltage along with an increased number of vesicles released during each release event, but then diminished above −40 mV as the anion driving force declined further (Fig. 20B). While overall release rate at depolarized potentials increased with temperature, the number of quanta in a burst at −40 mV did not increase (17 ± 7 at room temperature, n =22; versus 11 ± 6

at 35 °C, n = 5, p = 0.5, unpaired t-test). Events were speeded by increasing temperature (half-width RT = 216 ± 69 ms, n = 22; 35 °C= 125 ± 33, n = 5, p = 0.03, unpaired t-test, n = 5) The interburst interval was shortened by higher temperatures (interburst interval RT = 2756 ± 596 ms, n = 14; 35 °C = 1130 ± 665 ms, n = 5, p < 0.001, unpaired t-test). The overall increase in rate with temperature is likely a combination of the slight increase in quanta per burst and an increase in the rate of bursting.

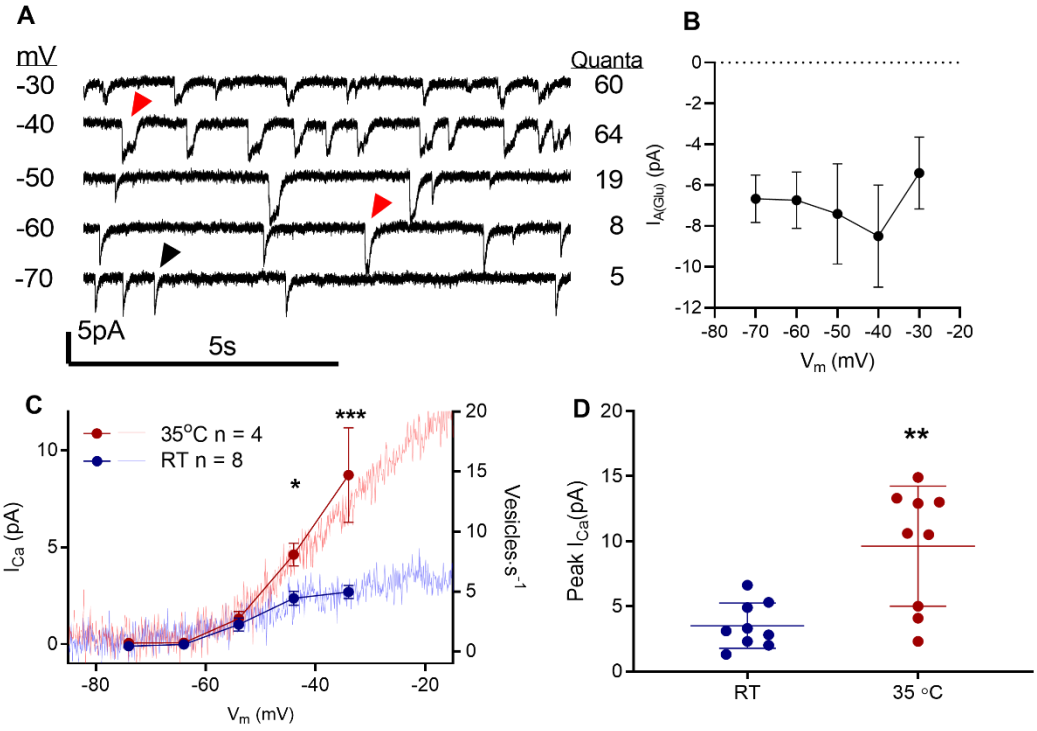

Figure 20. **A.** Vesicle release events in rods measured from $I_{A(glu)}$ increased in frequency with depolarization. As the holding potential approached −40 mV, vesicle release events were organized in bursts of 10-20 vesicles (red arrowheads) rather than unitary events that predominated in rods held at −70 mV (black arrowhead). The number of quanta released during each of these traces is denoted at the right. Quanta in a burst were calculated by charge transfer divided by the charge transfer of a unitary event at that voltage. **B.** As bursts started to appear at −50 mV, the amplitude and variance of $I_{A(glu)}$ increases. Data shown is from the same cell as the representative trace in panel A. **C.** Rates of release increased linearly with I_{Ca} at room temperature and 35 °C. Release rates (filled circles) at each voltage (liquid junction potential corrected) followed Ca^{2+} influx. Both voltage and temperature affect release rate ($p < 0.001$, 2-way ANOVA). Release rate at −44 and −34 mV were increased significantly by temperature ($p = 0.02$ and $p = 0.0002$, respectively, 2-way ANOVA, Tukey's

multiple comparisons) **C.** The peak amplitude of I_{Ca} increased with temperature ($p = 0.004$, paired t-test, $n = 9$).

Bursts and single vesicle fusion events were both enhanced by using SCN^- in the patch pipette, but bursts were not an artefact of using this anion since we also observed similar (albeit smaller) bursts using a Cl^- based pipette solution ($n = 4$) and did not see bursts in cones using the same pipette solution. As described later, bursts were not observed in rods after genetic elimination of the exocytotic Ca^{2+} sensor molecule, synaptotagmin-1 (Syt1). I_{Ca} and passive membrane properties were unchanged in rods lacking Syt1 and so the absence of bursts in these cells indicates that bursts were not due to artefactual bursts of Ca^{2+} channel activity in synaptic terminals (e.g., from a loss of voltage clamp).

Interspersed between bursts were occasional single vesicle fusion events (Fig. 21A-B). Bursts were longer in duration and larger in amplitude than individual events. Fig. 21C and D shows the amplitude histogram from a rod voltage-clamped at −40 mV. This rod showed more unitary events at −40 mV than most, allowing us to construct frequency distributions for both unitary and burst events. There were a number of small individual events with a mean amplitude of ~4 pA along with larger bursts that averaged 12 pA in amplitude. In order to estimate the number of vesicles released during a bursting episode, the charge transfer of each burst was divided by the average charge transfer of unitary events in the same cell. The high density of transporters in rods is unlikely to be saturated during glutamate release (Hasegawa et al., 2006) and we assumed $I_{A(glu)}$ events add linearly. Consistent with this assumption, the amplitude of large, multivesicular $I_{A(glu)}$ release events in salamander rods were linearly correlated in amplitude with simultaneously measured post-synaptic currents (Chapter 2)(Hays et al., 2020). Fig. 21C plots the frequency distribution for charge transfer measurements of large and small events from this cell. Fig. 21D illustrates a burst and a unitary event recorded at the same potential. While the amplitude of bursts was threefold larger than the single quantal amplitude, the charge transfer of bursts was six-fold

larger than the single vesicle charge transfer suggesting that the bursts in this example consisted of an average of 6 vesicles apiece. Bursts more often (81%, n = 22 cells) consisted of 10-20 vesicles with an apparent upper limit of 45-60 vesicles (3%, n = 22 cells). Quanta per burst calculated by charge transfer (17 ± 7, n = 22) was always larger than calculated by amplitudes (3 ± 1; p <0.0001, n = 22 cells, t-test), suggesting that many vesicles are released sequentially during a burst.

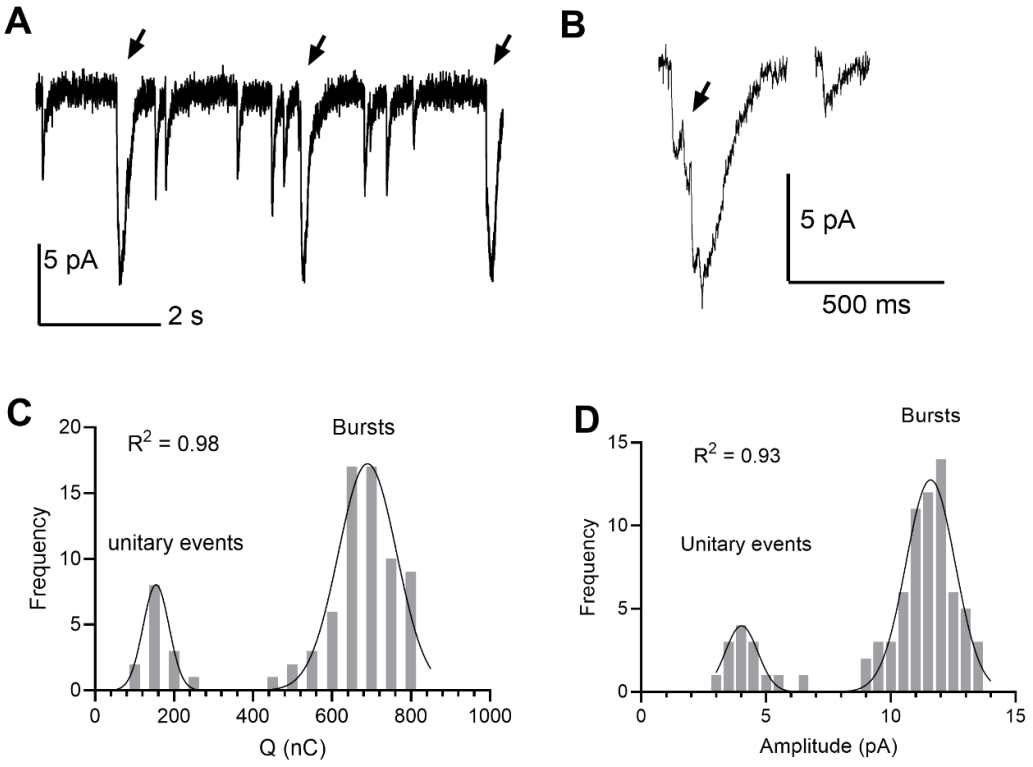

Figure 21 Bursts are multiples of unitary events. **A**. Example trace of burst events (arrows) and unitary events at −40 mV. **B.** Bursts (left) typically show a more asynchronous rise compared to the smooth rise of the unitary event (right).**C.** Charge transfer frequency distribution from the same cell suggested that each burst consisted of ~6 vesicles. Multiple Gaussian fit with 154.5 ± 32.9 and 689.9 ± 73.8 (mean ± SD) **D.** A. Amplitude frequency distribution of unitary and burst events in a rod voltage clamped at −40 mV. Multiple Gaussian fit with 4.0 ± 0.7 and 11.7 ± 1.0 (mean ± SD). This record was chosen for an abundance of unitary events

Consistent with sequential fusion of individual vesicles, many bursts showed multiple inflection points during the initial inward current (e.g., Fig. 22A and B). One could also see individual peaks during the burst consistent with sequential fusion of additional vesicles during the

burst. On the other hand, in some cases, multiple vesicles appeared to be released synchronously during bursts. In 50 ± 31% (mean ± SD, n = 11 cells) of the cells, bursts began with a large smooth, uninterrupted increase in the inward current suggesting that the fusion of some vesicles could also be highly synchronized. Event half-widths varied widely (60 − 709 ms) but averaged 216 ± 69 ms, n = 22 cells). The examples in Fig. 22C and D show large smooth increases in $I_{A(glu)}$ that are two to three times larger than the corresponding single vesicle events, suggesting the possibility of synchronous fusion of two or three vesicles.

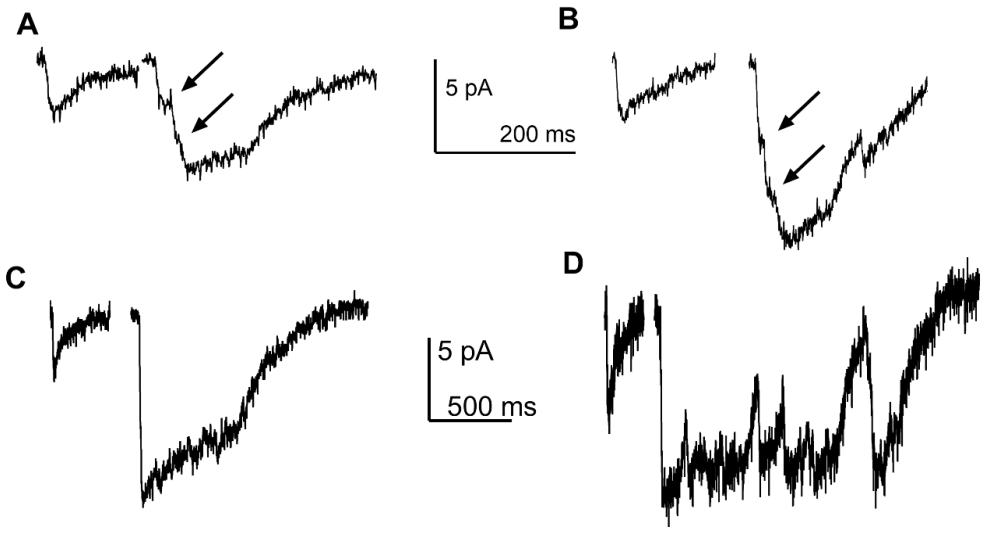

Figure 22. Comparing waveforms of unitary and burst events in cells held at −40 mV suggests both sequential and synchronous fusion of multiple vesicles during bursts. Often, the initial inward current during a burst showed multiple inflection points occurring at intervals similar to the amplitude as individual single vesicle events, suggesting sequential fusion of vesicles during the burst (e.g., A, B.), In other cases, the initial inward current increased smoothly to an amplitude that was two to three times larger than an individual event suggesting synchronous fusion of multiple vesicles (e.g., C, D). In the example in D, one can also see multiple peaks suggesting sequential fusion during the burst.

Cones voltage-clamped at −40 mV did not show the same bursting behavior as rods, but instead showed large individual release events that appeared to involve a more synchronous release mechanism (Fig. 23). As suggested by the example recordings and amplitude histogram in Fig. 23A, even during spontaneous release in cones held at −70 mV, there were many large events that appeared to arise from synchronous multiquantal release. This differed from rods where

multiquantal release only emerged at more depolarized potentials. An increase in the number of multiquantal release events at more depolarized potentials may explain why event amplitude did not diminish with voltage despite a decrease anion driving force (Fig. 23C). Unitary events in cones had a faster 10- 90% rise time (7.4 ± 0.5 ms, n > 40 events in 3 cells) than rods (9.3 ± 0.1 ms, n =12 rods, $p < 0.001$, t-test) suggesting a faster rise in synaptic cleft glutamate. The decay time constant (49.8 ± 6.9 ms, n > 40 events in 3 cells), which is shaped by the glutamate transporter cycle time, was not different from rods ($p = 0.33$, t-test). These data show that the bursting behavior

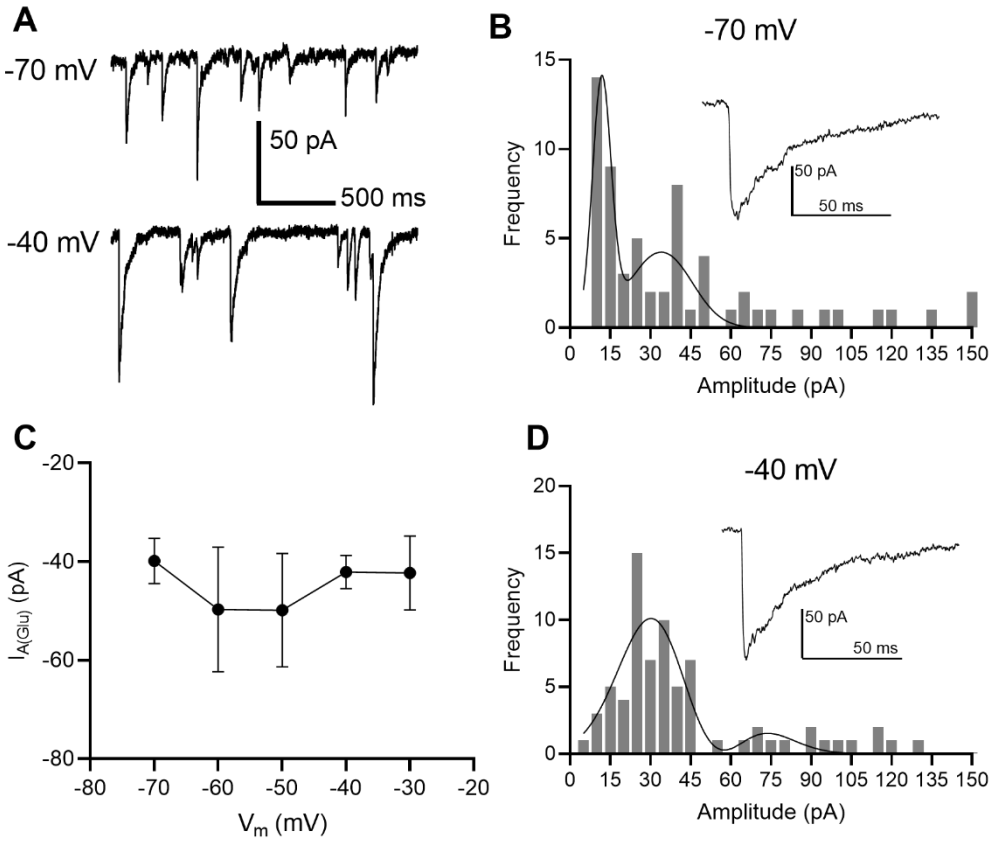

is specific to rods, suggesting it may play a role in signaling information under dim light conditions.

Figure 23 Bursting appears to be a characteristic exclusive to rods. **A.** Example recording of spontaneous events in in a cone held at −70 and −40 mV. **B.** Amplitude histogram of spontaneous $I_{A(glu)}$ release events (n = 61) recorded in a cone voltage-clamped at −70 mV. Inset shows the waveform of a single multiquantal (30 vesicles) spontaneous release event. The presence of many large events in this plot and the example traces in A suggest cones are capable of synchronous release of multiple vesicles. **C.** Plot of $I_{A(glu)}$ event amplitude as a function of holding potential in this same cone. **D** Amplitude histogram of spontaneous $I_{A(glu)}$ release events (n = 72) recorded in a cone voltage-clamped at −40 mV shows the presence of numerous large events. The waveform of a

synchronous multiquantal (34 vesicles) release event at −40 mV (inset). showed the same kinetics as events at −70 mV suggesting a more synchronized mechanism of multivesicular release than occurs in rods.

Bursts in rods held steadily at −40 mV and release events evoked by brief strong depolarizing stimuli both appear to originate from the same pool of vesicles. With a strong depolarizing test step (25 ms, −70 to −10 mV) that should release the entire readily releasable pool, release events averaged 21 ± 12 vesicles (n = 9) as measured from $I_{A(glu)}$ charge transfer following termination of the step. This is similar to the number of vesicles in bursts ($p = 0.17$, unpaired t-test). To compare these pools more directly, we voltage clamped rods at −40 mV for 30 s and then applied a brief depolarizing step to −10 mV (25 ms) to deplete the releasable pool, and then returned the membrane potential to −40 mV for another 30 s. Bursts measured before and after the depolarizing step were nearly equal in amplitude. Mean burst/evoked response ratio did not differ significantly from unity (before = 1.10 ± 0.17, $p = 0.9$, t-test, n =10; after = 0.88 ± 0.06, $p = 0.8$, t-test, n = 10). This is illustrated in Fig. 24A in which the depolarizing step evoked an inward current that was similar to bursts that occurred before and after the step. Interestingly, in the next trial, a burst occurred immediately before the step to −10 mV and the subsequent depolarizing step failed to evoke release (Fig. 24B). Because bursts were relatively infrequent, we were not fortunate enough to see other examples where the burst immediately preceded the test step, but the recording shown in Fig. 24 provides evidence that bursts can deplete the releasable pool available for depolarization-evoked release.

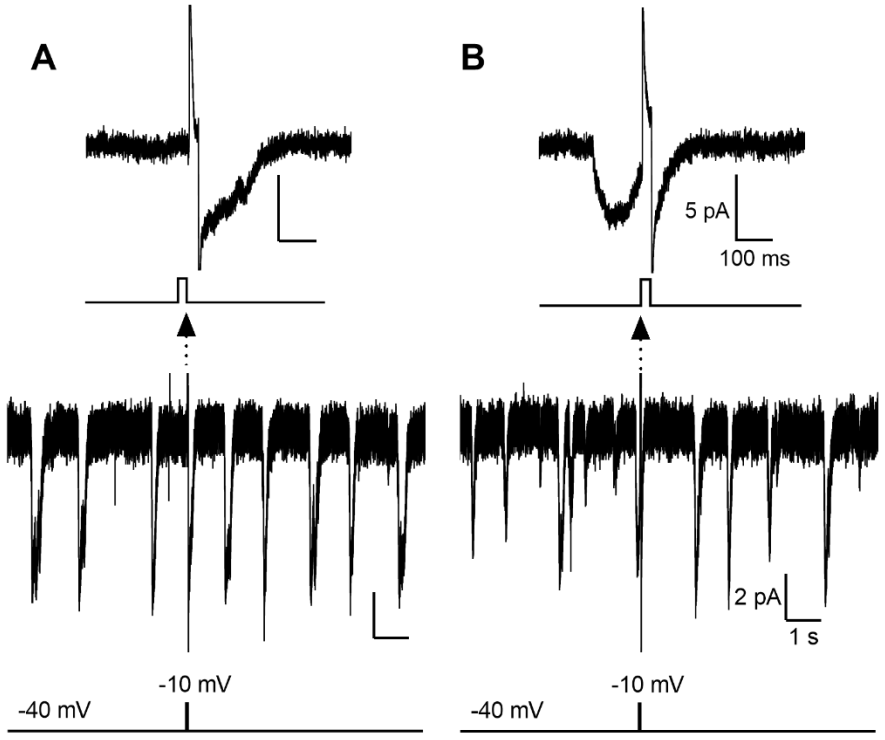

Figure 24 Rod voltage clamped at −40 mV and stepped briefly to −10 mV to test for cross-depletion of pools that contribute to bursting and evoked release. **A.** The amplitude of an $I_{A(glu)}$ release event evoked by a 25 ms step to −10 mV matched the amplitude of preceding and subsequent burst events before. **B.** Release was not evoked when a burst immediately preceded the step to −10 mV, suggesting a shared vesicle pool.

Bursts Depend on Calcium

The increased rate of release with depolarization tracked the increase in I_{Ca} suggesting it was Ca^{2+}-dependent. The essential role of Ca^{2+} influx was confirmed by eliminating this voltage-dependent in increase in release rate with addition of the voltage gated Ca^{2+} channel blocker Cd^{2+} to the external solution (n = 3) (Fig. 25A). The persistence of some release events even in the presence of Cd^{2+} is consistent with studies in salamander retina showing the capability for Ca^{2+}-independent spontaneous release from rods(Cork et al., 2016) (Cork et al., 2016).

As shown in Fig. 20C the membrane voltage of −40 mV approaches the midpoint activation voltage (V_{50}) for rod I_{Ca} (Babai and Thoreson, 2009) so we investigated whether increasing the

open time of L-type Ca^{2+} channels extended burst duration by recruiting extra vesicles. Lengthening Ca^{2+} channel openings by bath application of BayK8644 (2 µM) did not significantly alter release properties at –40 mV. Bursts consisted of 24 ± 9 (n =3, mean ± SD) vesicles in control conditions compared to 25 ± 14 vesicles in BayK8644 (p = 0.8, n = 3 cells, paired t-test). Burst event duration was also unchanged by extending Ca^{2+} channel open times (control half-width was 209 ± 87 ms, n =3, versus 211± 143 ms in BayK8644, p = 0.96, paired t-test, n = 3 cells). The frequency of individual uniquantal events in periods of 30 seconds (2.5 ± 0.7 events) was also not significantly increased with BayK8644 treatment (4.0 ± 0.9 events; n =3, p = 0.2, paired t-test). Thus, overall release rates at −40 mV were not increased with BayK8644 treatment (Figure 25B). These data suggest that while the influx of Ca^{2+} through Ca^{2+} channels is required to trigger a burst, the number of vesicles in each burst is not strongly shaped by further influx and diffusion of Ca^{2+} from voltage-gated Ca^{2+} channels.

Results from mouse and salamander retina have shown that Ca^{2+} released from internal stores by Ca^{2+}-induced Ca^{2+} release (CICR) helps to promote release when rods are tonically depolarized(Cadetti et al., 2006;Suryanarayanan and Slaughter, 2006;Babai et al., 2010b) (Cadetti et al., 2006;Suryanarayanan and Slaughter, 2006;Babai et al., 2010b). We tested contributions from CICR by introducing a ryanodine receptor inhibitor, dantrolene (100 µM), through the patch pipette and observed a modest reduction in release rate when CICR was blocked (p = 0.006; mixed model ANOVA), suggesting that Ca^{2+} from internal stores may boost release at depolarized potentials (Fig. 25C). However, CICR was not required for coordinating bursts as they persisted after introducing dantrolene into rods through the patch pipette (Fig. 26A). Dantrolene did not extend interburst intervals (3340 ± 2489 ms, n = 6) compared with control (2756 ± 596 ms, n = 14, p =

0.3, unpaired t-test) nor did it reduce the number of quanta in each burst from control (dantrolene: 21 ± 9, n = 6; control: 17 ± 7, n = 22, p = 0.1, unpaired t-test).

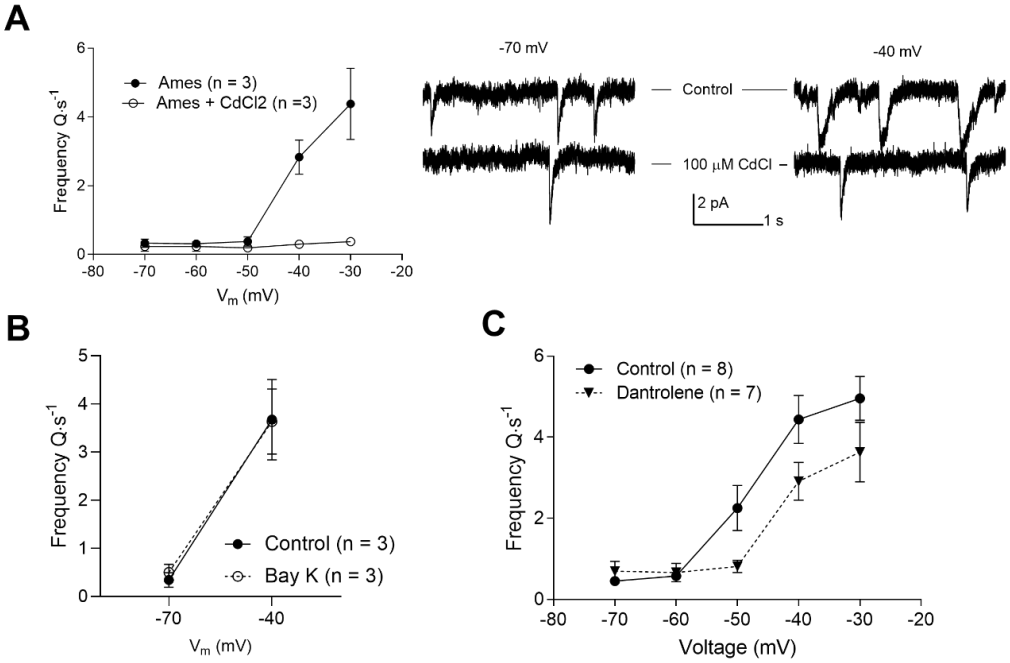

Figure 25 Bursting depends on Ca^{2+} from voltage-gated Ca^{2+} channels. **A.** Including $CdCl_2$ in the extracellular medium abolished bursts of release at depolarized potentials, although some Ca^{2+}-independent spontaneous release events remained (p = 0.0009, 2-way ANOVA). **B.** Including BayK8644 (2 µM) in the extracellular solution did not increase release rate measured at either −70 or −40 mV (p = 0.93, paired t-test). **C.** Application of a ryanodine receptor inhibitor, dantrolene (100 µM), in the pipette solution modestly reduced overall release frequency (p = 0.006, 2-way ANOVA)

Bursts were also not blocked by introducing a high antagonist concentration (100 µM) of ryanodine (n = 4) through the patch pipette (Fig. 26B). Likewise, the replenishment of internal stores by store operated channels (SOC) does not appear necessary for bursts as application of SOC Orai/Stim1 blocker SKF96368 through the patch pipette did not eliminate bursting behavior (Fig. 8C, n = 3). We also tested whether horizontal cell feedback might be responsible for organizing bursts, but bursts at −40 mV appeared to be unchanged by bath application of 10 µM AMPAR blocker NBQX (n = 3, Fig. 26D).

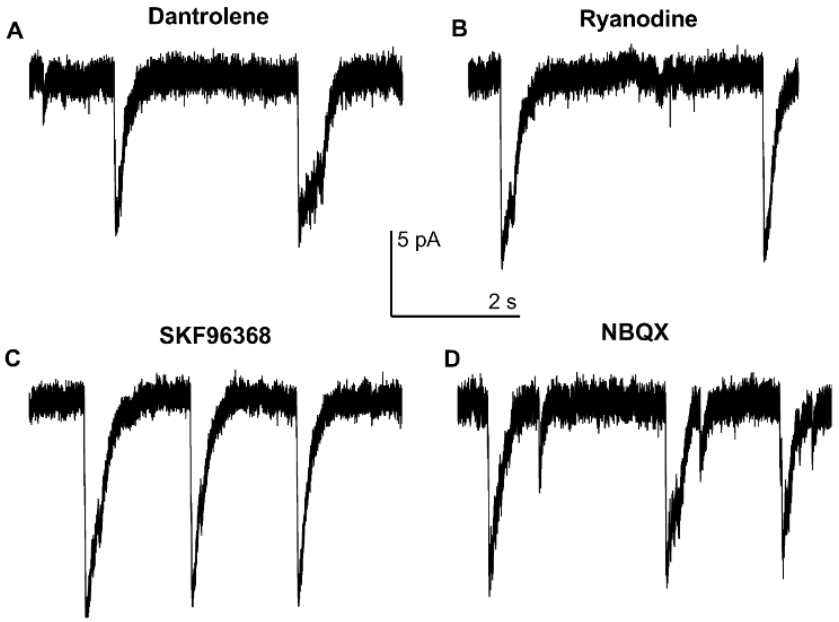

Figure 26 A, B. Inhibiting CICR with a high concentration of dantrolene (100 µM) or ryanodine (100 µM) in the patch pipette did not eliminate bursting behavior. **C.** Inhibiting the replenishment of internal Ca^{2+} stores with the SOC channel blocker SKF96368 (10 µM) in the bath also did not eliminate bursts. **D.** Adding an AMPAR blocker NBQX (10 µM) to the bath to block horizontal cell feedback did not eliminate bursting.

We manipulated intracellular Ca^{2+} buffering to probe the spatiotemporal Ca^{2+} distribution controlling release rates and bursting behavior. Typically, our pipette solution contained 5 mM EGTA as the principal Ca^{2+} buffer. Replacing this with the faster Ca^{2+} buffer, BAPTA, reduced the voltage-dependent increase in release rates to a similar extent with both 1 and 10 mM BAPTA ($p = 0.0004$, n = 5-8, mixed model ANOVA, Fig. 27). Neither concentration of BAPTA eliminated the bursting behavior observed at −40 mV and the number of quanta in each burst was unchanged (12.5 ± 1.4 versus 13.1 ± 2.1 and 11.3 ± 1.3 for 1 and 10 mM BAPTA, respectively; $p = 0.9$, 1-way ANOVA, n =5 cells in each condition). However, switching from EGTA to BAPTA lengthened the intervals between burst events from 2756 ± 596 in control conditions with 5 mM EGTA (n = 14 cells) to 4805 ± 1524 ms with 1 mM BAPTA ($p = 0.02$, ANOVA, n = 5 cells) and 6523 ± 2535 with 10 mM BAPTA ($p = 0.008$, ANOVA, n = 4 cells). The number of individual quanta released

between bursts was also not reduced by 1 or 10 mM BAPTA buffering (10 mM, p = 0.6, t-test, n = 5 cells of each condition) consistent with other evidence that these events result from Ca^{2+}-independent spontaneous release.

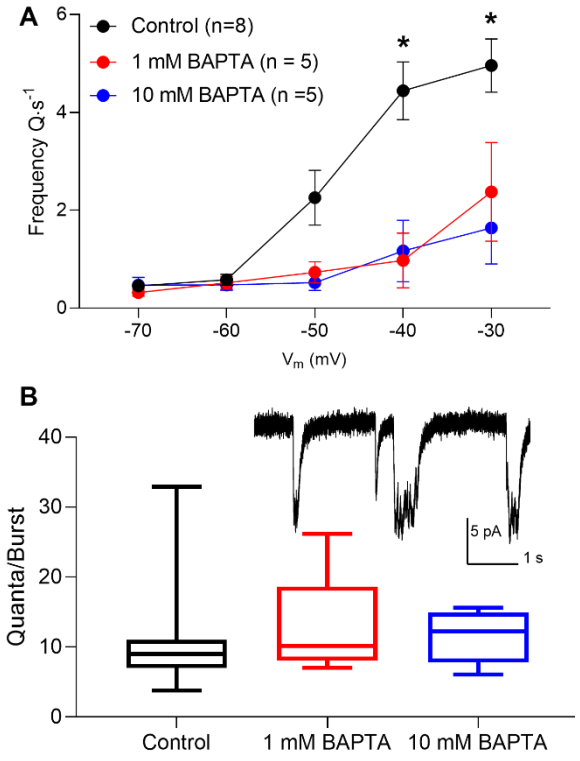

Figure 27 Replacing EGTA in the patch recording pipette with the faster Ca^{2+} buffer BAPTA reduced overall release rates during 30 s steps (p = 0.0004, 2-way ANOVA). **A.** Release rate was reduced by 1 mM BAPTA buffering compared to control 5 mM EGTA at −40 mV (p = 0.004; 2-way ANOVA, Tukey's multiple comparisons). Ten mM BAPTA significantly reduced release rates at −40 and −30 mV (p < 0.01; 2-way ANOVA, Tukey's multiple comparisons). **B.** Buffering by BAPTA did not eliminate bursting, and bursts consisted of the same number of quanta compared to control (p > 0.05, 1-way ANOVA, Tukey's multiple comparisons) Boxes represent interquartile range and median, and whiskers show minimum to maximum values.

Unlike individual single-vesicle release events, bursts were blocked by Cd^{2+} and so the persistence of bursts in the presence of 10 mM BAPTA indicates that they must involve release sites located within Ca^{2+} nanodomains extremely close to Ca^{2+} channels. Ca^{2+} channels are clustered beneath ribbons (Morgans, 2001;Specht et al., 2009;Mercer and Thoreson, 2011;Lv et al., 2012b) and so this suggests that ribbon-associated vesicles participate in bursting. This agrees with results suggesting that bursts share the readily releasable pool with evoked release, which is commonly thought to be ribbon-dependent. The finding that use of a faster buffer BAPTA increased the intervals between bursts suggests that more distant changes in $[Ca^{2+}]$ play a role in preparing bursts

for release. This may reflect the Ca^{2+}-dependence of vesicle replenishment at ribbons (Babai et al., 2010a;Van Hook et al., 2014;Van Hook and Thoreson, 2015).

Calcium-Activated Chloride Currents Emerge with Depolarization

In addition to bursts of release, another characteristic of rods that becomes apparent around −40 mV are large sustained inward currents that involve activation of Ca^{2+}-activated Cl^- currents ($I_{Cl(Ca)}$)(Thoreson and Burkhardt, 1991;Barnes and Deschenes, 1992). Much of the time, these currents were observed immediately after a step to −30 or −40 mV as illustrated in Fig. 28A (arrows show the initiation of these large currents), but they could also arise in the middle of long periods of depolarization as well. They were blocked by bath application of $CdCl_2$ (0.1 mM, Fig. 28A) and promoted by lower Ca^{2+} buffering from 5 to 0.1 mM EGTA. In fact, with weak intracellular Ca^{2+} buffering (0.1 mM EGTA), the frequency of large $I_{Cl(Ca)}$ during 30-s steps at −30 and −40 mV obscured accurate measurements of glutamate release during bursts. These large inward currents appeared to be anion currents since they were reduced at more positive potentials and by replacing KSCN with CsGluconate (n = 5) in the pipette solution, but were not blocked by TBOA (100 µM, n = 3). These large inward currents persisted even after strong buffering with 10 mM BAPTA, suggesting that sustained Ca^{2+} influx can saturate buffering.

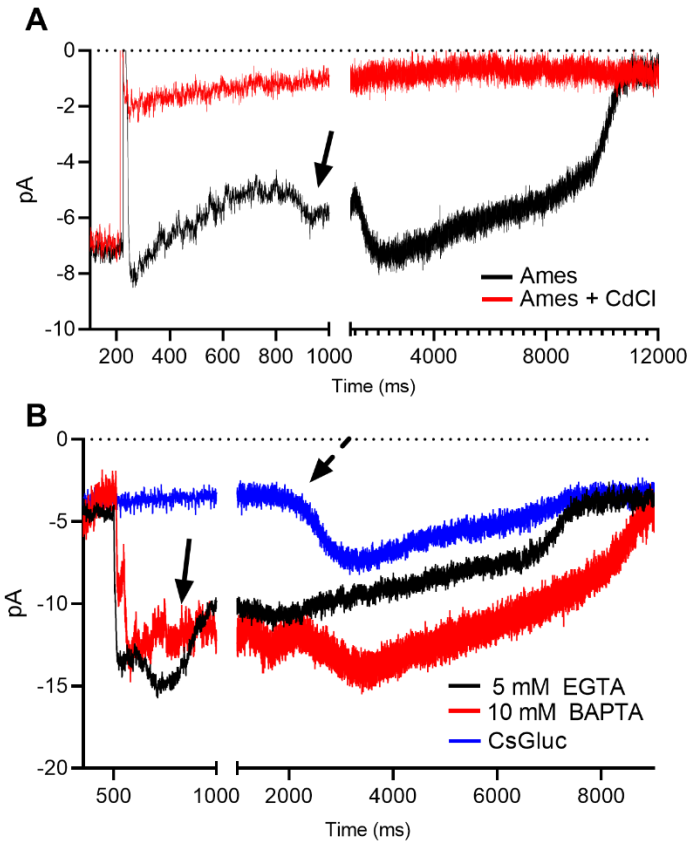

Figure 28 Large, long Ca^{2+} activated Cl^- currents ($I_{Cl(Ca)}$) emerge during sustained depolarization. Many time these currents were initiated after depolarization as in Panel A, but were also occasionally preceded by large burst events as in panel B. **A.** Representative current trace with 5 mM EGTA buffering shows that these large inward currents were eliminated when $CdCl_2$ was included in the Ames extracellular solution. Black arrow indicates start of $I_{Cl(Ca)}$ **B.** Using a CsGluconate-based internal solution rather than the KSCN solution reduced $I_{Cl(Ca)}$. $I_{Cl(Ca)}$ persisted even with 10 mM BAPTA in the KSCN internal solution suggesting that Ca^{2+} buffers could be saturated by the sustained Ca^{2+} influx during 30-s depolarizing steps. Black arrow shows onset of $I_{Ca(Cl)}$ immediately after a burst event, dashed arrow shows onset of $I_{Ca(Cl)}$ not preceded by a burst event with CsGluconate internal solution.

We also tested effects of Ca^{2+} buffering on release evoked by a strong depolarizing step. As illustrated in Fig. 29, steps from −70 to −10 mV evoked inward currents in rods as glutamate was retrieved. Fig. 29 examines the impact of different intracellular Ca^{2+} buffers. Panels A, B and C, show example recordings under four different buffering conditions evoked by steps of 5, 25, and 500 ms duration, respectively. With 5 mM EGTA, steps of 5 and 25 ms duration evoked similar amplitude inward currents. Larger currents were evoked by a 500-ms step (filled circles, Fig. 29D).

Using 1 mM BAPTA to restrict the spread of Ca^{2+} to nanodomains close to Ca^{2+} channels, similar amplitude currents were evoked by 5- and 25-ms steps, but there was no further increase with 500-ms steps (open triangles). More strongly buffering Ca^{2+} with 10 mM BAPTA eliminated $I_{A(Glu)}$ at all step durations (filled triangles) compared to 5 mM EGTA (5 ms $p = 0.002$, 25 ms $p = 0.003$, 500 ms $p < 0.0001$, 2-way ANOVA, Tukey's multiple comparisons). While 10 mM BAPTA is capable of buffering Ca^{2+} during relatively short steps, the persistence of $I_{Cl(Ca)}$ currents and bursts described above suggests that this buffer can be saturated with continued influx of Ca^{2+} during 30-s steps. With weaker Ca^{2+} buffering using 0.1 mM EGTA, responses evoked by 5-ms steps were unchanged ($p = 0.92$) and responses to longer steps were enhanced, although the change was not significant ($p = 0.1$). Taken together, these data say that fast synchronous release evoked by short 5-ms test steps involves vesicles located within Ca^{2+} nanodomains close to Ca^{2+} channels whereas slower release evoked by longer steps involves more distant sites. Since Ca^{2+} channels are clustered beneath ribbons, this suggests that fast release that is closely synchronized with Ca^{2+} channel activation occurs predominantly at the ribbon whereas slower release that is less tightly synchronized to the initial depolarization involves ectopic non-ribbon site.

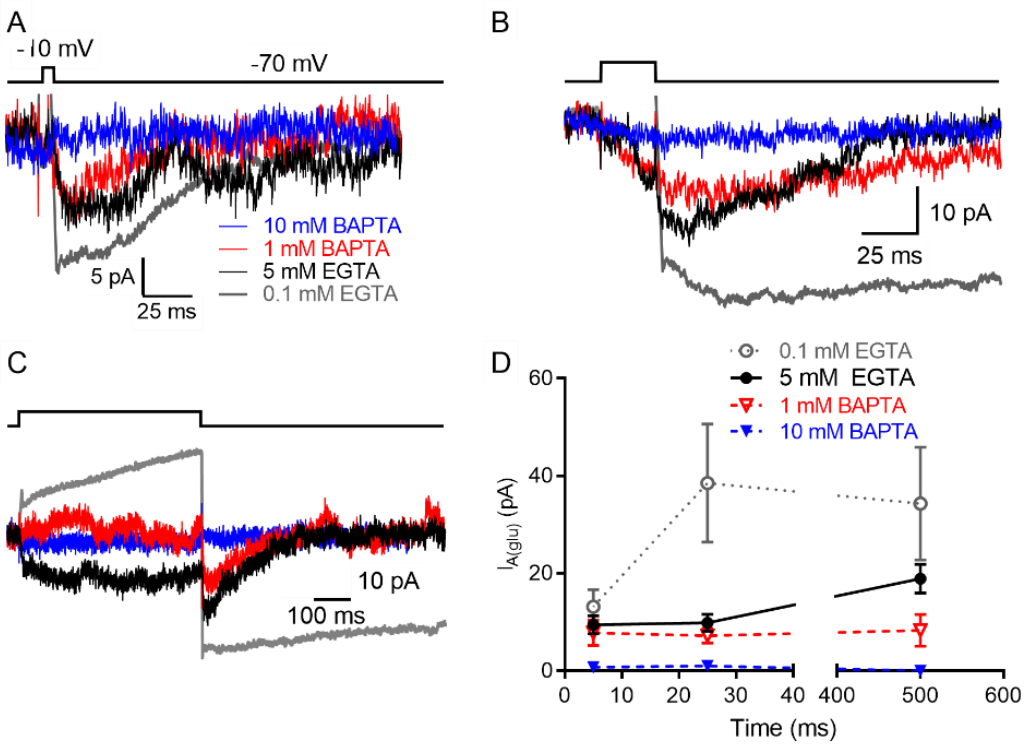

Figure 29 Effects of intracellular Ca^{2+} buffering on $I_{A(glu)}$ evoked in rods from C57Bl6 mice using strongly depolarizing steps (-70 to −10 mV). A. Representative $I_{A(glu)}$ evoked by 5 (A), 25 (B) and 500 (C) ms steps. Overlaid traces show currents evoked with different intracellular Ca^{2+} buffers introduced into rods through the patch whole cell recording pipette (0.1 mM EGTA, n =10, gray; 5 mM EGTA, black; 1 mM BAPTA, red; 10 mM BAPTA, blue). The stimulus trace is shown at the top of each panel. D. Summary data showing changes in $I_{A(glu)}$ with the various buffers. Buffering with 1 mM BAPTA (n =11) reduced $I_{A(glu)}$ evoked by 500 ms step significantly compared to control conditions (5 mM EGTA, n =16, p=0.0086, t-test corrected for multiple comparisons). 0.1 mM EGTA (n =10) significantly enhanced responses evoked by 25 ms steps (p=0.0018). Responses evoked by strong depolarizing steps were abolished by 10 mM BAPTA (n =3) compared to 5 mM EGTA with all step durations (p = 0.002, 5 ms; p = 0.008, 25 ms; p < 0.0001; 500 ms; Tukey's multiple comparisons test)

Ca^{2+} Sensors, Syt1 and Syt7, Contribute to Sustained Release

We then tested how Ca^{2+} sensors Syt1 and Syt7 shape evoked and sustained release. Selective elimination of Syt1 from mouse rods abolished fast, synchronous Ca^{2+}-dependent exocytosis evoked by brief depolarizing steps but a slower component of release persisted (Grassmeyer et al., 2019). The high affinity Ca^{2+} sensor, Syt7, is believed to be the sensor for slow, asynchronous release at bipolar cell ribbon synapses as well as a number of conventional synapses (Sun et al., 2007;Bacaj et al., 2015;Luo et al., 2015). To examine the role of Syt7 in release from

rods, the UNMC Mouse Genome Engineering core used EasiCRISPR to generate a floxed mouse line with loxP sites flanking exon 7 (Quadros et al., 2017). PCR experiments showed proper insertion of both LoxP sites. For selective elimination of Syt7 from rods, this line was crossed with mice that express Cre recombinase specifically in rods under control of the rhodopsin promoter (Rho-iCre) (Li et al., 2005). The generation of Syt1 flox mice was described previously (Quadros et al., 2017;Grassmeyer et al., 2019).

Fig. 30 shows examples of inward $I_{A(glu)}$ in rods from different mouse lines with and without Syt1 and Syt7. Fig. 30D plots the amplitude of $I_{A(glu)}$ as a function of test step duration. All data were obtained using 5 mM EGTA as the buffer and the data from control C57Bl6 mice are the same as those plotted in Fig. 29 (black, filled circles). Blocking the glutamate transporter with the inhibitor TBOA blocked depolarization-evoked inward currents, confirming that they arise from activation of glutamate transporter anion currents (filled triangles). Consistent with data from Grassmeyer et al. (2019), eliminating Syt1 from rods abolished responses to 5 ms steps ($p = 0.002$) and greatly reduced responses to 25 ms steps ($p = 0.01$, 2-way ANOVA, Tukey's multiple comparisons) (Grassmeyer et al., 2019). The earlier study only tested step durations up to 25 ms. As shown in Fig. 30C, eliminating Syt1 did not reduce the amplitude of $I_{A(glu)}$ evoked at the end of long 500 ms steps ($p = 0.97$, 2-way ANOVA, Tukey's multiple comparisons). Presumably, the glutamate released by Syt1 early during the step does not contribute significantly to the level of glutamate present after 500 ms.

We next recorded from rods in which Syt7 had been eliminated. Elimination of Syt7 had no effect on release evoked by 5- and 25-ms steps ($p = 0.99$, 2-way ANOVA, Tukey's multiple comparisons), but substantially reduced release evoked by 500-ms steps ($p = 0.003$). This suggests that Syt7 is the sensor that mediates slow release from rods. Consistent with this, in double conditional knockout mice where we eliminated both Syt1 and Syt7 from rods, release appeared to be entirely eliminated at all step durations ($p < 0.03$). The small residual inward currents that

remained in these rods did not differ significantly from the small inward currents that remained after bath application of TBOA (Fig. 30D). Together with the results of Fig. 29 suggesting that fast release occurs predominantly at the ribbon whereas slow release involves non-ribbon sites, these results suggest that Syt1 mediates ribbon release whereas Syt7 predominately mediates non-ribbon release.

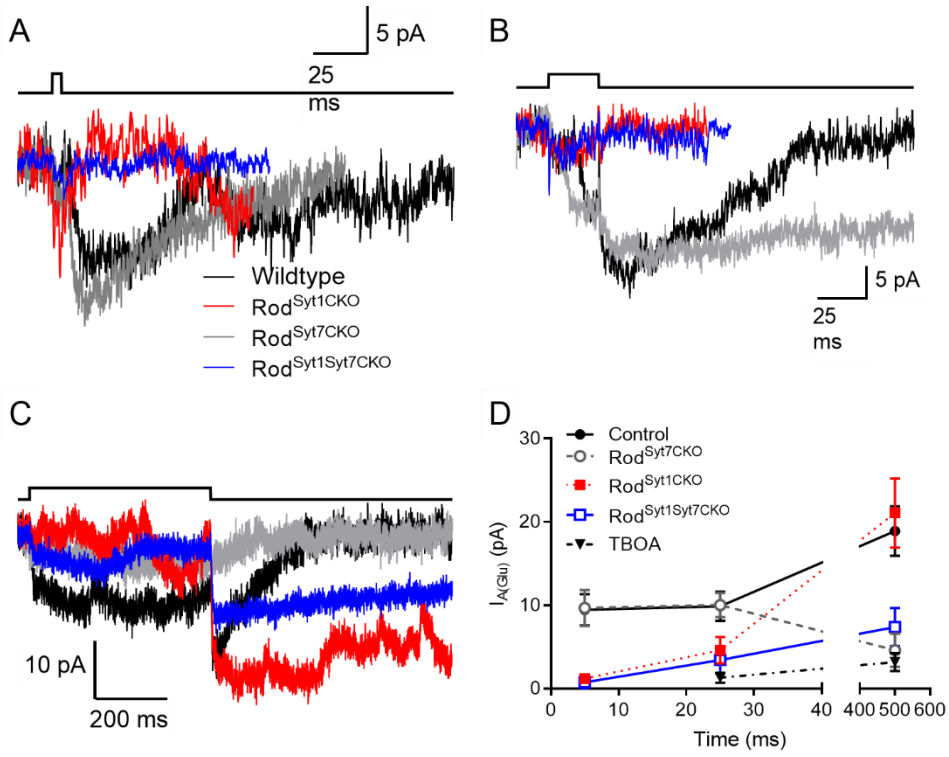

Figure 30 Single cell recording shows that eliminating Syt7 diminishes slower components of depolarization-evoked glutamate release. The traces in A, B and C show overlaid examples of glutamate transporter anion currents ($I_{A(glu)}$) recorded from rods in four different mouse lines: wildtype C57Bl6 (black traces), Rod^{Syt1CKO} (red traces), Rod^{Syt7CKO} (gray traces), and Rod^{Syt7Syt1CKO} (red traces) Currents were leak subtracted using a P/8 protocol to remove passive membrane properties.. C. Plot of $I_{A(glu)}$ amplitude as a function of test step duration (-70 to −10 mV) in single cell rod recordings from Wildtype (n =16), wildtype + TBOA (0.3 mM, filled triangles, n =8), Rod^{Syt1CKO} (filled squares, n = 29), Rod^{Syt7CKO} (n = 5), and Rod^{Syt1Syt7CKO} (open circles, n = 6). The amplitude of $I_{A(glu)}$ was measured immediately following the test step.

While deletion of Syt1 eliminates fast, evoked release, it also significantly elevates the rate of spontaneous release in rods voltage-clamped at −70 mV(Grassmeyer et al., 2019) (Grassmeyer

et al., 2019). This is consistent with findings from other systems that Syt1 helps to clamp the SNARE apparatus and prevent spontaneous fusion(Xu et al., 2009;Courtney et al., 2019;Grushin et al., 2019) (Xu et al., 2009;Courtney et al., 2019;Grushin et al., 2019). In rods lacking Syt1, we saw a significant overall increase in spontaneous release ($p < 0.001$) but there was also a further increase in release rates with depolarization at membrane potentials above −50 mV. Rates at −40 and −30 mV in Syt1CKO rods matched those in rods from control mice (Fig. 31). The smaller voltage-dependent increase seen after eliminating Syt1 suggests that unclamping Syt1 may facilitate fusion of vesicles that would normally be released only by an increase in Ca^{2+}. The residual voltage-dependent increase in release at −40 and −30 mV that remained after eliminating Syt1 from rods was abolished by replacing 5 mM EGTA with 1 mM BAPTA in the patch pipette (Fig 13B). This suggests that this residual release occurred at non-ribbon release sites and thus may be mediated by the high affinity sensor, Syt7(Xu et al., 2009) (Xu et al., 2009). Eliminating Syt7 from rods did not change the rate of spontaneous release at −60 or −70 mV but slightly depressed the increase at more positive potentials, although the effect was not significant ($p = 0.6$, 2-way ANOVA, n = 7-8 cells, Fig. 31). After eliminating both Syt1 and Syt7 from rods, spontaneous release at −60 and −70 mV was increased but the voltage dependent increase in release rates at −40 and −30 mV was eliminated ($p > 0.05$, 2-way ANOVA). Genetic elimination of the Ca^{2+} sensors Syt9 and Doc2B, also expressed in rods, did not have an effect on voltage dependent sustained release rates ($p = 0.45$, n = 3-8, mixed model ANOVA)(Fig. 31D).

Interestingly, when the calcium sensor Syt1 was conditionally knocked out in rods, roughly the same number of quanta were released over long periods of time (30 s) but events were largely uniquantal and not organized in bursts (Fig. 31A). These data suggest that the clamping function of Syt1 is necessary to maintain inactive periods between bursts, thus allowing accumulation of a

sufficient number of vesicles to initiate a burst at −40 mV. The absence of the sensors Syt7, Syt9, or Doc2b had no effect on bursts.

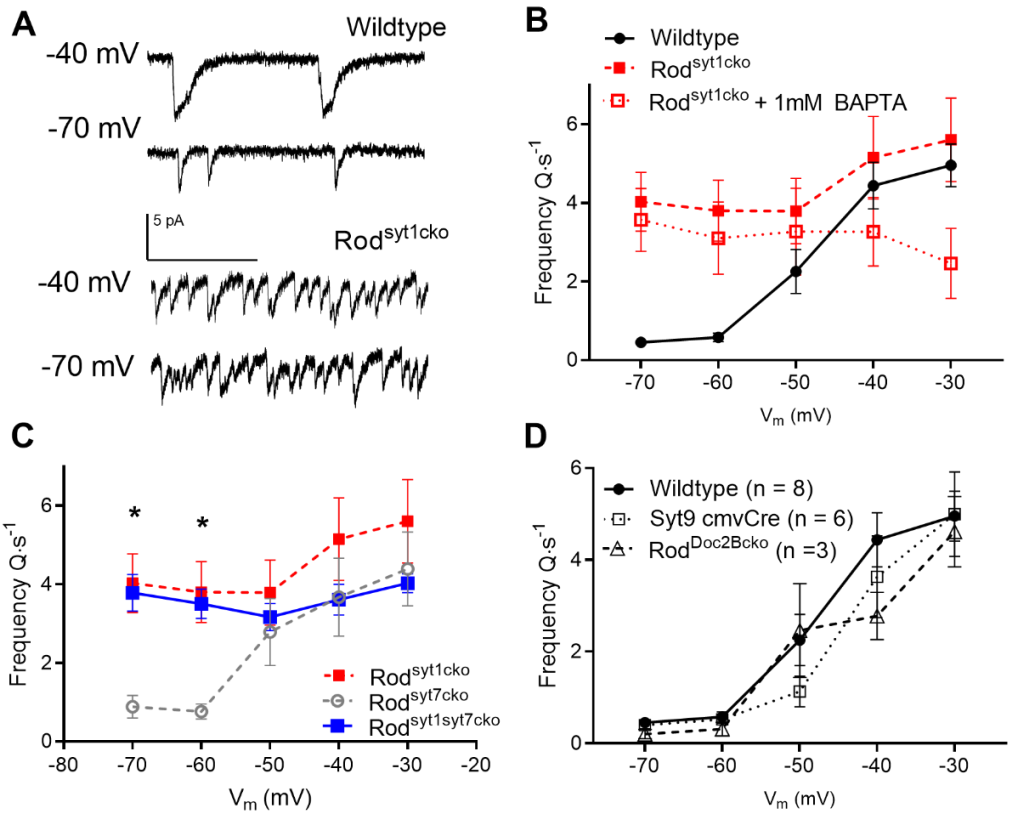

Figure 31. Syt1 and Syt7 mediate sustained release during long (30 s) depolarizations ***A.*** Representative traces at −40 and −70 mV illustrate the differences in release characteristics in wildtype and Rod^{Syt1CKO} knockout rods. ***B.*** After Syt1 elimination, voltage-dependent increases in release rate at −40 and −30 mV remained but were reduced by using the fast Ca^{2+} buffer, BAPTA (1 mM), rather than EGTA (5 mM). **C.** After eliminating Syt1, the voltage dependent increases in release rate that remained were attenuated by additionally removing Syt7 from rods. Syt7 knockout alone did not unclamp fusion at hyperpolarized potentials like Syt1 removal. **D.** Whole animal knockout of Syt9 and rod-specific elimination of Doc2b did not eliminate spontaneous release, prevent bursting or alter the voltage-dependent increase in sustained release rates.

Discussion

An appreciation of mechanisms of tonic release of glutamate-containing vesicles from rods, graded by membrane potential, is critical to understanding how synaptic transmission is regulated by light-evoked changes in rod membrane potential. Using $I_{A(glu)}$ we were able to show

that Ca^{2+} sensors Syt1 and Syt7 both contribute to the voltage-dependence of sustained and evoked vesicle release. At depolarized potentials in times of darkness, rods release vesicles at a slow rate, using a method for multivesicular release that recruits ribbon-associated vesicles near Ca^{2+} channels.

Glutamate release from vertebrate rods has been found to show a linear dependence on intraterminal [Ca^{2+}] and a shallow Ca^{2+} cooperativity (Thoreson et al., 2004;Heidelberger et al., 2005). Earlier assessments of Ca^{2+}-dependence of release were performed in non-mammalian retina and relied on techniques such as capacitance jumps, postsynaptic current measurements evoked by brief depolarizing steps, and fluorescent probes to evaluate fusion over longer period(Thoreson et al., 2004;Choi et al., 2005) (Thoreson et al., 2004;Choi et al., 2005). In the present study, we show that the sustained release of vesicles from mouse rods possessing a single ribbon also show the linear dependence on I_{Ca} demonstrated earlier.

Voltage-dependent changes in glutamate release rate tracked with I_{Ca}, even when the temperature of the system was increased to physiological levels. Fusogenicity of the SNARE complex, employed by rods for exocytosis, is controlled by entropic forces, so complex formation and zippering is not aided by increases in temperature (Mostafavi et al., 2017). Thus, rate appears to depend chiefly on the increase in I_{Ca} that accompanies increasing temperature that we found to have Q_{10} = 2.1. Voltage-gated Ca^{2+} channels in rods are L-type channels containing the Ca_V α subunit 1.4, with several splice variants that have different kinetics and gating properties (Tan et al., 2012;Haeseleer et al., 2016). While the gating properties of some voltage gated ion channels are strongly temperature-dependent (Q_{10} 5-10) (Lee and Deutsch, 1990;DeCoursey and Cherny, 1998;Hille, 2001), our experiments agree with the relatively weaker temperature-dependence of $Ca_v1.4$ (Q_{10} = 2-4) measured in various systems (Herve et al., 1992;Allen, 1996;Hope et al., 2005). Studies of synaptic release from bullfrog inner hair cells that also contain synaptic ribbons and employ L-type Ca^{2+} channels (Brandt et al., 2005) describe a stronger temperature

dependence of release frequency, but agree with the present study that increases in release are likely due to enhanced ion currents rather than changes in the fusion machinery itself (Sabatini and Regehr, 1996;Chen and von Gersdorff, 2019). It is possible that other parts of the synaptic vesicle cycle are speeding with temperature; however, the mouse rod is less reliant on fast endocytosis for refilling of the RRP than conventional neurons (von Gersdorff and Matthews, 1997). The tight relationship of release with Ca^{2+} influx improves linearity in the transformation of light-evoked changes in membrane potential into synaptic release.

We have previously shown that Ca^{2+}-dependent release evoked by brief depolarizing steps in rods and cones are both mediated by Syt1 (Grassmeyer et al., 2019). While Syt1 appears to mediate all of the evoked release in cones, rods retained the capability for a slower component of release after removal of Syt1. In the present study, we found that release could be evoked by strong depolarizing steps of 500 ms duration after deletion of Syt1 from rods. This slow release was abolished by eliminating Syt7. At other CNS synapses, including retinal bipolar cells, Syt1 and Syt7 work together, with the former initiating fast fusion and the latter slow, asynchronous fusion of vesicles from a separate pool (Geppert et al., 1994;Weber et al., 2014;Deng et al., 2020). Similarly, our results show that Syt1 mediates fast synchronous release and Syt7 mediates slow asynchronous release from rods. Slow asynchronous release was also abolished in rods by using 1 mM BAPTA as the Ca^{2+} buffer. Replacing the slower buffer EGTA with this fast buffer constrains the spread of Ca^{2+} to nanodomains close to Ca^{2+} channels. Since Ca^{2+} channels in rods are clustered near ribbons (Nachman-Clewner et al., 1999;Morgans, 2001;Dolphin et al., 2020), the persistence of fast release mediated by Syt1 suggests it involves vesicles at the base of synaptic ribbons. Conversely, the loss of slow release with 1 mM BAPTA suggests that Syt7-mediated asynchronous release involves sites further from ribbon-associated Ca^{2+} channels. There may also be a role for Syt7 in maintaining release during prolonged (e.g., 30 s) steps. At potentials above −50 mV when more Ca^{2+} channels are opening, non-ribbon vesicles appear to be recruited for

release. Buffering with 1 mM BAPTA eliminated the voltage dependent increase in ongoing vesicle release rates at −40 and −30 mV in Syt1 knockout rods. Eliminating Syt7 also reduced ongoing release rates at −40 and −30 mV but the effects were small suggesting a minor contribution from this sensor.

Spontaneous release can be important for circuit development, synaptic plasticity and shaping spiking patterns (McKinney et al., 1999;Carter and Regehr, 2002;Andreae et al., 2012). As in other neurons, spontaneous release in rods can be triggered by the stochastic opening of L-type Ca^{2+} channels, but vesicles can also be released independent of Ca^{2+} influx (Cork et al., 2016). Our results show that mouse rods are also capable of Ca^{2+}-independent spontaneous release since strong buffering by 10 mM BAPTA or inclusion of $CdCl_2$ in the extracellular medium did not eliminate spontaneous fusion events. At hyperpolarized potentials where Ca^{2+} channels are minimally active, spontaneous release rate were slow, consistent with previous measurements in mouse rod of ~0.9 Hz at −70 mV (Grassmeyer et al., 2019). This is similar to the rate of Ca^{2+}-independent release in amphibian rods after accounting for differences in the number of ribbons (1.3 v/s/ribbon)(Cork et al., 2016;Hays et al., 2020). The spontaneous rate in mouse cones averaged ~5 Hz and our serial reconstructions of mouse cones (n = 4 cones) show they have ~10 ribbons/cone (Li et al., 2005), yielding a rate of 0.5 v/s/ribbon. Salamander cones have 13 ribbons/cone (Pang et al., 2008a;Bartoletti et al., 2010) and a spontaneous rate of 11-12 Hz or 0.8-0.9 v/s/ribbon.(Sterling and Matthews, 2005).

While spontaneous release from rods held at −70 mV appeared to involve the stochastic release of individual vesicles, when rods were depolarized to −40 mV, we saw the emergence of multiquantal bursts of release, each involving 10-20 vesicles. We consider the mechanisms involved in the bursts below. In addition to their voltage-dependence, bursts were blocked by Cd^{2+} indicating that they require activation of voltage-dependent Ca^{2+} channels. Like Ca^{2+}-dependent release evoked by brief depolarizing steps, bursting at −40 mV was not observed in rods lacking

Syt1 (Grassmeyer et al., 2019). Elimination of Syt7 did not alter bursting. The loss of bursting that accompanied the loss of Syt1 may directly interrupt bursting or indirectly deplete an overlapping pool of vesicles, but these results nevertheless indicate that the vesicles involved in bursting can be released by Syt1-mediated mechanisms. Inclusion of 10 mM BAPTA in the patch pipette did not abolish the bursting that accompanied depolarization maintained for tens of second but did block release evoked by short depolarizing steps. It is likely that the buffering capacity was overwhelmed by the continued influx of Ca^{2+} during prolonged depolarizing stimulation. Consistent with this, large inward currents reflecting the activation of Ca^{2+}-activated Cl^- channels also persisted with 10 mM BAPTA. The persistence of bursting in the presence of BAPTA indicates that it involves vesicles that are within nanodomains that are close to Ca^{2+} channels and thus likely involves ribbon-associated vesicles.

The periods between bursts are not likely to be due to cessation of Ca^{2+} influx since $Ca_V1.4$ channels show minimal inactivation. The failure of AMPAR blocker NBQX to eliminate bursting suggests that horizontal cell feedback is not required for bursting behavior. The dihydropyridine agonist BayK8644, which extends the open time of L-type Ca^{2+} channels, did not reduce interburst intervals or extend burst duration. The interburst intervals were, however, extended by BAPTA, which may be due to a slower rate of replenishment with less available intracellular Ca^{2+} (Babai et al., 2010a). CICR contributes to slow release from rods (Cadetti et al., 2006;Babai et al., 2010b;Chen et al., 2014;Chen et al., 2015), but bursts were not abolished by a high concentration of ryanodine, the ryanodine receptor inhibitor dantrolene or an SOC inhibitor.

Burst sizes are likely constrained by the number of vesicles available for release. Synaptic ribbons appear specialized for multiquantal release. Multiquantal release can be sequential or tightly coordinated so that multiple vesicles are released simultaneously(Glowatzki and Fuchs, 2002;Singer et al., 2004;Graydon et al., 2011;Hays et al., 2020) (Glowatzki and Fuchs, 2002;Singer et al., 2004;Graydon et al., 2011;Hays et al., 2020). Synchronous fusion of multiple vesicles can

occur if multiple nearby vesicles are located within the same rapidly rising Ca^{2+} nanodomains (Graydon et al., 2011) or it can result from homotypic fusion of vesicles prior to release (Matthews and Sterling, 2008;Hays et al., 2020).

The BAPTA results suggest that vesicles involved in bursts are closely associated with ribbons. The apparent cross-depletion between vesicle pools involved in bursts and depolarization-evoked release, along with evidence that the number of vesicles in bursts roughly matched the number of vesicles released by a brief strong depolarizing step, together suggest that the pool of vesicles involved in bursts overlaps with the readily releasable pool of vesicles evident during strong depolarization. This latter pool is thought to reflect vesicles tethered at the base of the ribbon (Mennerick and Matthews, 1996;LoGiudice and Matthews, 2009). While bursts appear to be initiated by vesicles at the base of the ribbon located within Ca^{2+} channel nanodomains, the release of subsequent vesicles during the burst appears to involve sequential fusion of additional vesicles. The large smooth rise of the initial inward current during bursts suggests that some vesicles may also fuse synchronously as seen in salamander rods and mouse bipolar cells (Singer et al., 2004;Hays et al., 2020). The sequential nature of vesicle fusion during these bursts may be similar to multiquantal release in hair cells (Grant et al., 2010). In hair cells, it has been suggested that the complex release events reflect flickering of fusion pores (Chapochnikov et al., 2014). In our hands, $I_{A(glu)}$ were very uniform in both kinetics and magnitude at −70 mV suggesting full vesicle fusion, releasing one whole quantum during spontaneous release. The burst events at −40 mV consistently had larger charge transfer than spontaneous events, so it seems unlikely that they originate from a single vesicle.

One strategy for achieving reliable transmission of single photon responses at the rod synapse is to maintain extremely fast release rates; however, we found that release from rods at −40 mV and 35 °C averaged only ~10 v/s/ribbon, substantially lower than the rate of ~100 vesicles/s that is needed for reliable transmission assuming a purely Poisson release process (Rao

et al., 1994;Rao-Mirotznik et al., 1998;van Rossum and Smith, 1998). There may be two advantages to keeping the overall release rate low. First, as the quantal rate increases, the fractional change in rate produced by photon absorption increases (Schein and Ahmad, 2006). Furthermore, maintaining a high rate of release during long periods of darkness requires a tremendous amount of energy and other cellular resources (Okawa et al., 2008;Linton et al., 2010;Yuan et al., 2018). An alternative strategy for making release more reliable is to make it more regular. This can improve the ability of downstream bipolar cells to detect small changes in release rate caused by small single photon responses (Schein and Ahmad, 2005;2006). At the dark resting membrane potential of −40 mV, we consistently observed large multivesicular release events that occurred at semi-regular intervals. These bursts were characteristic of rods but not cones, suggesting a particular role for transmitting scotopic signals. The role of bursting in transmission of single photon light response of rods is explored further in Chapter 4.

CHAPTER 4: Rod signaling at the dark potential

Abstract

Rod photoreceptors are specialized to transduce and transmit single photon responses to the visual system. This remarkable proficiency depends on reducing the rate of glutamate release sufficiently to be appreciated post-synaptically in rod bipolar cells. We discovered that at their resting membrane potential in darkness, rods release coordinated bursts of vesicles rather than rapid stochastic uniquantal release events. In this chapter, we examined the statistical properties of release and tested sensitivity of bursting to small voltage changes similar to those produced in rods by absorption of a single photon. Spontaneous release of individual vesicles in rods voltage-clamped below the threshold for activating voltage-gated Ca^{2+} currents occurred stochastically and obeyed Poisson statistics. The transition from uniquantal release to bursts appeared reliably as the membrane potential approached −40 mV in rods. Hyperpolarizing rods from −40 to −43.5 mV, similar to the voltage change evoked by a single photon response, reduced burst frequency. The interval between bursts immediately following this step was significantly longer than the average interevent interval measured at −40 mV. Application of a voltage stimulus that mimicked the waveform of a 3.4 mV single photon response reduced the probability of seeing a burst nearly to zero with a rebound increase in probability at stimulus offset. Using white noise stimuli, the waveform that preferentially triggered bursts was a small hyperpolarization followed by depolarization with a time course similar to single photon responses. Simulations of release frequency suggest that the sensitivity of bursting to small voltage changes may contribute to a non-linearity at the rod synapse that discards responses below a certain threshold to favor larger responses.

Introduction

One of the most impressive features of the vertebrate visual system is the ability to detect signals from single photons. Pioneering psychophysical studies showed that humans can see light flashes consisting of a dozen or less photons falling on the retina, suggesting that individual rods must be capable of responding to absorption of single photons of light (Hecht et al., 1942). The ability of rods to respond to single photons was later confirmed by electrophysiological recordings from single rods (Baylor et al., 1984;Rieke and Baylor, 1998;Gross et al., 2015;Reingruber et al., 2015). In primates, absorption of a single photon evokes a response of approximately 1 mV (Schneeweis and Schnapf, 1995;Hornstein et al., 2005). In mouse rods, single photon responses are a bit larger, averaging around 3.4 mV (Cangiano et al., 2012). The perception of single photons by the visual system requires that rods reliably transmit these small voltage changes to downstream neurons.

In darkness, rods maintain a relatively depolarized membrane potential near −40 mV. This membrane potential is sufficiently depolarized to activate $Ca_V1.4$ L-type Ca^{2+}channels that control synaptic glutamate release from rods. $Ca_V1.4$ channels show minimal voltage- and Ca^{2+}-dependent inactivation, allowing for sustained Ca^{2+} influx into rod terminals in darkness (Baumann et al., 2004;Waldner et al., 2018). This in turn promotes the continued release of glutamate by rods that acts on ON-type rod bipolar cells. As rods hyperpolarize to light, the resulting decline in Ca^{2+} channel activity slows the rate of ongoing vesicle release leading to the opening of TRPM1 cation channels in rod bipolar cells and thus membrane depolarization.

Synaptic release is an intrinsically noisy process that is typically described by Poisson statistics (Zhang and Peskin, 2015;Malagon et al., 2016;Miki, 2019). The challenge for a recipient rod bipolar cell is to distinguish a genuine slowing of release caused by a small hyperpolarizing single photon response from a random pause in release. One proposed solution is to sustain a very high rate of release. Given Poisson statistics, for true single photon- driven pauses to be reliably

distinguished from a random long interevent interval, the minimum quantal release rate has been calculated to be 80-100 vesicles per second (Rao et al., 1994;Rao-Mirotznik et al., 1998;van Rossum and Smith, 1998;Schein and Ahmad, 2005). This is substantially faster than most conventional neurons (Rao et al., 1994) although ribbon synapses in turtle cones may be capable of sustaining release rates of up to 80 v/s/ribbon (Copenhagen et al., 1983). However, salamander rods, salamander cones, and gecko rods all appear to release vesicles at slower rates of 10-20 v/s/ribbon (Sheng et al., 2007). Post-synaptic measurements suggest that release from mammalian cones is also relatively slow with a rate of 18 v/s/ribbon (Berntson and Taylor, 2003). Our results reported in Chapter 3 report the first direct measurements of release rates at a mammalian rod synapse and find a sustained release at a rate of ~10 v/s/ribbon at −40 mV, much slower than that required for accurate single photon detection.

A second strategy to avoid detection of false positive events due to random intervals is to make release more regular. Schein and Ahmad formulated the clockwork hypothesis which proposes that the rate of release is not purely Poisson, but is a more regular Erlang process that waits for a large number of Poisson event intervals before triggering a release event(Schein and Ahmad, 2005) (Schein and Ahmad, 2005). The sustained release of glutamate from rods involves a plate-like, presynaptic structure known as the synaptic ribbon. Ribbons tether vesicles along their planar surfaces and then deliver them to release sites at the base (Snellman et al., 2011;Vaithianathan et al., 2016). Sustained release at photoreceptor ribbon synapses is thus limited by the rate at which vesicles are delivered to release sites (Jackman et al., 2009). It was proposed that the wait times required for delivery and docking of vesicles at the base of the ribbon (i.e., replenishment) would be one possible mechanism that could yield an Erlang process at rod synapses.

Spontaneous release of vesicles from salamander rods and cones shows an exponential distribution of interevent intervals consistent with Poisson release statistics (Cadetti et al.,

2005;Cork et al., 2016) but amphibian rods have ~7 ribbons and amphibian cones have ~13 ribbons making it difficult to assess release properties at an individual ribbon. By contrast, mammalian rods have only a single ribbon. We took advantage of this feature and recorded individual glutamate release events from mouse rods to examine release statistics at single ribbon synapses. To measure release, we recorded presynaptic anion currents coupled to glutamate transporter activity in rod terminals. The glutamate transporters in rods (largely EAAT 5) are linked to an uncoupled anion conductance so that as glutamate is retrieved, an anion channel is opened (Arriza et al., 1997;Schneider et al., 2014). Using this approach, we found that when rods were voltage-clamped at −70 mV, spontaneous release of single vesicles occurred stochastically at rates that followed Poisson statistics; however, when rods were held at the typical resting membrane potential in darkness of −40 mV, sustained release occurred in regularly spaced bursts of ~17 vesicles apiece. Small hyperpolarizing steps and voltage waveforms that simulated single photon responses both produced abrupt decrements in the rate of these bursts. Event-triggered average waveforms obtained from white noise stimuli showed that bursts were preferentially triggered by a small hyperpolarizing voltage excursion followed by a larger depolarizing excursion, with a time course similar to single photon responses of rods. A key property of transmission from rods to rod bipolar cells is the presence of a thresholding non-linearity that discards synaptic noise along with some small but genuine responses. Our results are consistent with other evidence that this non-linear threshold occurs prior to summation of rod inputs in the rod bipolar cell (van Rossum and Smith, 1998;Field and Rieke, 2002;Sampath and Rieke, 2004). Furthermore, we suggest that the sensitivity of this bursting behavior to small voltage changes may be an important presynaptic component to this thresholding non-linearity.

Methods

Animals

Control mice of predominately or wholly C57/Bl6 backgrounds were kept on 12-hour dark-light cycles and experimentation was performed with the approval of the University of Nebraska Medical Center Institutional Animal Care and Use Committee. Mice of both sexes aged 4-12 weeks were euthanized in accordance with the AVMA Guidelines for the Euthanasia of Animals by CO2 asphyxiation and cervical dislocation.

Electrophysiology

Rod cells were visualized in a flatmount preparation performed on an upright fixed-stage microscope (Nikon E600FN) under a 60x water-immersion objective. Rod inner segments and cell bodies were identified morphologically and targeted with positive pressure using recording electrodes mounted on Huxley-Wall micromanipulators (Sutter Instruments). Rod recordings were performed in whole-cell voltage clamp using an Axopatch 200B amplifier (Axon Instruments/Molecular Devices) and signals were digitized with DigiData 1550 (Axon Instruments/Molecular Devices). Data acquisition and analysis was performed on pClamp 10 Software (Molecular Devices). Voltages were not corrected for liquid junction potential (KSCN pipette solution: 3.9 mV). All experiments were performed in room light.

Flatmount preparations were continuously superfused with room temperature Ames solution (US Biological) bubbled with 95% O_2 /5%CO_2 at ~1 mL /minute unless otherwise noted. Intracellular solutions for $I_{A(glu)}$ measurements contained (in mM): 120 KSCN, 10 TEA-Cl, 10 HEPES, 1 $CaCl_2$, 1 $MgCl_2$, 0.5 Na-GTP, 5 Mg-ATP, 5 phospho-creatine, pH 7.3. Intracellular solution was buffered with 5 mM EGTA. Passive membrane properties averaged C_m = 3.2 ± 0.2 pF; R_s = 2.3 ± 0.04 GΩ (mean ± SD, n = 20).

$I_{A(glu)}$ event frequency, kinetics, and charge transfer were identified with the event finder function in pClamp directed by a template that included a sampling of ~10 manually curated events. Statistical analysis was performed on GraphPad Prism 7 and all data are represented as mean ± SEM unless otherwise noted.

Statistical Analysis

To test whether release rate reflected a Poisson process at −70 and −40 mV, interevent interval histograms were fit with a one-phase exponential decay. In another approach, the number of release events was tallied over a long period (30 s) to calculate the average number of release events per second (λ). A fractional frequency distribution of events was then made using 1-second bins and fit with a Poisson model (see equation 1 below) where *P* is the probability of observing *x* number of events, and *e* is Euler's constant. We calculated the best fit λ value (mean events in an interval) in that cell using GraphPad Prism 7.

$$\text{Equation 1: } P(x) = \frac{\lambda^x e^{-\lambda}}{x!}$$

Results

As described in chapter 3, we recorded $I_{A(glu)}$ from individual rods in flatmount mouse retina preparations to study the voltage- and Ca^{2+}- dependent changes in release at single rod ribbons (Fig. 32). Spontaneous inward currents in rods voltage-clamped at −70 mV showed a unimodal amplitude distribution suggesting they consist entirely of uniquantal events (Fig. 19, Chapter 3). The increased rate of vesicle release with membrane depolarization involves a switch to more coordinated forms of release with semiregular bursts dominating release in rods held at −40 mV (Fig. 32). As described in the last chapter, these bursts consist of 10-20 vesicles (17 ± 7, mean ± SD), are triggered by Ca^{2+} influx and derive from a readily releasable pool of vesicles shared with evoked release. Release rates increase with temperature in proportion to rod I_{Ca} (Ref. Chapter 3), attaining a rate of ~10 v/s/ribbon at the dark resting membrane potential of −40 mV at

35 °C. This is too slow to reliably encode small single photon voltage responses by simple changes in rate, assuming Poisson release statistics (Rao et al., 1994;Schein and Ahmad, 2006).

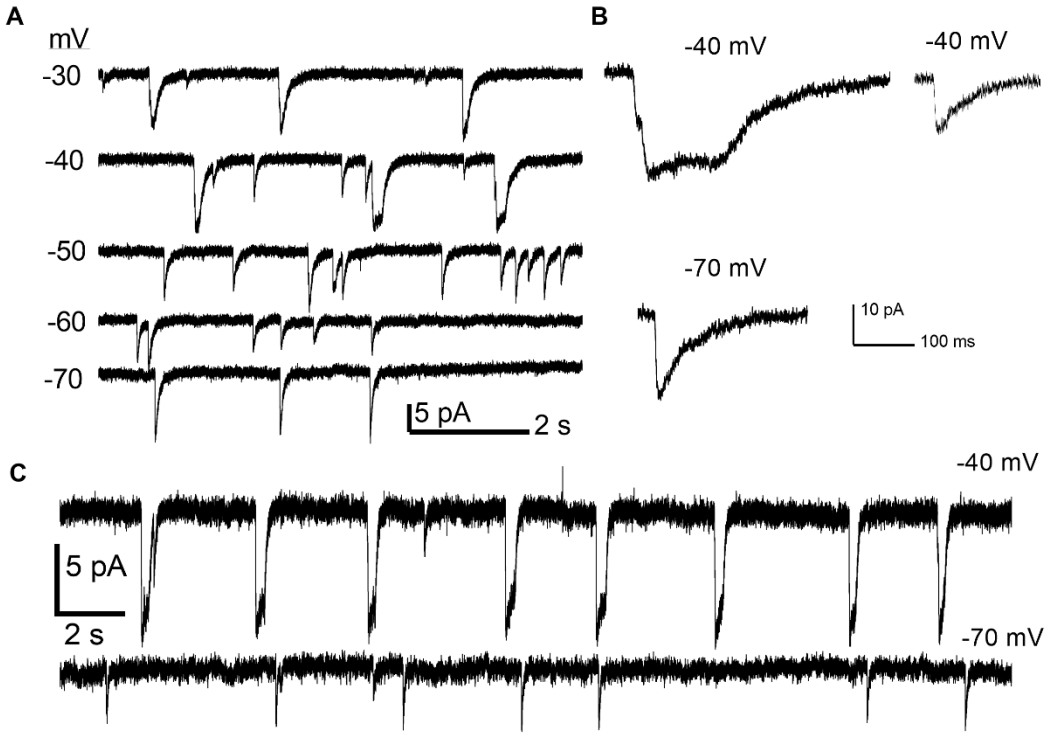

Figure 32 The quantity of glutamate released, measured by $I_{A(glu)}$, increases with depolarization but near −40 mv, release is coordinated in bursts of 10-20 vesicles rather than single vesicle fusion events. **A.** Representative traces from a single rod clamped at various voltages. **B.** Panel B illustrates a burst and unitary event at −40 mV and a unitary event at −70 mV. **C.** Panel C shows long recording segments to illustrate the stochastic release of individual events at −70 mV and more regular bursting at −40 mV.

Release in Bursts is not Modeled by Poisson Statistics

It is generally accepted that under conditions of low release probability, vesicle exocytosis occurs stochastically, obeying Poisson statistics (Zhang and Peskin, 2015;Malagon et al., 2016;Miki, 2019). Spontaneous release can occur due to chance openings of voltage-gated Ca^{2+} channels or can be Ca^{2+}-independent (Kavalali, 2015;Cork et al., 2016;Kavalali, 2019). The persistence of spontaneous release events in rods held at −70 mV even in the presence of

extracellular Cd^{2+} or intracellular 10 mM BAPTA showed that they are Ca^{2+}-independent events (Chapter 3). For analyzing frequency distributions of events, only rods in which we observed >50 spontaneous or burst events were included in the data set. The frequency distributions of interevent intervals for release events detected in rods voltage-clamped at −70 mV consistently exhibited a one-phase exponential decay as predicted for a Poisson release process (R^2 = 0.96 ± 0.05, mean ± SD, n = 8) (Fig. 33A) The probability of the number of release events that occur in a 1 s interval was also well fit by assuming a Poisson distribution (Fig. 33C). The Poisson fit for spontaneous events was robust (R^2= 0.94 ± 0.07, mean ± SD, n = 8) and the best fit value of the mean number of events per second, λ, was similar to the actual mean number of events observed in the sample (p = 0.72, n = 8).

These results indicate that the rate of Ca^{2+}-independent spontaneous release from rods is a Poisson process. What about higher rates when Ca^{2+}-dependent release is engaged at more depolarized potentials? If we treat bursts as single release events, histograms of interburst intervals cannot be fit by single exponential decay (Fig. 33C). Fitting the interburst intervals with a Gaussian function yielded better fits (mean R^2 = 0.84 ± 0.12) than an exponential decay and suggested a coefficient of variation of 0.64 ± 0.20 (n =8). If the multiple vesicles released in a burst are considered as separate events, the distribution of such events in time also cannot be modeled by a Poisson distribution. When time was binned into 1-second intervals, there were either many vesicles (a burst) or none released during each time interval. This caused events to be distributed in a bimodal fashion. We attempted fitting the frequency distribution with the Poisson model equation (equation 1), with λ constrained to the measured number of mean events/s. As illustrated in Fig. 33D, the fit was quite poor and yielded $-R^2$ values (-0.5 ± 05, n = 8) indicating that the Poisson distribution does not appropriately model this phenomenon.

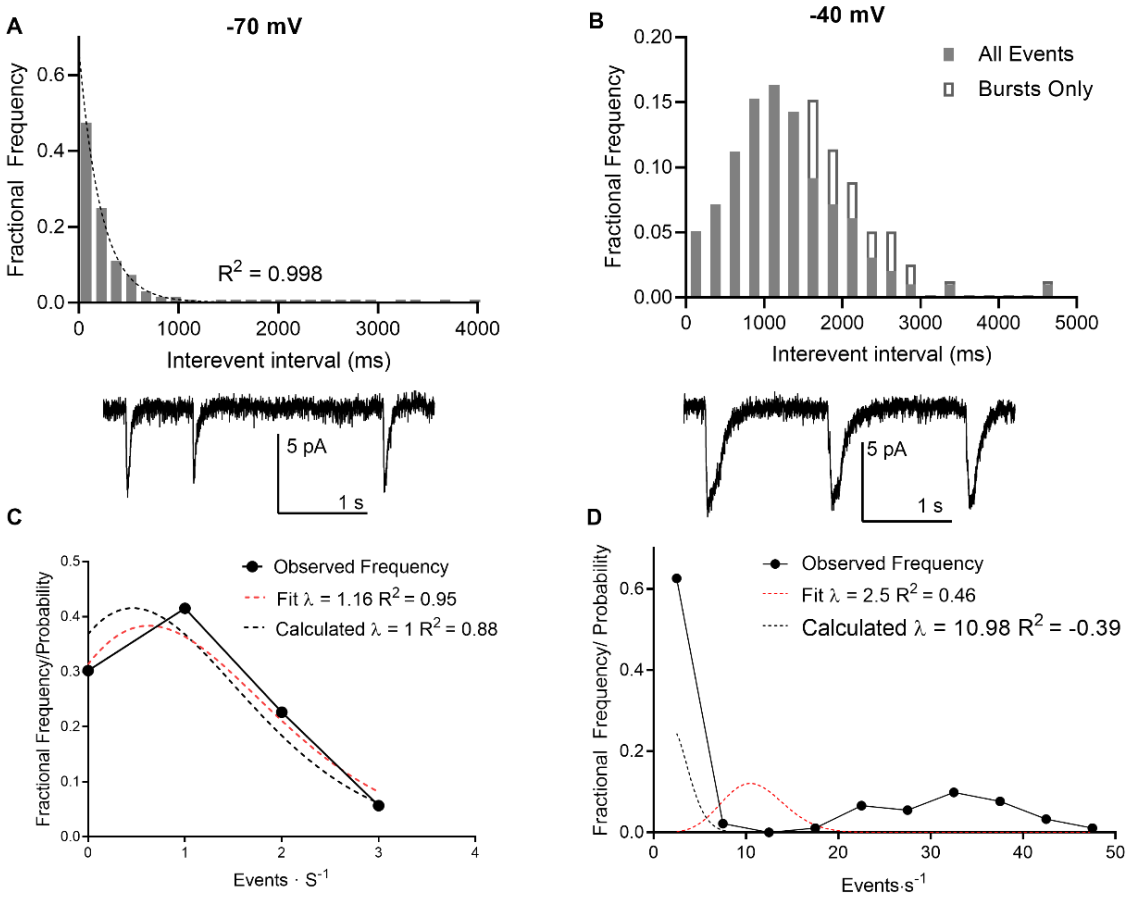

Figure 33 Sustained release rate in bursts is not Poisson. Panels **A** and **C** show spontaneous release obeys the Poisson model. A. Interevent intervals fit a one phase exponential decay (τ = 220). **B**. If bursts are considered single events, their interevent intervals do not show an exponential decline consistent with a Poisson model, even when also considering the unitary events between bursts. **C.** Using equation 1, we fit the probability of seeing a number of events in 1 second bins to the frequency per second measured over 90 − 180 s recording. We obtained a good fit when we constrained the fit to the calculated mean events per second of $\lambda = 1$ (dashed black line, calculated, R^2 =0.88) and obtained an event better fit with a similar value for λ when it was unconstrained (dashed red line, fit $\lambda = 1.16$, $R^2 = 0.95$). **D.** Because bursts are asynchronous, if we consider the quanta released in a burst to be separate release events, there are either 0 or ~35 events happening per second. This is also not well modeled by Poisson statistics, both when the software was constrained the λ was constrained to match the mean rate of 2.5 (dashed red line, $R^2 = 0.46$) calculated from long observations, or when λ was unconstrained (dashed black line, best fit $\lambda = 10.98$, $R^2 = -0.39$).

Bursting is Sensitive to Small Voltage Changes

As shown in Chapter 3, the bursting behavior was not observed in cones, occurred only near the typical membrane potential in darkness, and was not distributed in time in a Poisson

manner. Therefore, we hypothesized a role for this form of coordinated release in the synaptic transmission of small single photon events. Cangiano et al. measured the photovoltage in mouse to average 3.44 mV; we applied a hyperpolarizing step of 3.5 mV to investigate its effects on burst frequency(Cangiano et al., 2012) (Cangiano et al., 2012). After significant (30 s) periods of time clamped at –40 mV, a 3.5 mV hyperpolarizing step to −43.5 mV caused a pause in bursting. Comparing the average interburst intervals measured for 30 s at −40 mV with those measured for 30 s at −43.5 mV, we saw significantly longer intervals (1846 ± 1055 ms vs 3106 ± 1808, $p < 0.0001$, paired t-test, $n = 4$). When we looked at the period immediately after applying the step to −43.5 mV, bursts were delayed substantially so that bursts were absent for seconds afterwards (red triangles in Fig. 34B). The shortest interburst interval (3 s) seen after stepping to −43.5 mV (red triangles) exceeded the standard deviation of interburst intervals measured at −40 mV. Smaller hyperpolarizing steps of −1 ($n = 3$; filled circles, Fig. 34B) and −2 mV ($n = 3$; stars, Fig. 34B) also caused an appreciable pause in bursting immediately after the step.

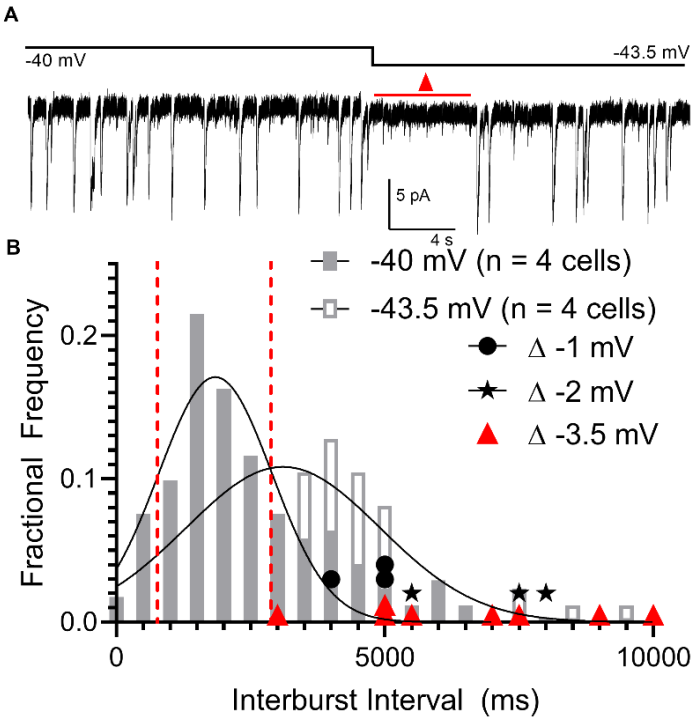

Figure 34 Bursts were sensitive to small hyperpolarizing steps. A. Example trace showing that bursts of $I_{A(glu)}$ release events paused for several seconds immediately after hyperpolarizing the rod from −40 to −43.5 mV and the rate of bursting remained slower for the duration of the step. Red triangle denotes the time interval we were measuring to plot as red triangles in panel B. **B.** Frequency distribution of intervals between bursts measured at −40 and −43.5 mV (n = 4), each fit with a single Gaussian. Hyperpolarization slightly extended the mean interburst from 1846 ± 1055 ms to 3106 ± 1808 ms interval during the entire 30 s step to −43.5 mV ($p < 0.0001$, paired t-test). Filled circle, star and triangles show the longer interval measured directly after hyperpolarizing steps of 1, 2, or 3.5 mV, respectively. All of these intervals were >1 standard deviation of the mean interburst interval at −40 mV (red dashed lines).

To further investigate the capability of a single photon absorption event to reduce bursting, we clamped rods at –40 mV and applied a voltage stimulus waveform mimicking a single photon voltage response (Fig. 35A). The simulated single photon response was constructed from a two exponential function that rose with a time constant of 1 s and declined with a time constant of 2.5 s, attaining a peak amplitude of 3.4 mV with a time to peak of 245 ms (Fig. 35A)(Cangiano et al., 2012). For each cell held at −40 mV, the simulated single photon voltage stimulus was repeated for 30 trials (Fig. 35B). When a rod received 30 consecutive simulated photons, a burst event was

almost never observed during the hyperpolarizing stimulus, suggesting that rods are able to adjust release probability for even these small voltage changes. The probability of observing the onset of a burst event during the 300 ms period of the simulated single photon was 0.016, significantly lower ($p = 0.008$, $n = 6$ rods, repeated measures ANOVA) than the probability of observing a burst in 300 ms time bins randomly chosen at any time prior to the simulated flash (0.15) and even lower than the probability (0.27) of observing a burst event during the 300 ms period immediately following the simulated single photon response ($p = 0.002$, $n = 6$, repeated measures ANOVA; Fig. 4C). The voltage stimulus prevented further bursting during the hyperpolarization but did not truncate bursts that had started just prior to the stimulus because bursts that were operating during the stimulus had the same number of quanta, measured by charge transfer, to those prior ($p = 0.53$, t-test , $n = 5$ rods).

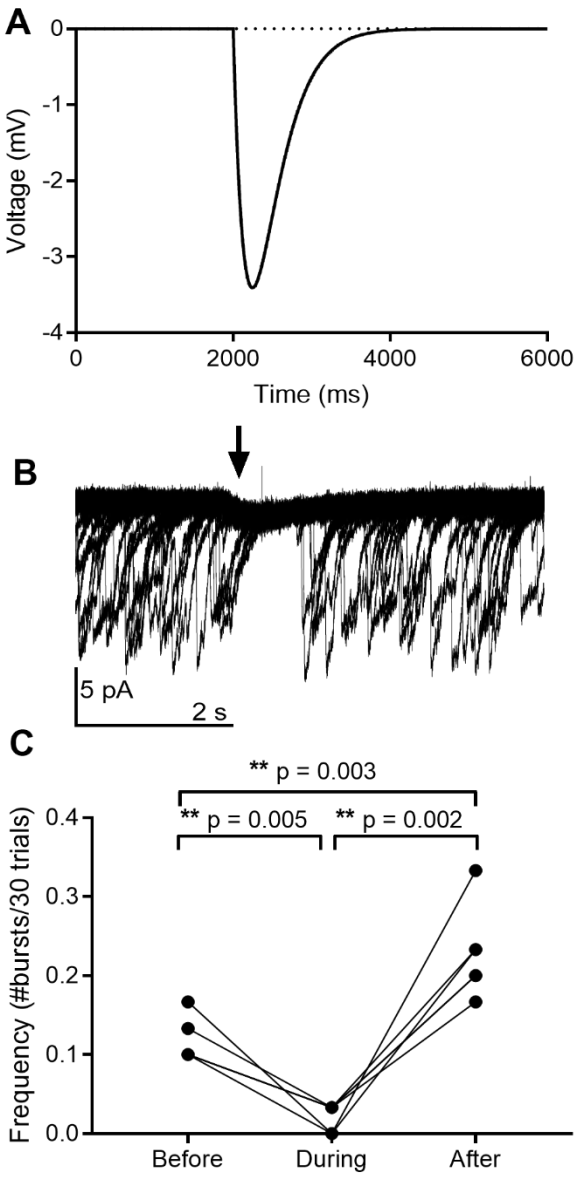

Figure 35 Rods voltage clamped at −40 were presented a simulated single photon voltage stimulus. A. Voltage stimulus had an amplitude of −3.4 mV and time to peak of 245 ms, matching the single photon responses measured in mouse rods by Cangiano et al. (2012)(Cangiano et al., 2012). B. When a rod was presented with the stimulus 30 consecutive times (black arrow), there was an appreciable pause in release during hyperpolarization. C. Summary data showing the number of burst events, out of a maximum possible 30, initiated in 300 ms intervals at a random time before the stimulus, beginning 50 ms into the stimulus and immediately following the stimulus. Burst events were almost never observed during the single photon waveform. The probability of observing a burst before, during, or after the stimulus was different p = 0.0005, 2-way ANOVA, Tukey's multiple comparisons, n = 6)

Fig. 36A illustrates the effect of 1 rod absorbing a photon among a population of 20 rods assuming linear convergence onto a single rod bipolar cell (Rao-Mirotznik et al., 1998;Calkins and Sterling, 1999). In this example, we overlaid a single trace recorded from a rod stimulated by application of a single photon voltage waveform on top of 19 traces from 3 rods that did not receive a simulated photon. It is difficult to distinguish the stimulus from a random pause in release (asterisk). When we repeated this by overlaying 5 responses from 1 rods onto 15 non-responding traces from 5 rods, the change in bursting induced by the simulated photon was more easily distinguished from random pauses (Fig. 36B). Occurrence of the flash was even more easily distinguished when we overlaid 10 responding rods and 10 non-responders (Fig. 36C).

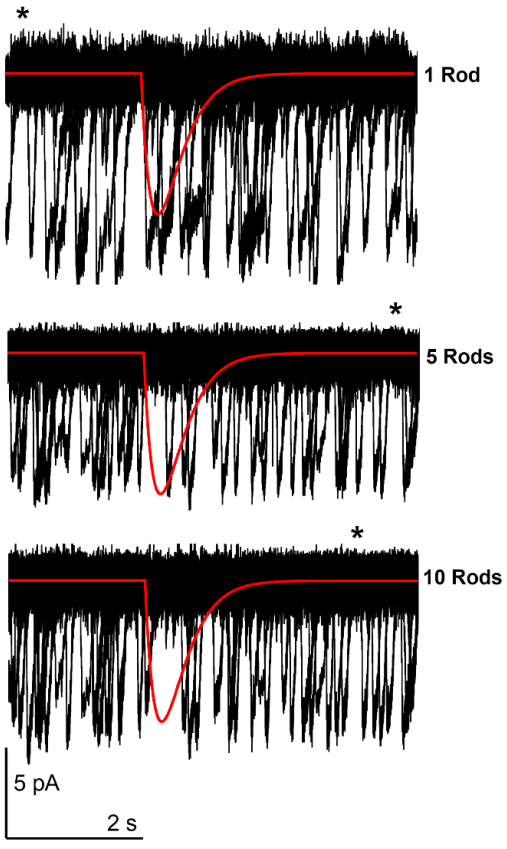

Figure 36 Examples overlaying 20 rod traces in which 1, 5, or 10 rods received simulated single photon voltage stimuli while the remaining rods were held continuously at −40 mV. Black asterisks denote possible false positives. Traces where voltage stimulus was applied came from the same rod, while the remaining traces came from random 6 s samples of 3 rods held at −40 mV. The red trace shows the single photon voltage stimulus.

Release Simulations

The initial increase in rod $I_{A(glu)}$ integrates the rise in cleft glutamate levels. $I_{A(glu)}$ events associated with individual vesicles declined with a time constant close to 50 ms, consistent with the slow cycle time for glutamate transport (Arriza et al., 1997;Gameiro et al., 2011). In salamander rods, the glutamate transporters were estimated to be at least 3 microns from release sites (Hays et al., 2020). The mGluR6 glutamate receptors of rod bipolar cells are located 400-800 nm from ribbons (Rao-Mirotznik et al., 1998). mGluR6 receptors act through G_o proteins to close TRPM1 channels in the rod bipolar cell membrane (Morgans et al., 2009;Morgans et al., 2010). This cascade has slow kinetics of activation during glutamate onset with and then slowly de-activates, with latencies of tens of milliseconds similar to $I_{A(glu)}$ kinetics (Snellman et al., 2008;Morgans et al., 2010). As a first approximation, $I_{A(glu)}$ provides a reasonable estimate for the kinetics of rod bipolar cell currents evoked by glutamate release from rods.

To examine the ability of a post-synaptic neuron to detect changes in release produced by absorption of a photon, we compared Gaussian distributions of $I_{A(glu)}$ release rates in rods held at −40 mV to simulate rates in darkness and rates observed while applying the voltage waveform for a single photon response. In the trials described above, the rate of bursting measured at −40 mV averaged 0.46 ± 0.15 bursts/s (S.D., n = 7). This rate declined to 0.06 ± 0.06 bursts/s during the 300 ms interval of the single photon voltage waveform and then rebounded to 0.752 $\underline{+}$ 0.188 bursts/s during the 300 ms immediately afterwards. Fig. 37A compares these distributions. There is very little overlap between the burst frequencies seen in darkness and following absorption of a photon and even less overlap between the single photon response and the rates measured immediately afterward. This indicates that absorption of a single photon could be readily detected at that synapse, but only if the sampling window was long enough.

When we plotted interburst intervals against time after patch rupture, we saw a small but significant rundown in the rate of bursting during the recording ($m = 0.002$, $p < 0.01$, $n = 4$). As

described in Chapter 3, physiological temperatures permitted faster bursting by a factor of 2.2. These data suggest that our calculations of burst rates made during sustained periods of depolarization may underestimate rates of bursting and variance. The fastest rate of bursting at room temperature was 0.7 bursts/s, suggesting that at physiological temperatures, a rod may be able to achieve a rate of 1.5 bursts/s *in situ*. As we consider in the general discussion, this faster rate improves the likelihood that a bipolar cell may sense the change in absorption of a photon by a presynaptic rod.

Previous studies suggested a non-linearity in the transmission of small responses from rods to rod bipolar cells and that this non-linearity occurs in the bipolar cell dendrite prior to summation of responses in the soma (Field and Rieke, 2002;Taylor and Smith, 2004;Okawa and Sampath, 2007). We multiplied the mean rate and variance in darkness by 20 to simulate linear summation of responses from 20 rods into a rod bipolar cell. We then simulated photon absorption in 1, 5 or 10 rods, matching the conditions illustrated by the overlaid waveforms in Fig. 36. To do so, we replaced the "dark" mean rate and variance from 1, 5 or 10 rods with the lower mean and variance measured during a simulated flash. As illustrated in Fig. 37B, because the rate change produced by a response in one rod was only a small fraction of the total rate, linear summation of inputs obscured the ability of the post-synaptic neuron to detect absorption of a photon by one rod in the total population of 20. If we assumed that 10 photons were absorbed simultaneously in the population of 20 rods, the post-synaptic bipolar cell could reliably detect the light flash if the rate by setting a detection threshold of 5.9 bursts/s. However, this comes with a cost that 12.9% of random changes in rate during darkness would also be falsely detected as light responses. Doubling the overall rates to simulate the rates at 35 °C did not noticeably improve detection thresholds (not shown). These data are consistent with other evidence for the presence of a nonlinear thresholding mechanism placed prior to summation of responses in the bipolar cell soma (Field and Rieke, 2002;Sampath and Rieke, 2004).

We next compared the benefits of semi-regular bursting behavior to a simple Poisson distribution. In this case, we assumed that the rate of release in darkness followed Poisson statistics, showing variance equal to the mean rate. From the results of Chapter 3, we used the mean overall vesicle release rate of 9 v/s measured at −40 mV and reduced that this rate to 7 v/s during the light flash. As illustrated in Fig. 37C, the difference in release rates produced in a single rod is not sufficient for detection of a single photon (assuming a neurometric threshold of 75% correct). Linearly summing inputs from 20 cells and assuming that the rate dropped to zero during the flash (Fig. 37D), the overall distributions were not much different from the distributions seen when summing inputs from 20 cells but using the properties of bursting (Fig. 37B). These data suggest that without some coordination among rods, the semi-regular bursting behavior is not, by itself, enough to greatly improve detection thresholds. Instead, the most important property of bursting behavior is the tremendous fall in the likelihood of a burst occurring during the single photon flash. This suggests that in addition to non-linearities involving the rod bipolar cell mGluR6 glutamate receptor, there is also a significant presynaptic non-linearity that shapes the time course and size of glutamate pulses detected by these receptors.

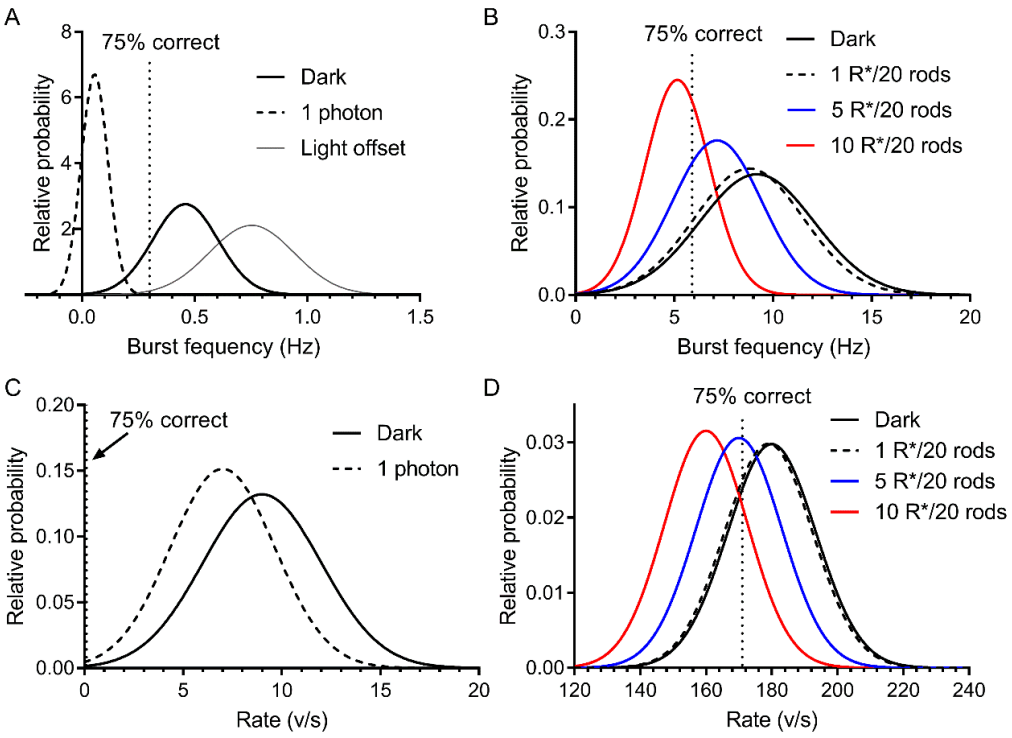

Figure 37 Assessing the capability for photon detection. A) Gaussian distributions of burst rates measured in rods held at −40 mV (data from Fig. 4, 0.459 ± 0.145 bursts/s, S.D., n = 7, black trace), rates observed while applying the voltage waveform for a single photon response (0.056 ± 0.059 bursts/s, dashed trace), and rate measured during a 300 ms period after the end of the stimulus (0.752 ± 0.188 bursts/s, gray trace). B. Mean rate and variance from 20 rods assuming linear summation. Absorption of a photon by 1 (dashed trace), 5 (blue trace) or 10 (red trace) rods, was simulated by replacing the "dark" mean rate and variance with the lower mean and variance measured during a simulated flash for 1, 5 or 10 rods. C) Distribution of rates assuming Poisson statistics for single vesicle release rates of 9 ± 3 v/s in darkness (black trace) and 7 ± 2.2 v/s (dashed trace) during the light flash. D) Photon absorption by 1 (dashed trace), 5 (blue trace) or 10 (red trace) rods was simulated with Poisson statistics in a population of 20 rods by assuming that the rate and variance dropped to zero if a rod absorbed a photon. For all panels, probabilities were normalized relative to a rate of 1 event/s. Neurometric threshold of 75% correct is shown as a vertical dashed line.

White Noise Analysis

To identify the voltage changes that preferentially evoke bursting in rods, we held rods at −40 mV and applied a white noise voltage stimulus with a standard deviation of 3.5 mV and high frequency cutoff of 5 Hz, consistent with the rod power spectrum (Chichilnisky and Rieke, 2005). The average stimulus waveform that preceded each burst, i.e., the event triggered average (ETA)

waveform, consisted of a small hyperpolarizing excursion followed by a larger depolarizing excursion with a total time course roughly similar to that of a single photon response. (n = 4; Fig. 38A). Using a white noise voltage stimulus with a smaller standard deviation (0.8 mV), the ETA showed a waveform with a similar shape and time course (Fig. 38B). When we tested a similarly small stimulus but with 20 Hz cutoff, the ETA appeared as noise (Fig. 38C), suggesting the rod terminal preferentially responds to slow voltage changes with the frequency response characteristics of rods in light and dark, filtering out faster frequency membrane voltage noise. These data reinforce the idea that rods are very sensitive to small voltage changes similar to those experienced during a single photon response, consistent with a role of these bursts in helping to encode small light responses at the rod ribbon synapse.

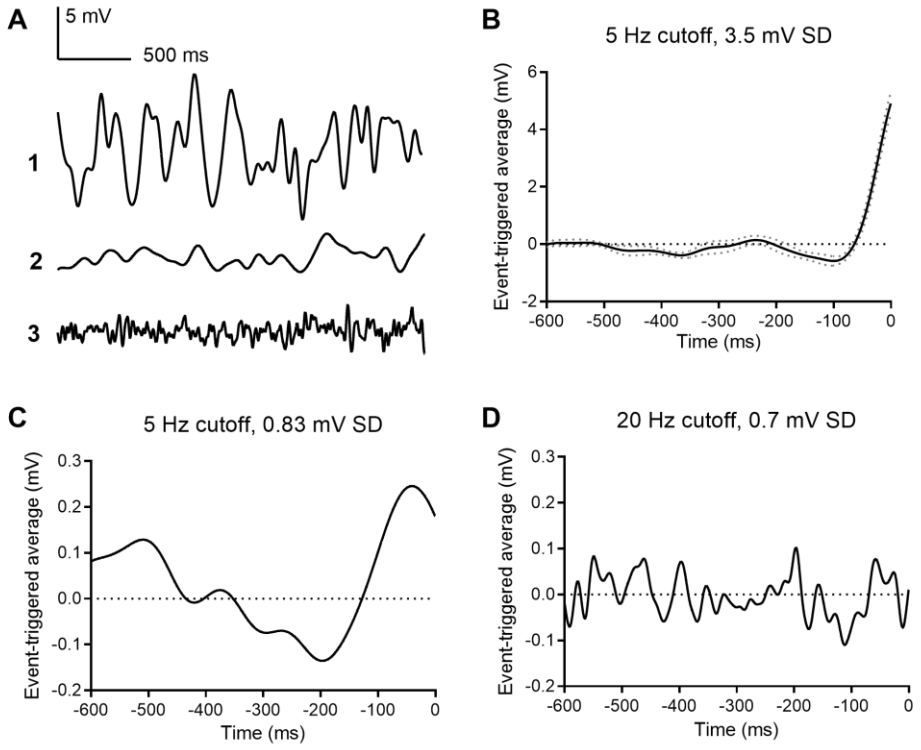

F**igure 38** Event triggered averages (ETAs) were compiled from 600 ms segments of the white noise voltage stimulus. **A.** 2.5 s segments of white noise voltage stimulus with 5 Hz cut-off and 3.5 mV SD. **B.** ETA evoked by the same white noise stimulus. **C.** ETA evoked by a smaller stimulus with 5 Hz cutoff but only 0.8 mV SD. **D.** ETA evoked by a white noise stimulus with 20 Hz cut-off and 0.8 mV SD appeared as noise.

Discussion

In this study, we examined the mechanisms by which tonic release from rods can be regulated by small changes in membrane potential. Using $I_{A(glu)}$ to measure release presynaptically, we found that at a membrane potential similar to that experienced in darkness, rods released glutamate-filled vesicles in coordinated bursts at rates that were not modeled by Poisson statistics. These bursts of release were exquisitely sensitive to small voltage changes. In the discussion below we consider their possible role in transmitting small single photon responses of rods.

The ability of the vertebrate visual system to detect single photons signals arises from the high photon capture rates and high gain of the phototransduction cascade in rods. Next, the small changes in membrane voltage produced by absorption of a single photon must produce an appreciable change in the rate of release at the rod synapse. At the synapse from rods to rod bipolar cell dendrites, there is a non-linear thresholding mechanism in which only responses that exceed a certain size are transmitted, removing baseline noise along with smaller responses that fall below that threshold (Field and Rieke, 2002;Berntson et al., 2004b;Sampath and Rieke, 2004). In mouse retina, where ~20 rods converge onto each rod bipolar cell (Rao-Mirotznik et al., 1998;Calkins and Sterling, 1999), comparisons of recordings from rods and rod bipolar cells found thresholds that excluded 40-85% of the single photon events in rods (Field and Rieke, 2002;Berntson et al., 2004b;Schein and Ahmad, 2006). In rabbit retina, where 100 rods converge onto each rod bipolar cell, as many as 90% of the single photon responses are removed by the thresholding mechanism (Trexler et al., 2011). Finally, as many as 75,000 rods eventually converge onto a single ganglion cell, allowing the capture of scarce single photons to produce detectable changes in retinal output (Taylor and Smith, 2004;Okawa and Sampath, 2007).

Computer simulations suggested that, assuming a purely Poisson release process, post-synaptic detection by rod bipolar cells requires rod release rates of 80-100 $Q \cdot s^{-1}$ (Rao et al., 1994;van Rossum and Smith, 1998). However, as shown in Chapter 3, the overall rate of release

from rods only attained 9 or 10 v/s at −40 mV and 35 deg C, with rates half as slow at room temperature (Chapter 3). Similarly low rates have been found in experiments from non-mammalian rods using activity-dependent dyes, with gecko rods show a release rate in darkness of 2.5 v/s/ribbon and salamander rods a rate of 18 v/s/ribbon suggesting these low rates are conserved feature among rods (Sheng et al., 2007).

A second strategy suggested to overcome noise in release rates is to make release more regular. At hyperpolarized membrane potentials, we found that glutamate release from rods followed a Poisson distribution similar to that seen at many other neurons (Malagon et al., 2016;Miki, 2019). This nearly ubiquitous feature of neurons was established in the 1950s by Bernard Katz who modeled spontaneous release events to develop the quantal hypothesis of neurotransmission (Kavalali, 2015;2018). However, as the membrane potential approached −40 mV, release from rods was coordinated in bursts at fairly regular intervals. Amplitude distributions of release events and rates of release could not be explained by Poisson statistics. Intervals between bursts were instead more consistent with an Erlang process, having a coefficient of variance (CV) half as wide as what expected from a strictly Poisson process. Erlang processes wait a certain number of Poisson intervals between each event. The accumulation of Poisson intervals thus effectively averages and regularizes release. It was suggested that an Erlang process might play a role in transmitting single photon responses from rods (Schein and Ahmad, 2005;2006). However, to achieve reliable single photon detection, even with a rate of 100 v/s/ribbon, Schein and Ahmad found that they needed an Erlang process with an Erlang factor of 66 (i.e., an accumulation of 66 Poisson intervals) (Schein and Ahmad, 2006). Our experimental data showed a narrower distribution than expected for a Poisson process by an order of 2-3, suggesting an aggregate of 4-9 Poisson processes comprise the burst event, many fewer than that required in the modeling by Schein and Ahmad (2005, 2006). The modest increase in regularity that accompanies bursting thus seems less important than the sensitivity of bursting behavior to small voltage changes.

The non-linear thresholding mechanisms used at rod bipolar synapses is thought to occur before summation of rod responses in the rod bipolar cell soma (Field and Rieke, 2002;Sampath and Rieke, 2004). Consistent with this, when we summed responses linearly among 20 rods, the ability of a bipolar cell to detect absorption of a photon was poor, regardless of whether one assumed Poisson release statistics or bursting behavior. One mechanism that has been shown to contribute to this non-linear thresholding is that glutamate levels in the cleft are thought to keep the rod bipolar cell in saturation and that a small voltage change in one rod reduces glutamate sufficiently at one dendrite to re-open numerous TRPM1 channels in the rod bipolar cell, producing a relatively large voltage response (Sampath and Rieke, 2004). We hypothesize that one mechanism that may keep glutamate levels high enough at individual synaptic clefts to saturate receptors during darkness are the regular bursts of release.

When we simulated the changes sensed at a single rod synapse, if we assumed Poisson statistics using our measured rates, it was virtually impossible to distinguish a single photon response from noise. On the other hand, the abrupt cessation of bursting produced by a single photon response could be readily detected. However, this would only be possible for the bipolar cell if the sampling interval was long enough, and the integration time for the bipolar cell is estimated to be ~200 ms (Taylor and Smith, 2004;Schein and Ahmad, 2005). So what can we say about burst rates and their potential impact on rod bipolar cell membrane potential?

Rates of mGluR6 activation and deactivation operate on a similar time scale as $I_{A(glu)}$ suggesting that changes in $I_{A(glu)}$ provide a reasonable estimate of glutamate levels sensed by a post-synaptic rod bipolar cell (Nawy, 2000;Snellman et al., 2008;Gameiro et al., 2011). At room temperature, interburst intervals averaged 2.6 s with each burst lasting ~0.2 s, suggesting a burst of glutamate would be present in the synaptic cleft for < 10% of the time. However, release ran down during whole cell recording and rates were higher at 35 °C, suggesting that the true interburst interval *in vivo* may be as short as 0.7 s followed by bursts of 0.2 s (1.5 burst/s). This would

suggest that 4-5 out of 20 presynaptic rods would be actively releasing glutamate onto a rod bipolar cell at any moment, while the others would be between bursts. Flashes applied during a burst did not appear to terminate bursts early, but flashes nevertheless delayed the next burst considerably. Given a sampling interval of 200 ms by the rod, delaying a burst that was "scheduled" to appear during that 200 ms interval will have a much bigger impact on detection that delaying a burst that would have occurred later. In other words, photons that are absorbed by a rod during or immediately after a burst would likely produce voltage changes in the rod bipolar cell that are to be too small and slow to be detected. This in turn suggests that, at any moment, only about one rod in three is actually providing a useful signal concerning capture of a photon to post-synaptic bipolar cells. This is consistent with the idea that the non-linear thresholding mechanism employed by rod bipolar cells discards 2/3 single photon responses. If maintaining the rod bipolar cell membrane potential only requires overlapping inputs from 4-5 rods, then eliminating only one of these inputs by preventing a burst of glutamate with absorption of a single photon could produce as much as 25% change in the rod bipolar cell response. Multivesicular bursts of glutamate release at individual dendrites provide a mechanism to achieve the saturation of mGluR6 receptors that has been shown to be important in the thresholding non-linearity at the rod bipolar cell synapse.(Sampath and Rieke, 2004)

In this study, we report the first direct measurements of release properties at single rod photoreceptor synaptic ribbons. These results constrain models of rod signaling by showing that rods release vesicles at a rate of only 9-10 v/s/ribbon in darkness with release coordinated in bursts of vesicles occurring about once per second. Data in the previous chapter suggest that bursts involve a ribbon-associated releasable pool of vesicles and that the intervals between bursts may be shaped by replenishment of this pool. The cumulative wait times for replenishment of multiple vesicles to the releasable pool provides a mechanism for achieving an Erlang process to enhance regularity in release rates. However, the modest increase in regularity that accompanies bursting

appears less important to signaling at rod synapses than the sensitivity of bursting to small voltage changes. Even voltage changes as small as 1 mV produced detectable changes in bursting and white noise voltage stimuli showed that very small depolarizing excursions could trigger bursts.

Our results suggest that this bursting behavior may contribute to the presynaptic non-linearity in rod signaling. Reliance on bursts filters out high frequency noise, noise introduced by spontaneous individual vesicle release events, and other sources. Because photon absorption events have less immediate effects on bursting in some rods than others, our results suggest that, during each 200 ms sampling window, signals from many of the presynaptic rods would have only a small impact on the post-synaptic bipolar cell membrane potential. Thus, in addition to non-linearities introduced by maintaining glutamate receptors in a state of saturation, our results suggest that the rod bipolar cell membrane potential is controlled by glutamate released from only a subset of rods at any moment. The cost of this arrangement is discarding inputs from many presynaptic rods (Field and Rieke, 2002;Berntson et al., 2004b;Schein and Ahmad, 2006;Trexler et al., 2011), but the benefit is that the fractional change in glutamate receptor activity produced by the loss of input from a single rod upon photon absorption is enhanced. Thus, the bursts of vesicle release in rods and their sensitivity to small voltage changes in darkness may be critical for generating detectable responses to single photons in rod bipolar cells that receive inputs from 20 or more rods.

Chapter 5: DISCUSSION

Our ability to perceive light at the absolute limit of sensitivity imposed by the quantal nature of light has fascinated retinal physiologists since this possibility was first established in pioneering psychophysical studies by Hecht and colleagues (Hecht et al., 1942). This process begins with absorption of single photons by rod photoreceptors but also requires reliable transmission of these small single photon responses to second-order retinal bipolar cells. Most of the presynaptic characteristics of release involved in signal transmission at rod synapses in mammals have been derived largely from models. The studies in this dissertation employed methods for directly measuring glutamate release from rods in salamander and mouse retina to provide a deeper understanding of the mechanisms that shape transmission at rod synapses.

Early studies suggested that most synapses released at most one vesicle in response to an incoming action potential (Korn et al., 1981;Redman and Walmsley, 1983;Redman, 1990). However, it has since become evident that many neurons employ multivesicular release operations to create analog codes and increase reliability at certain synapses. Ribbon-bearing neurons are particularly adept at this form of release (Singer et al., 2004;Graydon et al., 2011;Rudolph et al., 2015) and retinal bipolar cells of zebrafish appear to use multiquantal release as a means of encoding contrast (James et al., 2019). Mechanistically, multiquantal release can arise from sequential fusion, synchronous fusion of multiple vesicles with the plasma membrane, or homotypic fusion between neighboring vesicles prior to compound fusion with the plasma membrane. Homotypic fusion is common in many secretory systems and results of chapter 2 show evidence for this mechanism in rod photoreceptor cells (Hansen et al., 1999;Klein et al., 2017;Gutierrez et al., 2018). Photoreceptors share a common SNARE protein isoform, syntaxin3, with mast cells and pancreatic beta cells where syntaxin 3b mediates homotypic fusion (Curtis et al., 2008;Zhu et al., 2013;Sanchez et al., 2018). Similarly, we found that inhibiting syntaxin3b prevented multiquantal glutamate release from salamander rods. Damaging the ribbon also reduced

multiquantal release. In ribbon-bearing neurons, compound fusion has been suggested as a mechanism for releasing many vesicles with a rapid elevation of intracellular Ca^{2+} (Heidelberger et al., 1994;Heidelberger, 1998). Morphological studies have shown large invaginations and endosome-like cisternae near ribbons (Hama and Saito, 1977;Hama, 1980;Lenzi et al., 2002) that may arise from pre-fused vesicles or bulk endocytosis. Parsons and Sterling proposed that one possible purpose of the ribbon is to facilitate compound fusion of neighboring vesicles, a hypothesis that agrees with our findings in Chapter 2 (Parsons and Sterling, 2003).

The two pools of vesicles involved in evoked and spontaneous release appeared to be distinct as they did not cross-deplete. This suggests a functional difference likely conferred by different populations of vesicular SNARE proteins (Crawford and Kavalali, 2015a). We have shown that syntaxin 3b is involved in multiquantal release and it is possible that the ribbon could maintain an enriched population of syntaxin3b-expressing vesicles through local vesicle cycling.

Controlling the likelihood of multiquantal release by Ca^{2+} as we observed in salamander provides a means of rapidly increasing glutamate in the cleft to very high levels. In darkness, intraterminal Ca^{2+} would be high, promoting sustained multiquantal release such that when a rod absorbs a single photon, the relative reduction in glutamate released will be more than if it were only releasing one quanta at a time. Releasing multiple quanta through a single fusion pore would also prevent catastrophic disruption of the terminal membrane that would occur (Wen et al., 2018) if the rod cannot endocytose vesicles quickly enough to match the rate of release.

Our studies also provided further evidence of the presence of spatially segregated active zones in salamander retina; which further enhances the coding repertoire of the rod that only transmits signals in analog form. Photoreceptors may be able to enrich their output to higher centers by controlling release from different sites to preferentially activate distinct populations of post-synaptic receptors. This type of synaptic heterogeneity is evident in cortical neurons (Atasoy et al.,

2008;Scheefhals and MacGillavry, 2018), where the postsynaptic neuron expresses spatially segregated receptor types. Multiquantal release from rod ribbons may preferentially excite ON bipolar cells that appose the rod terminal at different distances and orientation. Bipolar cell mGluR6 receptors are far enough (~800 nm) away from the rod terminal that the influence of single quanta would be diminished by diffusional filtering, helping to eliminate the noise that accompanies spontaneous release. The AMPA receptors that mediate responses of horizontal cells have a relatively low affinity for glutamate (EC_{50} > 50 μM) so multiquantal release may also enhance signaling to horizontal cells.

In mouse rods, we observed random Ca^{2+}-independent release of vesicles at rods when they were voltage-clamped at -70 mV, below the activation range for voltage-dependent I_{Ca}. Spontaneous release, or exocytosis of neurotransmitter that occurs in the absence of an incoming action potential, occurs in almost all synapses with a variety of cell-type specific characteristics. Though never evoked, spontaneous release can be Ca^{2+}-dependent or -independent. The Ca^{2+} dependence has been shown by several intracellular Ca^{2+} buffers with variable chelating abilities which demonstrated a decline in spontaneous release rate. Ca^{2+} dependent spontaneous release may depend on the occasional stochastic openings of Ca^{2+} channels even at very negative membrane potentials. This is more likely to be true in inhibitory neurons whereas in excitatory terminals, the source of intracellular Ca^{2+} that drives Ca^{2+}-dependent spontaneous release is more likely to be release from internal stores (Williams and Smith, 2018). Our experiments with extracellular Cd^{2+} suggest that most spontaneous release in mouse rods is independent of influx through VGCCs. As in salamander, we did not observe a role for ryanodine receptor-mediated Ca^{2+} release in spontaneous activity. The absence of Ca^{2+} dependent forms of spontaneous release keeps spontaneous fusion at its lowest possible rate, limiting synaptic noise.

When mouse rods were depolarized to -40 mV, the resting membrane potential in darkness, $I_{A(glu)}$ appeared as coordinated bursts of multiquantal release. These bursts involved synchronous

fusion (like salamander rods) but also sequential fusion of vesicles. The bursts depended on the exocytotic Ca^{2+} sensor Syt1. Elimination of Syt1 from rods almost completely eliminated ERG b-waves in the scotopic range and greatly increased spontaneous release at all potentials. Loss of Syt1 rendered rods insensitive to small voltage changes, contributing to loss of the b-wave in electroretinography (Grassmeyer et al., 2019). However, in addition to abolishing voltage-dependent changes in glutamate release, the rampant spontaneous vesicle fusion that accompanies loss of Syt1 may also impair transmission to rod bipolar cells by saturating post-synaptic mGluR6 receptors. A "clamping" function of Syt1 has also been shown in other neurons, where knocking out Syt1 increases spontaneous release (Chicka et al., 2008;Courtney et al., 2019). In rods, the clamping function allowed for seconds long intervals between bursts when Syt1 was present. As shown by the rapid release of vesicles during bursts, rods are capable of releasing vesicles at high rates, at least for a short time. Modeling studies had suggested that in order to detect the change in rate of release produced by small single photon responses, rods must sustain release rates of nearly 100 vesicles/s for indefinite periods (Rao et al., 1994). However, our measurements in individual rods showed that sustained release rates had a shallow relationship with voltage, rising in parallel with I_{Ca} and achieving an overall rate of only ~10 vesicles/s/ribbon at the dark resting membrane potential.

While the overall release rate was low, we found that vesicle release at the dark potential in mouse rods occurred in semiregular bursts triggered by rapid Ca^{2+} increases localized to intracellular nanodomains immediately beneath Ca^{2+} channels. Burst duration was not strongly influenced by global terminal Ca^{2+} levels but restricting the intracellular diffusion of Ca^{2+} closer to ribbons lengthened the intervals between bursts. Rods use a $Ca_V1.4$ Ca^{2+} channel that is resistant to inactivation allowing for tonic steady influx during long periods of depolarization (Baumann et al., 2004;Pangrsic et al., 2018;Waldner et al., 2018) leading to slow changes in global Ca^{2+}. The global elevation of Ca^{2+} that accompanies this sustained influx makes it difficult to rapidly decrease

Ca^{2+} to reduce release upon absorption of a photon. Linking release frequency to Ca^{2+} channel openings rather than global Ca^{2+} helps to solve this problem. This mechanism is also suited to the low affinity Ca^{2+} sensor Syt1. We found that Syt1 was essential for bursting as well as fast synchronous release but not spontaneous release or release evoked by long depolarizing steps that fully activate I_{Ca}. The heterogeneity of responses to Ca^{2+} in the rod suggests that a combination of Ca^{2+} sensors must mediate release, but sensors other than Syt1 in rods had not previously been investigated. Our results in Chapter 3 also suggest that if depolarization requires further release, global Ca^{2+} may then dictate release from non-ribbon sites by using high affinity exocytotic Ca^{2+} sensor Syt7. We began to see the influence of Syt7 on evoked release only with long (500 ms) and strong depolarizing steps that are not representative of physiological conditions. However, it also promoted sustained release at -40 and -30 mV.

Lastly, in Chapter 4, we examine the role for bursting in transmitting single photon responses. While the overall rate of glutamate release tracked linearly with I_{Ca} over the normal physiological range of voltages attained by rods (-70 to –30 mV), the coordination of release in burst was extremely sensitive to small voltage changes (1-3.5 mV) near the dark resting potential -40 mV. These small voltage changes are similar to those experienced by rods upon absorption of a single photon.

Given the convergence of 20 rods to 1 rod bipolar cell, our findings may emulate a coding scheme observed in cortical networks. Cortical neurons, especially of sensory and motor systems, apply an energy efficient, sparse (< 1 Hz) code of action potentials. It is hypothesized that these sparse codes are a result of energy demands; only 1 neuron in a population of 50 have the metabolic capacity to be active at a particular time. In the retina, this computation might instead be necessary due to sparse signals (scarce single photon absorptions), and the incredible energy demands of sustained transmitter release over long periods of darkness. As mentioned, modeling studies suggested that rates of 100 v/s/ribbon are need to produce a reliably detectable change in release at

a given rod ribbon synapse in response to the small voltage changes produced by absorption of a single photon. This places an enormous energy demand on the retina. This conclusion assumed that the voltage-dependence of release paralleled voltage-dependent changes in I_{Ca}. While we found that the overall rate of release averaged over long periods did indeed mirror changes in I_{Ca}, release was not maintained continuously at the same rate but instead showed long pauses punctuated by rapid bursts of release as the rod approached the dark resting membrane potential. The likelihood of bursting was exquisitely sensitive to small voltage changes near the dark resting membrane potential. Thus, rather than maintaining a continuously high rate of release from all rods simultaneously, our results suggest that only a handful of rods are active at any moment and that the glutamate released from a few rods is sufficient to strongly hyperpolarize a rod bipolar cell. Effectively, the rod bipolar cell thus samples from a subset of active rods at any time, allowing the others to rest. It is known that rod bipolar cells do not respond to every photon absorbed presynaptically. It has been suggested that this non-linearity arises entirely at the mGluR6 receptors themselves (Field and Rieke, 2002;Sampath and Rieke, 2004) but our results suggest that some single photon responses may also be discarded presynaptically because they occur early in a pause between bursts and thus have less of an impact on the likelihood of a subsequent burst of release. The nervous system continuously balances energy demands with the need for sensitivity. The high rates of continuous release that would be needed to encode every photon at every rod synapse require enormous amounts of energy. By allowing some rods to rest and discarding their inputs, this bursting strategy permits high sensitivity to small voltage changes in other rods while minimizing the overall energy demands across the population.

Recall that rods contact rod bipolar cells at an invaginating synapse that isolates a rod's signal to its paired dendritic tip. In mouse retina, approximately twenty rods converge onto each rod bipolar cell via mGluR6 (Tsukamoto et al., 2001;Berntson et al., 2004b). A slowing of glutamate release from rods, relieves the saturation of mGluR6 allowing for the opening of

downstream TRPM1 cation channels and depolarization. One of the issues with a strictly Poisson rate of univesicular release is the continually changing glutamate concentration in the cleft. This may be overcome if bursts of vesicles saturate mGluR6 such that every release event leads to the same magnitude of voltage change at the rod bipolar cell dendrite. Ca^{2+} dependent inhibition may then also shorten signals so each voltage change exhibits the same kinetics as well. In salamander, Ca^{2+} dependent inhibition may be too slow (Nawy, 2000;2004) but in mouse, Berntson and Taylor found it to be on the order of milliseconds.(Berntson et al., 2004a). Additionally, fast glutamate binding and removal by presynaptic EAAT can help to make the signal more transient (Hasegawa et al., 2006). These mechanisms combined help to make synapse to detect single photons, effectively "binarizing" the synapse. Berntson and Taylor measured the half saturating intensity of the synapse to be 0.7 R*, suggesting the exclusive duty of the rod is to signal single photons (Berntson et al., 2004b). If this is true, grading release as an analog signal would be unnecessary and a binary system (photon or no photon) would be sufficient.

We found that $I_{A(glu)}$ rates were approximated by an Erlang distribution (k = 4-9) at –40 mV where the probability of release decreases during the single photon response followed by a relative increase in release probability after depolarization back to the dark potential. It has been proposed that enhancing regularity of release by implementing an Erlang process could help in discriminating single photon responses from noise (Schein and Ahmad, 2005;2006). However, the modest increase in the regularity of release that we observed did not achieve a high enough Erlang factor to greatly improve predictability. One of the challenges in transmitting single photon responses is inherent voltage noise due to thermal isomerizations of rhodopsin (rare) and phosphodiesterase (more common) in the rod outer segment (Taylor and Smith, 2004;Okawa and Sampath, 2007). It has been suggested that a mechanism for reducing the impact of dark noise in rods is a temporal filter where release rate is only modulated by frequencies of voltage changes that could contain a single photon response (< 5 Hz) (Chichilnisky and Rieke, 2005). Consistent with

this, we observed that slow depolarizing excursions of a white noise stimulus with a 5 Hz cutoff could trigger bursting while a 20 Hz white noise filter could not. Another mechanism for removing noise is implementation of a thresholding mechanism that does not transmit small signals and noise but only large signals.

One hypothesis for enhancing the transmission of scotopic signals is rod-rod gap junctional coupling (Jin et al., 2015). If absorption of a photon by one rod can hyperpolarize neighboring rods, their probability of releasing a burst also would also decrease. Some voltage change may be lost by the resistance though a gap junction and voltage noise is shared, but if the photovoltage is 3.44 mV, our data suggest that 60% of that voltage change may be lost and still initiate a meaningful pause in release. We have not yet investigated the impact of coupling on this bursting behavior. Gap-junctional conductance is reduced in light-adapted retinas such as those we used for out studies. Furthermore, C57Bl6 mice show weaker coupling among rods than some other mouse strains. In chapter 4, we discuss how bursting may contribute to such a thresholding non-linearity at the rod to rod bipolar cell synapse. In future studies, we plan to pursue further models of the contribution of bursting to the ability of rod bipolar cells to detect single photons, investigating the impact of variations in release rate, Erlang factor, coupling among rods and other factors.

BIBLIOGRAPHY

Ala-Laurila, P., and Rieke, F. (2014). Coincidence detection of single-photon responses in the inner retina at the sensitivity limit of vision. *Curr Biol* 24**,** 2888-2898.

Allen, T.J. (1996). Temperature dependence of macroscopic L-type calcium channel currents in single guinea pig ventricular myocytes. *J Cardiovasc Electrophysiol* 7**,** 307-321.

Alvarez De Toledo, G., and Fernandez, J.M. (1990). Compound versus multigranular exocytosis in peritoneal mast cells. *The Journal of general physiology* 95**,** 397-409.

Andreae, L.C., Fredj, N.B., and Burrone, J. (2012). Independent vesicle pools underlie different modes of release during neuronal development. *J Neurosci* 32**,** 1867-1874.

Arriza, J.L., Eliasof, S., Kavanaugh, M.P., and Amara, S.G. (1997). Excitatory amino acid transporter 5, a retinal glutamate transporter coupled to a chloride conductance. *Proceedings of the National Academy of Sciences of the United States of America* 94**,** 4155-4160.

Atasoy, D., Ertunc, M., Moulder, K.L., Blackwell, J., Chung, C., Su, J., and Kavalali, E.T. (2008). Spontaneous and evoked glutamate release activates two populations of NMDA receptors with limited overlap. *J Neurosci* 28**,** 10151-10166.

Awatramani, G.B., and Slaughter, M.M. (2000). Origin of transient and sustained responses in ganglion cells of the retina. *J Neurosci* 20**,** 7087-7095.

Babai, N., Bartoletti, T.M., and Thoreson, W.B. (2010a). Calcium regulates vesicle replenishment at the cone ribbon synapse. *J Neurosci* 30**,** 15866-15877.

Babai, N., Morgans, C.W., and Thoreson, W.B. (2010b). Calcium-induced calcium release contributes to synaptic release from mouse rod photoreceptors. *Neuroscience* 165**,** 1447-1456.

Babai, N., Sendelbeck, A., Regus-Leidig, H., Fuchs, M., Mertins, J., Reim, K., Brose, N., Feigenspan, A., and Brandstatter, J.H. (2016). Functional Roles of Complexin 3 and Complexin 4 at Mouse Photoreceptor Ribbon Synapses. *J Neurosci* 36**,** 6651-6667.

Babai, N., and Thoreson, W.B. (2009). Horizontal cell feedback regulates calcium currents and intracellular calcium levels in rod photoreceptors of salamander and mouse retina. *J Physiol* 587**,** 2353-2364.

Bacaj, T., Wu, D., Burre, J., Malenka, R.C., Liu, X., and Sudhof, T.C. (2015). Synaptotagmin-1 and -7 Are Redundantly Essential for Maintaining the Capacity of the Readily-Releasable Pool of Synaptic Vesicles. *PLoS Biol* 13**,** e1002267.

Bacaj, T., Wu, D., Yang, X., Morishita, W., Zhou, P., Xu, W., Malenka, R.C., and Sudhof, T.C. (2013). Synaptotagmin-1 and synaptotagmin-7 trigger synchronous and asynchronous phases of neurotransmitter release. *Neuron* 80**,** 947-959.

Baden, T., Berens, P., Franke, K., Roman Roson, M., Bethge, M., and Euler, T. (2016). The functional diversity of retinal ganglion cells in the mouse. *Nature* 529**,** 345-350.

Bal, M., Leitz, J., Reese, A.L., Ramirez, D.M., Durakoglugil, M., Herz, J., Monteggia, L.M., and Kavalali, E.T. (2013). Reelin mobilizes a VAMP7-dependent synaptic vesicle pool and selectively augments spontaneous neurotransmission. *Neuron* 80**,** 934-946.

Barnes, S., and Deschenes, M.C. (1992). Contribution of Ca and Ca-activated Cl channels to regenerative depolarization and membrane bistability of cone photoreceptors. *J Neurophysiol* 68**,** 745-755.

Barnes, S., and Kelly, M.E. (2002). Calcium channels at the photoreceptor synapse. *Adv Exp Med Biol* 514**,** 465-476.

Bartoletti, T.M., Babai, N., and Thoreson, W.B. (2010). Vesicle pool size at the salamander cone ribbon synapse. *J Neurophysiol* 103**,** 419-423.

Bartoletti, T.M., Jackman, S.L., Babai, N., Mercer, A.J., Kramer, R.H., and Thoreson, W.B. (2011). Release from the cone ribbon synapse under bright light conditions can be controlled by the opening of only a few Ca(2+) channels. *Journal of neurophysiology* 106**,** 2922-2935.

Bartoletti, T.M., and Thoreson, W.B. (2011). Quantal amplitude at the cone ribbon synapse can be adjusted by changes in cytosolic glutamate. *Mol Vis* 17**,** 920-931.

Baumann, L., Gerstner, A., Zong, X., Biel, M., and Wahl-Schott, C. (2004). Functional characterization of the L-type Ca2+ channel Cav1.4alpha1 from mouse retina. *Invest Ophthalmol Vis Sci* 45**,** 708-713.

Baylor, D.A., Lamb, T.D., and Yau, K.W. (1979). Responses of retinal rods to single photons. *J Physiol* 288**,** 613-634.

Baylor, D.A., Nunn, B.J., and Schnapf, J.L. (1984). The photocurrent, noise and spectral sensitivity of rods of the monkey Macaca fascicularis. *J Physiol* 357**,** 575-607.

Beckwith-Cohen, B., Holzhausen, L.C., Wang, T.M., Rajappa, R., and Kramer, R.H. (2019). Localizing Proton-Mediated Inhibitory Feedback at the Retinal Horizontal Cell-Cone Synapse with Genetically-Encoded pH Probes. *J Neurosci* 39**,** 651-662.

Behrendorff, N., Dolai, S., Hong, W., Gaisano, H.Y., and Thorn, P. (2011). Vesicle-associated membrane protein 8 (VAMP8) is a SNARE (soluble N-ethylmaleimide-sensitive factor attachment protein receptor) selectively required for sequential granule-to-granule fusion. *The Journal of biological chemistry* 286**,** 29627-29634.

Bello, O.D., Jouannot, O., Chaudhuri, A., Stroeva, E., Coleman, J., Volynski, K.E., Rothman, J.E., and Krishnakumar, S.S. (2018). Synaptotagmin oligomerization is essential for calcium control of regulated exocytosis. *Proceedings of the National Academy of Sciences of the United States of America* 115**,** E7624-E7631.

Bendahmane, M., Bohannon, K.P., Bradberry, M.M., Rao, T.C., Schmidtke, M.W., Abbineni, P.S., Chon, N.L., Tran, S., Lin, H., Chapman, E.R., Knight, J.D., and Anantharam, A.

(2018). The synaptotagmin C2B domain calcium-binding loops modulate the rate of fusion pore expansion. *Mol Biol Cell* 29**,** 773-880.

Berntson, A., Smith, R.G., and Taylor, W.R. (2004a). Postsynaptic calcium feedback between rods and rod bipolar cells in the mouse retina. *Vis Neurosci* 21**,** 913-924.

Berntson, A., Smith, R.G., and Taylor, W.R. (2004b). Transmission of single photon signals through a binary synapse in the mammalian retina. *Vis Neurosci* 21**,** 693-702.

Berntson, A., and Taylor, W.R. (2003). The unitary event amplitude of mouse retinal on-cone bipolar cells. *Vis Neurosci* 20**,** 621-626.

Berntson, A.K., and Morgans, C.W. (2003). Distribution of the presynaptic calcium sensors, synaptotagmin I/II and synaptotagmin III, in the goldfish and rodent retinas. *J Vis* 3**,** 274-280.

Blank, U. (2011). The mechanisms of exocytosis in mast cells. *Advances in Experimental Medicine and Biology* 716**,** 107-122.

Borisovska, M. (2018). Syntaxins on granules promote docking of granules via interactions with munc18. *Scientific reports* 8**,** 193-017-18597-z.

Brandt, A., Khimich, D., and Moser, T. (2005). Few CaV1.3 channels regulate the exocytosis of a synaptic vesicle at the hair cell ribbon synapse. *J Neurosci* 25**,** 11577-11585.

Braun, R.D., Linsenmeier, R.A., and Goldstick, T.K. (1995). Oxygen consumption in the inner and outer retina of the cat. *Invest Ophthalmol Vis Sci* 36**,** 542-554.

Brose, N., Petrenko, A.G., Sudhof, T.C., and Jahn, R. (1992). Synaptotagmin: a calcium sensor on the synaptic vesicle surface. *Science* 256**,** 1021-1025.

Byrne, J.H., Heidelberger, R., Waxham, M.N., and Alberini, C.M. "From molecules to networks : an introduction to cellular and molecular neuroscience". Third edition. ed.).

Byrne, J.H., Heidelberger, R, Waxham, M.N (2014). *From Molecules to Networks: An Introduction to Cellular and Molecular Neuroscience.* San Diego, CA: Elsevier.

Byzov, A.L., and Trifonov Yu, A. (1981). Ionic mechanisms underlying the nonlinearity of horizontal cell membrane. *Vision Res* 21**,** 1573-1578.

Cadetti, L., Bryson, E.J., Ciccone, C.A., Rabl, K., and Thoreson, W.B. (2006). Calcium-induced calcium release in rod photoreceptor terminals boosts synaptic transmission during maintained depolarization. *Eur J Neurosci* 23**,** 2983-2990.

Cadetti, L., and Thoreson, W.B. (2006). Feedback effects of horizontal cell membrane potential on cone calcium currents studied with simultaneous recordings. *J Neurophysiol* 95**,** 1992-1995.

Cadetti, L., Tranchina, D., and Thoreson, W.B. (2005). A comparison of release kinetics and glutamate receptor properties in shaping rod-cone differences in EPSC kinetics in the salamander retina. *J Physiol* 569**,** 773-788.

Cai, J., Nelson, K.C., Wu, M., Sternberg, P., Jr., and Jones, D.P. (2000). Oxidative damage and protection of the RPE. *Prog Retin Eye Res* 19**,** 205-221.

Calkins, D.J., and Sterling, P. (1999). Evidence that circuits for spatial and color vision segregate at the first retinal synapse. *Neuron* 24**,** 313-321.

Cangiano, L., Asteriti, S., Cervetto, L., and Gargini, C. (2012). The photovoltage of rods and cones in the dark-adapted mouse retina. *J Physiol* 590**,** 3841-3855.

Carter-Dawson, L.D., and Lavail, M.M. (1979). Rods and cones in the mouse retina. II. Autoradiographic analysis of cell generation using tritiated thymidine. *J Comp Neurol* 188**,** 263-272.

Carter, A.G., and Regehr, W.G. (2002). Quantal events shape cerebellar interneuron firing. *Nat Neurosci* 5**,** 1309-1318.

Chanaday, N.L., and Kavalali, E.T. (2018). Presynaptic origins of distinct modes of neurotransmitter release. *Curr Opin Neurobiol* 51**,** 119-126.

Chapman, E.R. (2008). How does synaptotagmin trigger neurotransmitter release? *Annu Rev Biochem* 77**,** 615-641.

Chapochnikov, N.M., Takago, H., Huang, C.H., Pangrsic, T., Khimich, D., Neef, J., Auge, E., Gottfert, F., Hell, S.W., Wichmann, C., Wolf, F., and Moser, T. (2014). Uniquantal release through a dynamic fusion pore is a candidate mechanism of hair cell exocytosis. *Neuron* 83**,** 1389-1403.

Chen, M., Krizaj, D., and Thoreson, W.B. (2014). Intracellular calcium stores drive slow non-ribbon vesicle release from rod photoreceptors. *Front Cell Neurosci* 8**,** 20.

Chen, M., Van Hook, M.J., and Thoreson, W.B. (2015). Ca2+ Diffusion through Endoplasmic Reticulum Supports Elevated Intraterminal Ca2+ Levels Needed to Sustain Synaptic Release from Rods in Darkness. *J Neurosci* 35**,** 11364-11373.

Chen, M., Van Hook, M.J., Zenisek, D., and Thoreson, W.B. (2013). Properties of ribbon and non-ribbon release from rod photoreceptors revealed by visualizing individual synaptic vesicles. *J Neurosci* 33**,** 2071-2086.

Chen, M., and Von Gersdorff, H. (2019). How to Build a Fast and Highly Sensitive Sound Detector That Remains Robust to Temperature Shifts. *J Neurosci* 39**,** 7260-7276.

Chichilnisky, E.J., and Rieke, F. (2005). Detection sensitivity and temporal resolution of visual signals near absolute threshold in the salamander retina. *J Neurosci* 25**,** 318-330.

Chicka, M.C., Hui, E., Liu, H., and Chapman, E.R. (2008). Synaptotagmin arrests the SNARE complex before triggering fast, efficient membrane fusion in response to Ca2+. *Nat Struct Mol Biol* 15**,** 827-835.

Choi, S.Y., Sheng, Z., and Kramer, R.H. (2005). Imaging light-modulated release of synaptic vesicles in the intact retina: retinal physiology at the dawn of the post-electrode era. *Vision Res* 45**,** 3487-3495.

Chung, C., Barylko, B., Leitz, J., Liu, X., and Kavalali, E.T. (2010). Acute dynamin inhibition dissects synaptic vesicle recycling pathways that drive spontaneous and evoked neurotransmission. *J Neurosci* 30**,** 1363-1376.

Connaughton, V. (1995). "Glutamate and Glutamate Receptors in the Vertebrate Retina," in *Webvision: The Organization of the Retina and Visual System,* eds. H. Kolb, E. Fernandez & R. Nelson. (Salt Lake City (UT)).

Copenhagen, D.R., Ashmore, J.F., and Schnapf, J.K. (1983). Kinetics of synaptic transmission from photoreceptors to horizontal and bipolar cells in turtle retina. *Vision Res* 23**,** 363-369.

Cork, K.M., Van Hook, M.J., and Thoreson, W.B. (2016). Mechanisms, pools, and sites of spontaneous vesicle release at synapses of rod and cone photoreceptors. *Eur J Neurosci* 44**,** 2015-2027.

Courtney, N.A., Bao, H., Briguglio, J.S., and Chapman, E.R. (2019). Synaptotagmin 1 clamps synaptic vesicle fusion in mammalian neurons independent of complexin. *Nat Commun* 10**,** 4076.

Courtney, N.A., Briguglio, J.S., Bradberry, M.M., Greer, C., and Chapman, E.R. (2018). Excitatory and Inhibitory Neurons Utilize Different Ca(2+) Sensors and Sources to Regulate Spontaneous Release. *Neuron* 98**,** 977-991 e975.

Crawford, D.C., and Kavalali, E.T. (2015a). Molecular underpinnings of synaptic vesicle pool heterogeneity. *Traffic (Copenhagen, Denmark)* 16**,** 338-364.

Crawford, D.C., and Kavalali, E.T. (2015b). Molecular underpinnings of synaptic vesicle pool heterogeneity. *Traffic* 16**,** 338-364.

Curtis, L., Datta, P., Liu, X., Bogdanova, N., Heidelberger, R., and Janz, R. (2010). Syntaxin 3B is essential for the exocytosis of synaptic vesicles in ribbon synapses of the retina. *Neuroscience* 166**,** 832-841.

Curtis, L.B., Doneske, B., Liu, X., Thaller, C., Mcnew, J.A., and Janz, R. (2008). Syntaxin 3b is a t-SNARE specific for ribbon synapses of the retina. *The Journal of comparative neurology* 510**,** 550-559.

Dacheux, R.F., and Raviola, E. (1986). The rod pathway in the rabbit retina: a depolarizing bipolar and amacrine cell. *J Neurosci* 6**,** 331-345.

Datta, P., Gilliam, J., Thoreson, W.B., Janz, R., and Heidelberger, R. (2017). Two Pools of Vesicles Associated with Synaptic Ribbons Are Molecularly Prepared for Release. *Biophysical journal* 113**,** 2281-2298.

De Robertis, E.D., and Bennett, H.S. (1955). Some features of the submicroscopic morphology of synapses in frog and earthworm. *J Biophys Biochem Cytol* 1**,** 47-58.

Decoursey, T.E., and Cherny, V.V. (1998). Temperature dependence of voltage-gated H+ currents in human neutrophils, rat alveolar epithelial cells, and mammalian phagocytes. *J Gen Physiol* 112**,** 503-522.

Del Castillo, J., and Katz, B. (1954). Quantal components of the end-plate potential. *J Physiol* 124**,** 560-573.

Demontis, G.C., Longoni, B., Barcaro, U., and Cervetto, L. (1999). Properties and functional roles of hyperpolarization-gated currents in guinea-pig retinal rods. *J Physiol* 515 (Pt 3)**,** 813-828.

Demontis, G.C., Moroni, A., Gravante, B., Altomare, C., Longoni, B., Cervetto, L., and Difrancesco, D. (2002). Functional characterisation and subcellular localisation of HCN1 channels in rabbit retinal rod photoreceptors. *J Physiol* 542**,** 89-97.

Deng, S., Li, J., He, Q., Zhang, X., Zhu, J., Li, L., Mi, Z., Yang, X., Jiang, M., Dong, Q., Mao, Y., and Shu, Y. (2020). Regulation of Recurrent Inhibition by Asynchronous Glutamate Release in Neocortex. *Neuron* 105**,** 522-533 e524.

Deniz, S., Wersinger, E., Schwab, Y., Mura, C., Erdelyi, F., Szabo, G., Rendon, A., Sahel, J.A., Picaud, S., and Roux, M.J. (2011). Mammalian retinal horizontal cells are unconventional GABAergic neurons. *J Neurochem* 116**,** 350-362.

Diamond, J.S. (2017). Inhibitory Interneurons in the Retina: Types, Circuitry, and Function. *Annu Rev Vis Sci* 3**,** 1-24.

Doering, C.J., Peloquin, J.B., and Mcrory, J.E. (2007). The Ca(v)1.4 calcium channel: more than meets the eye. *Channels (Austin)* 1**,** 3-10.

Dolphin, A.C., Insel, P.A., Blaschke, T.F., and Meyer, U.A. (2020). Introduction to the Theme "Ion Channels and Neuropharmacology: From the Past to the Future". *Annu Rev Pharmacol Toxicol* 60**,** 1-6.

Dolphin, A.C., and Lee, A. (2020). Presynaptic calcium channels: specialized control of synaptic neurotransmitter release. *Nat Rev Neurosci* 21**,** 213-229.

Druzin, M., Haage, D., Malinina, E., and Johansson, S. (2002). Dual and opposing roles of presynaptic Ca2+ influx for spontaneous GABA release from rat medial preoptic nerve terminals. *J Physiol* 542**,** 131-146.

Duncan, G., Rabl, K., Gemp, I., Heidelberger, R., and Thoreson, W.B. (2010). Quantitative analysis of synaptic release at the photoreceptor synapse. *Biophys J* 98**,** 2102-2110.

Eckly, A., Rinckel, J.Y., Proamer, F., Ulas, N., Joshi, S., Whiteheart, S.W., and Gachet, C. (2016). Respective contributions of single and compound granule fusion to secretion by activated platelets. *Blood* 128**,** 2538-2549.

Eggermann, E., Bucurenciu, I., Goswami, S.P., and Jonas, P. (2011). Nanodomain coupling between Ca(2)(+) channels and sensors of exocytosis at fast mammalian synapses. *Nat Rev Neurosci* 13**,** 7-21.

Eliasof, S., Arriza, J.L., Leighton, B.H., Amara, S.G., and Kavanaugh, M.P. (1998a). Localization and function of five glutamate transporters cloned from the salamander retina. *Vision research* 38**,** 1443-1454.

Eliasof, S., Arriza, J.L., Leighton, B.H., Kavanaugh, M.P., and Amara, S.G. (1998b). Excitatory amino acid transporters of the salamander retina: identification, localization, and function. *The Journal of neuroscience : the official journal of the Society for Neuroscience* 18**,** 698-712.

Eliasof, S., and Werblin, F. (1993). Characterization of the glutamate transporter in retinal cones of the tiger salamander. *J Neurosci* 13**,** 402-411.

Fahlke, C., Kortzak, D., and Machtens, J.P. (2016). Molecular physiology of EAAT anion channels. *Pflugers Arch* 468**,** 491-502.

Farrow, K., Isa, T., Luksch, H., and Yonehara, K. (2019). Editorial: The Superior Colliculus/Tectum: Cell Types, Circuits, Computations, Behaviors. *Front Neural Circuits* 13**,** 39.

Fatt, P., and Katz, B. (1952). Spontaneous subthreshold activity at motor nerve endings. *J Physiol* 117**,** 109-128.

Feigenspan, A., and Babai, N. (2015). Functional properties of spontaneous excitatory currents and encoding of light/dark transitions in horizontal cells of the mouse retina. *The European journal of neuroscience* 42**,** 2615-2632.

Felten, D.L., O'banion, M.K., and Maida, M.S. (2016). *Netter's atlas of neuroscience*. Philadelphia, PA: Elsevier.

Fernandez-Chacon, R., Shin, O.H., Konigstorfer, A., Matos, M.F., Meyer, A.C., Garcia, J., Gerber, S.H., Rizo, J., Sudhof, T.C., and Rosenmund, C. (2002). Structure/function analysis of Ca2+ binding to the C2A domain of synaptotagmin 1. *J Neurosci* 22**,** 8438-8446.

Fernandez, I., Arac, D., Ubach, J., Gerber, S.H., Shin, O., Gao, Y., Anderson, R.G., Sudhof, T.C., and Rizo, J. (2001). Three-dimensional structure of the synaptotagmin 1 C2B-domain: synaptotagmin 1 as a phospholipid binding machine. *Neuron* 32**,** 1057-1069.

Field, G.D., and Rieke, F. (2002). Nonlinear signal transfer from mouse rods to bipolar cells and implications for visual sensitivity. *Neuron* 34**,** 773-785.

Field, G.D., and Sampath, A.P. (2017). Behavioural and physiological limits to vision in mammals. *Philos Trans R Soc Lond B Biol Sci* 372.

Field, G.D., Sher, A., Gauthier, J.L., Greschner, M., Shlens, J., Litke, A.M., and Chichilnisky, E.J. (2007). Spatial properties and functional organization of small bistratified ganglion cells in primate retina. *J Neurosci* 27**,** 13261-13272.

Fox, M.A., and Sanes, J.R. (2007). Synaptotagmin I and II are present in distinct subsets of central synapses. *J Comp Neurol* 503**,** 280-296.

Freedman, M.S., Lucas, R.J., Soni, B., Von Schantz, M., Munoz, M., David-Gray, Z., and Foster, R. (1999). Regulation of mammalian circadian behavior by non-rod, non-cone, ocular photoreceptors. *Science* 284**,** 502-504.

Gameiro, A., Braams, S., Rauen, T., and Grewer, C. (2011). The discovery of slowness: low-capacity transport and slow anion channel gating by the glutamate transporter EAAT5. *Biophys J* 100**,** 2623-2632.

Geppert, M., Goda, Y., Hammer, R.E., Li, C., Rosahl, T.W., Stevens, C.F., and Sudhof, T.C. (1994). Synaptotagmin I: a major Ca2+ sensor for transmitter release at a central synapse. *Cell* 79**,** 717-727.

Glowatzki, E., and Fuchs, P.A. (2002). Transmitter release at the hair cell ribbon synapse. *Nature neuroscience* 5**,** 147-154.

Goswami, S.P., Bucurenciu, I., and Jonas, P. (2012). Miniature IPSCs in hippocampal granule cells are triggered by voltage-gated Ca2+ channels via microdomain coupling. *J Neurosci* 32**,** 14294-14304.

Grabner, C.P., Gandini, M.A., Rehak, R., Le, Y., Zamponi, G.W., and Schmitz, F. (2015). RIM1/2-Mediated Facilitation of Cav1.4 Channel Opening Is Required for Ca2+-Stimulated Release in Mouse Rod Photoreceptors. *J Neurosci* 35**,** 13133-13147.

Grabner, C.P., and Moser, T. (2018). Individual synaptic vesicles mediate stimulated exocytosis from cochlear inner hair cells. *Proc Natl Acad Sci U S A* 115**,** 12811-12816.

Grant, L., Yi, E., and Glowatzki, E. (2010). Two modes of release shape the postsynaptic response at the inner hair cell ribbon synapse. *The Journal of neuroscience : the official journal of the Society for Neuroscience* 30**,** 4210-4220.

Grassmeyer, J.J., Cahill, A.L., Hays, C.L., Barta, C., Quadros, R.M., Gurumurthy, C.B., and Thoreson, W.B. (2019). Ca(2+) sensor synaptotagmin-1 mediates exocytosis in mammalian photoreceptors. *Elife* 8.

Gray, E.G., and Pease, H.L. (1971). On understanding the organisation of the retinal receptor synapses. *Brain Res* 35**,** 1-15.

Graydon, C.W., Cho, S., Li, G.L., Kachar, B., and Von Gersdorff, H. (2011). Sharp Ca(2)(+) nanodomains beneath the ribbon promote highly synchronous multivesicular release at hair cell synapses. *J Neurosci* 31**,** 16637-16650.

Graydon, C.W., Zhang, J., Oesch, N.W., Sousa, A.A., Leapman, R.D., and Diamond, J.S. (2014). Passive diffusion as a mechanism underlying ribbon synapse vesicle release and resupply. *J Neurosci* 34**,** 8948-8962.

Grewer, C., Gameiro, A., Zhang, Z., Tao, Z., Braams, S., and Rauen, T. (2008). Glutamate forward and reverse transport: from molecular mechanism to transporter-mediated release after ischemia. *IUBMB Life* 60**,** 609-619.

Grimes, W.N., Baudin, J., Azevedo, A.W., and Rieke, F. (2018). Range, routing and kinetics of rod signaling in primate retina. *Elife* 7.

Grimes, W.N., Zhang, J., Tian, H., Graydon, C.W., Hoon, M., Rieke, F., and Diamond, J.S. (2015). Complex inhibitory microcircuitry regulates retinal signaling near visual threshold. *J Neurophysiol* 114**,** 341-353.

Gross, O.P., Pugh, E.N., Jr., and Burns, M.E. (2015). cGMP in mouse rods: the spatiotemporal dynamics underlying single photon responses. *Front Mol Neurosci* 8**,** 6.

Grove, J.C.R., Hirano, A.A., De Los Santos, J., Mchugh, C.F., Purohit, S., Field, G.D., Brecha, N.C., and Barnes, S. (2019). Novel hybrid action of GABA mediates inhibitory feedback in the mammalian retina. *PLoS Biol* 17**,** e3000200.

Grushin, K., Wang, J., Coleman, J., Rothman, J.E., Sindelar, C.V., and Krishnakumar, S.S. (2019). Structural basis for the clamping and Ca(2+) activation of SNARE-mediated fusion by synaptotagmin. *Nat Commun* 10**,** 2413.

Gutierrez, B.A., Chavez, M.A., Rodarte, A.I., Ramos, M.A., Dominguez, A., Petrova, Y., Davalos, A.J., Costa, R.M., Elizondo, R., Tuvim, M.J., Dickey, B.F., Burns, A.R., Heidelberger, R., and Adachi, R. (2018). Munc18-2, but not Munc18-1 or Munc18-3, controls compound and single-vesicle-regulated exocytosis in mast cells. *The Journal of biological chemistry* 293**,** 7148-7159.

Hack, I., Peichl, L., and Brandstatter, J.H. (1999). An alternative pathway for rod signals in the rodent retina: rod photoreceptors, cone bipolar cells, and the localization of glutamate receptors. *Proc Natl Acad Sci U S A* 96**,** 14130-14135.

Haeseleer, F., Williams, B., and Lee, A. (2016). Characterization of C-terminal Splice Variants of Cav1.4 Ca2+ Channels in Human Retina. *J Biol Chem* 291**,** 15663-15673.

Hama, K. (1980). Fine structure of the afferent synapse and gap junctions on the sensory hair cell in the saccular macula of goldfish: a freeze-fracture study. *J Neurocytol* 9**,** 845-860.

Hama, K., and Saito, K. (1977). Fine structure of the afferent synapse of the hair cells in the saccular macula of the goldfish, with special reference to the anastomosing tubules. *J Neurocytol* 6**,** 361-373.

Hansen, N.J., Antonin, W., and Edwardson, J.M. (1999). Identification of SNAREs involved in regulated exocytosis in the pancreatic acinar cell. *The Journal of biological chemistry* 274**,** 22871-22876.

Hasegawa, J., Obara, T., Tanaka, K., and Tachibana, M. (2006). High-density presynaptic transporters are required for glutamate removal from the first visual synapse. *Neuron* 50**,** 63-74.

Haverkamp, S., Grunert, U., and Wassle, H. (2001). The synaptic architecture of AMPA receptors at the cone pedicle of the primate retina. *J Neurosci* 21**,** 2488-2500.

Hays, C.L., Grassmeyer, J.J., Wen, X., Janz, R., Heidelberger, R., and Thoreson, W.B. (2020). Simultaneous Release of Multiple Vesicles from Rods Involves Synaptic Ribbons and Syntaxin 3B. *Biophys J* 118**,** 967-979.

He, L., Xue, L., Xu, J., Mcneil, B.D., Bai, L., Melicoff, E., Adachi, R., and Wu, L.G. (2009). Compound vesicle fusion increases quantal size and potentiates synaptic transmission. *Nature* 459**,** 93-97.

Hecht, S., Shlaer, S., and Pirenne, M.H. (1942). Energy, Quanta, and Vision. *J Gen Physiol* 25**,** 819-840.

Heidelberger, R. (1998). Adenosine triphosphate and the late steps in calcium-dependent exocytosis at a ribbon synapse. *J Gen Physiol* 111**,** 225-241.

Heidelberger, R. (2007). Mechanisms of tonic, graded release: lessons from the vertebrate photoreceptor. *J Physiol* 585**,** 663-667.

Heidelberger, R., Heinemann, C., Neher, E., and Matthews, G. (1994). Calcium dependence of the rate of exocytosis in a synaptic terminal. *Nature* 371**,** 513-515.

Heidelberger, R., Sterling, P., and Matthews, G. (2002). Roles of ATP in depletion and replenishment of the releasable pool of synaptic vesicles. *J Neurophysiol* 88**,** 98-106.

Heidelberger, R., Thoreson, W.B., and Witkovsky, P. (2005). Synaptic transmission at retinal ribbon synapses. *Prog Retin Eye Res* 24**,** 682-720.

Heidelberger, R., Wang, M.M., and Sherry, D.M. (2003). Differential distribution of synaptotagmin immunoreactivity among synapses in the goldfish, salamander, and mouse retina. *Vis Neurosci* 20**,** 37-49.

Herve, J.C., Yamaoka, K., Twist, V.W., Powell, T., Ellory, J.C., and Wang, L.C. (1992). Temperature dependence of electrophysiological properties of guinea pig and ground squirrel myocytes. *Am J Physiol* 263**,** R177-184.

Hille, B. (2001). *Ion channels of excitable membranes.* Sunderland, Mass.: Sinauer.

Hirasawa, H., Yamada, M., and Kaneko, A. (2012). Acidification of the synaptic cleft of cone photoreceptor terminal controls the amount of transmitter release, thereby forming the receptive field surround in the vertebrate retina. *J Physiol Sci* 62**,** 359-375.

Hoffman-Kim, D., Diefenbach, T.J., Eustace, B.K., and Jay, D.G. (2007). Chromophore-assisted laser inactivation. *Methods in cell biology* 82**,** 335-354.

Hope, C.I., Sharp, D.M., Hemara-Wahanui, A., Sissingh, J.I., Lundon, P., Mitchell, E.A., Maw, M.A., and Clover, G.M. (2005). Clinical manifestations of a unique X-linked retinal disorder in a large New Zealand family with a novel mutation in CACNA1F, the gene responsible for CSNB2. *Clin Exp Ophthalmol* 33**,** 129-136.

Hornstein, E.P., Verweij, J., Li, P.H., and Schnapf, J.L. (2005). Gap-junctional coupling and absolute sensitivity of photoreceptors in macaque retina. *J Neurosci* 25**,** 11201-11209.

Hui, E., Bai, J., Wang, P., Sugimori, M., Llinas, R.R., and Chapman, E.R. (2005). Three distinct kinetic groupings of the synaptotagmin family: candidate sensors for rapid and delayed exocytosis. *Proc Natl Acad Sci U S A* 102**,** 5210-5214.

Humeau, Y., Doussau, F., Vitiello, F., Greengard, P., Benfenati, F., and Poulain, B. (2001). Synapsin controls both reserve and releasable synaptic vesicle pools during neuronal activity and short-term plasticity in Aplysia. *J Neurosci* 21**,** 4195-4206.

Ichinose, T., and Hellmer, C.B. (2016). Differential signalling and glutamate receptor compositions in the OFF bipolar cell types in the mouse retina. *J Physiol* 594**,** 883-894.

Ingram, N.T., Sampath, A.P., and Fain, G.L. (2020). Membrane conductances of mouse cone photoreceptors. *J Gen Physiol* 152.

Innocenti, B., and Heidelberger, R. (2008). Mechanisms contributing to tonic release at the cone photoreceptor ribbon synapse. *J Neurophysiol* 99**,** 25-36.

Ishikawa, T., Sahara, Y., and Takahashi, T. (2002). A single packet of transmitter does not saturate postsynaptic glutamate receptors. *Neuron* 34**,** 613-621.

Ito, S., and Feldheim, D.A. (2018). The Mouse Superior Colliculus: An Emerging Model for Studying Circuit Formation and Function. *Front Neural Circuits* 12**,** 10.

Jackman, S.L., Babai, N., Chambers, J.J., Thoreson, W.B., and Kramer, R.H. (2011). A positive feedback synapse from retinal horizontal cells to cone photoreceptors. *PLoS Biol* 9**,** e1001057.

Jackman, S.L., Choi, S.Y., Thoreson, W.B., Rabl, K., Bartoletti, T.M., and Kramer, R.H. (2009). Role of the synaptic ribbon in transmitting the cone light response. *Nature neuroscience* 12**,** 303-310.

James, B., Darnet, L., Moya-Diaz, J., Seibel, S.H., and Lagnado, L. (2019). An amplitude code transmits information at a visual synapse. *Nature neuroscience* 22**,** 1140-1147.

Jarsky, T., Tian, M., and Singer, J.H. (2010). Nanodomain control of exocytosis is responsible for the signaling capability of a retinal ribbon synapse. *The Journal of neuroscience : the official journal of the Society for Neuroscience* 30**,** 11885-11895.

Jensen, A.A., Fahlke, C., Bjorn-Yoshimoto, W.E., and Bunch, L. (2015). Excitatory amino acid transporters: recent insights into molecular mechanisms, novel modes of modulation and new therapeutic possibilities. *Curr Opin Pharmacol* 20**,** 116-123.

Jin, N.G., Chuang, A.Z., Masson, P.J., and Ribelayga, C.P. (2015). Rod electrical coupling is controlled by a circadian clock and dopamine in mouse retina. *J Physiol* 593**,** 1597-1631.

Johnson, C.P., and Chapman, E.R. (2010). Otoferlin is a calcium sensor that directly regulates SNARE-mediated membrane fusion. *J Cell Biol* 191**,** 187-197.

Johnson, J.E., Jr., Perkins, G.A., Giddabasappa, A., Chaney, S., Xiao, W., White, A.D., Brown, J.M., Waggoner, J., Ellisman, M.H., and Fox, D.A. (2007). Spatiotemporal regulation of ATP and Ca2+ dynamics in vertebrate rod and cone ribbon synapses. *Mol Vis* 13**,** 887-919.

Kaeser, P.S., and Regehr, W.G. (2014). Molecular mechanisms for synchronous, asynchronous, and spontaneous neurotransmitter release. *Annu Rev Physiol* 76**,** 333-363.

Kanow, M.A., Giarmarco, M.M., Jankowski, C.S., Tsantilas, K., Engel, A.L., Du, J., Linton, J.D., Farnsworth, C.C., Sloat, S.R., Rountree, A., Sweet, I.R., Lindsay, K.J., Parker, E.D., Brockerhoff, S.E., Sadilek, M., Chao, J.R., and Hurley, J.B. (2017). Biochemical

adaptations of the retina and retinal pigment epithelium support a metabolic ecosystem in the vertebrate eye. *Elife* 6.

Kantardzhieva, A., Peppi, M., Lane, W.S., and Sewell, W.F. (2012). Protein composition of immunoprecipitated synaptic ribbons. *Journal of proteome research* 11**,** 1163-1174.

Kavalali, E.T. (2002). SNARE interactions in membrane trafficking: a perspective from mammalian central synapses. *Bioessays* 24**,** 926-936.

Kavalali, E.T. (2015). The mechanisms and functions of spontaneous neurotransmitter release. *Nat Rev Neurosci* 16**,** 5-16.

Kavalali, E.T. (2018). Spontaneous neurotransmission: A form of neural communication comes of age. *J Neurosci Res* 96**,** 331-334.

Kavalali, E.T. (2019). Neuronal Ca(2+) signalling at rest and during spontaneous neurotransmission. *J Physiol*.

Kavalali, E.T., and Plummer, M.R. (1996). Multiple voltage-dependent mechanisms potentiate calcium channel activity in hippocampal neurons. *J Neurosci* 16**,** 1072-1082.

Kim, I.J., Zhang, Y., Yamagata, M., Meister, M., and Sanes, J.R. (2008). Molecular identification of a retinal cell type that responds to upward motion. *Nature* 452**,** 478-482.

Klein, O., Roded, A., Zur, N., Azouz, N.P., Pasternak, O., Hirschberg, K., Hammel, I., Roche, P.A., Yatsu, A., Fukuda, M., Galli, S.J., and Sagi-Eisenberg, R. (2017). Rab5 is critical for SNAP23 regulated granule-granule fusion during compound exocytosis. *Scientific reports* 7**,** 15315-15017-15047-15318.

Koch, H.P., Brown, R.L., and Larsson, H.P. (2007). The glutamate-activated anion conductance in excitatory amino acid transporters is gated independently by the individual subunits. *J Neurosci* 27**,** 2943-2947.

Koenig, D., and Hofer, H. (2011). The absolute threshold of cone vision. *J Vis* 11.

Koike, C., Numata, T., Ueda, H., Mori, Y., and Furukawa, T. (2010a). TRPM1: a vertebrate TRP channel responsible for retinal ON bipolar function. *Cell Calcium* 48**,** 95-101.

Koike, C., Obara, T., Uriu, Y., Numata, T., Sanuki, R., Miyata, K., Koyasu, T., Ueno, S., Funabiki, K., Tani, A., Ueda, H., Kondo, M., Mori, Y., Tachibana, M., and Furukawa, T. (2010b). TRPM1 is a component of the retinal ON bipolar cell transduction channel in the mGluR6 cascade. *Proc Natl Acad Sci U S A* 107**,** 332-337.

Kolb, H., and Famiglietti, E.V. (1974). Rod and cone pathways in the inner plexiform layer of cat retina. *Science* 186**,** 47-49.

Kolomeisky, A.B. (2013). Motor proteins and molecular motors: how to operate machines at the nanoscale. *J Phys Condens Matter* 25**,** 463101.

Korn, H., Triller, A., Mallet, A., and Faber, D.S. (1981). Fluctuating responses at a central synapse: n of binomial fit predicts number of stained presynaptic boutons. *Science* 213**,** 898-901.

Kramer, R.H., and Davenport, C.M. (2015). Lateral Inhibition in the Vertebrate Retina: The Case of the Missing Neurotransmitter. *PLoS Biol* 13**,** e1002322.

Krispel, C.M., Chen, D., Melling, N., Chen, Y.J., Martemyanov, K.A., Quillinan, N., Arshavsky, V.Y., Wensel, T.G., Chen, C.K., and Burns, M.E. (2006). RGS expression rate-limits recovery of rod photoresponses. *Neuron* 51**,** 409-416.

Lam, D.M., Lasater, E.M., and Naka, K.I. (1978). gamma-Aminobutyric acid: a neurotransmitter candidate for cone horizontal cells of the catfish retina. *Proc Natl Acad Sci U S A* 75**,** 6310-6313.

Lam, P.P., Ohno, M., Dolai, S., He, Y., Qin, T., Liang, T., Zhu, D., Kang, Y., Liu, Y., Kauppi, M., Xie, L., Wan, W.C., Bin, N.R., Sugita, S., Olkkonen, V.M., Takahashi, N., Kasai, H., and Gaisano, H.Y. (2013). Munc18b is a major mediator of insulin exocytosis in rat pancreatic beta-cells. *Diabetes* 62**,** 2416-2428.

Lamb, T.D., and Pugh, E.N., Jr. (1992). A quantitative account of the activation steps involved in phototransduction in amphibian photoreceptors. *J Physiol* 449**,** 719-758.

Lasansky, A. (1978). Contacts between receptors and electrophysiologically identified neurones in the retina of the larval tiger salamander. *The Journal of physiology* 285**,** 531-542.

Lau, J.C., and Linsenmeier, R.A. (2012). Oxygen consumption and distribution in the Long-Evans rat retina. *Exp Eye Res* 102**,** 50-58.

Lee, S.C., and Deutsch, C. (1990). Temperature dependence of K(+)-channel properties in human T lymphocytes. *Biophys J* 57**,** 49-62.

Lenzi, D., Crum, J., Ellisman, M.H., and Roberts, W.M. (2002). Depolarization redistributes synaptic membrane and creates a gradient of vesicles on the synaptic body at a ribbon synapse. *Neuron* 36**,** 649-659.

Leskov, I.B., Klenchin, V.A., Handy, J.W., Whitlock, G.G., Govardovskii, V.I., Bownds, M.D., Lamb, T.D., Pugh, E.N., Jr., and Arshavsky, V.Y. (2000). The gain of rod phototransduction: reconciliation of biochemical and electrophysiological measurements. *Neuron* 27**,** 525-537.

Li, G.L., Cho, S., and Von Gersdorff, H. (2014). Phase-locking precision is enhanced by multiquantal release at an auditory hair cell ribbon synapse. *Neuron* 83**,** 1404-1417.

Li, G.L., Keen, E., Andor-Ardo, D., Hudspeth, A.J., and Von Gersdorff, H. (2009). The unitary event underlying multiquantal EPSCs at a hair cell's ribbon synapse. *J Neurosci* 29**,** 7558-7568.

Li, L., Eter, N., and Heiduschka, P. (2015). The microglia in healthy and diseased retina. *Exp Eye Res* 136**,** 116-130.

Li, S., Chen, D., Sauve, Y., Mccandless, J., Chen, Y.J., and Chen, C.K. (2005). Rhodopsin-iCre transgenic mouse line for Cre-mediated rod-specific gene targeting. *Genesis* 41**,** 73-80.

Li, W., Keung, J.W., and Massey, S.C. (2004). Direct synaptic connections between rods and OFF cone bipolar cells in the rabbit retina. *J Comp Neurol* 474**,** 1-12.

Liley, A.W. (1956). The quantal components of the mammalian end-plate potential. *J Physiol* 133**,** 571-587.

Linsenmeier, R.A. (1986). Effects of light and darkness on oxygen distribution and consumption in the cat retina. *J Gen Physiol* 88**,** 521-542.

Linton, J.D., Holzhausen, L.C., Babai, N., Song, H., Miyagishima, K.J., Stearns, G.W., Lindsay, K., Wei, J., Chertov, A.O., Peters, T.A., Caffe, R., Pluk, H., Seeliger, M.W., Tanimoto, N., Fong, K., Bolton, L., Kuok, D.L., Sweet, I.R., Bartoletti, T.M., Radu, R.A., Travis, G.H., Zagotta, W.N., Townes-Anderson, E., Parker, E., Van Der Zee, C.E., Sampath, A.P., Sokolov, M., Thoreson, W.B., and Hurley, J.B. (2010). Flow of energy in the outer retina in darkness and in light. *Proc Natl Acad Sci U S A* 107**,** 8599-8604.

Liu, J. (1995). "The Anatomy and Physiology of Direction-Selective Retinal Ganglion Cells," in *Webvision: The Organization of the Retina and Visual System,* eds. H. Kolb, E. Fernandez & R. Nelson. (Salt Lake City (UT)).

Liu, P., Khvotchev, M., Li, Y.C., Chanaday, N.L., and Kavalali, E.T. (2018). Copine-6 Binds to SNAREs and Selectively Suppresses Spontaneous Neurotransmission. *J Neurosci* 38**,** 5888-5899.

Liu, X., Heidelberger, R., and Janz, R. (2014). Phosphorylation of syntaxin 3B by CaMKII regulates the formation of t-SNARE complexes. *Molecular and cellular neurosciences* 60**,** 53-62.

Llano, I., and Gerschenfeld, H.M. (1993). Inhibitory synaptic currents in stellate cells of rat cerebellar slices. *J Physiol* 468**,** 177-200.

Loebel, A., Silberberg, G., Helbig, D., Markram, H., Tsodyks, M., and Richardson, M.J. (2009). Multiquantal release underlies the distribution of synaptic efficacies in the neocortex. *Front Comput Neurosci* 3**,** 27.

Logiudice, L., and Matthews, G. (2009). The role of ribbons at sensory synapses. *Neuroscientist* 15**,** 380-391.

Lollike, K., Lindau, M., Calafat, J., and Borregaard, N. (2002). Compound exocytosis of granules in human neutrophils. *Journal of leukocyte biology* 71**,** 973-980.

Luo, F., Bacaj, T., and Sudhof, T.C. (2015). Synaptotagmin-7 Is Essential for Ca2+-Triggered Delayed Asynchronous Release But Not for Ca2+-Dependent Vesicle Priming in Retinal Ribbon Synapses. *J Neurosci* 35**,** 11024-11033.

Luo, F., and Sudhof, T.C. (2017). Synaptotagmin-7-Mediated Asynchronous Release Boosts High-Fidelity Synchronous Transmission at a Central Synapse. *Neuron* 94**,** 826-839 e823.

Lv, C., Gould, T.J., Bewersdorf, J., and Zenisek, D. (2012a). High-resolution optical imaging of zebrafish larval ribbon synapse protein RIBEYE, RIM2, and CaV 1.4 by stimulation emission depletion microscopy. *Microscopy and microanalysis : the official journal of Microscopy Society of America, Microbeam Analysis Society, Microscopical Society of Canada* 18**,** 745-752.

Lv, C., Gould, T.J., Bewersdorf, J., and Zenisek, D. (2012b). High-resolution optical imaging of zebrafish larval ribbon synapse protein RIBEYE, RIM2, and CaV 1.4 by stimulation emission depletion microscopy. *Microsc Microanal* 18**,** 745-752.

Machtens, J.P., Kortzak, D., Lansche, C., Leinenweber, A., Kilian, P., Begemann, B., Zachariae, U., Ewers, D., De Groot, B.L., Briones, R., and Fahlke, C. (2015). Mechanisms of anion conduction by coupled glutamate transporters. *Cell* 160**,** 542-553.

Magee, J.C., Avery, R.B., Christie, B.R., and Johnston, D. (1996). Dihydropyridine-sensitive, voltage-gated Ca2+ channels contribute to the resting intracellular Ca2+ concentration of hippocampal CA1 pyramidal neurons. *J Neurophysiol* 76**,** 3460-3470.

Magi, S., Piccirillo, S., Amoroso, S., and Lariccia, V. (2019). Excitatory Amino Acid Transporters (EAATs): Glutamate Transport and Beyond. *Int J Mol Sci* 20.

Malagon, G., Miki, T., Llano, I., Neher, E., and Marty, A. (2016). Counting Vesicular Release Events Reveals Binomial Release Statistics at Single Glutamatergic Synapses. *J Neurosci* 36**,** 4010-4025.

Masland, R.H. (2011). Cell populations of the retina: the Proctor lecture. *Invest Ophthalmol Vis Sci* 52**,** 4581-4591.

Masland, R.H. (2012). The tasks of amacrine cells. *Vis Neurosci* 29**,** 3-9.

Masu, M., Iwakabe, H., Tagawa, Y., Miyoshi, T., Yamashita, M., Fukuda, Y., Sasaki, H., Hiroi, K., Nakamura, Y., Shigemoto, R., and Et Al. (1995). Specific deficit of the ON response in visual transmission by targeted disruption of the mGluR6 gene. *Cell* 80**,** 757-765.

Matthews, G., and Sterling, P. (2008). Evidence that vesicles undergo compound fusion on the synaptic ribbon. *J Neurosci* 28**,** 5403-5411.

Mckinney, R.A., Capogna, M., Durr, R., Gahwiler, B.H., and Thompson, S.M. (1999). Miniature synaptic events maintain dendritic spines via AMPA receptor activation. *Nat Neurosci* 2**,** 44-49.

Mehta, B., Snellman, J., Chen, S., Li, W., and Zenisek, D. (2013). Synaptic ribbons influence the size and frequency of miniature-like evoked postsynaptic currents. *Neuron* 77**,** 516-527.

Mennerick, S., and Matthews, G. (1996). Ultrafast exocytosis elicited by calcium current in synaptic terminals of retinal bipolar neurons. *Neuron* 17**,** 1241-1249.

Mercer, A.J., and Thoreson, W.B. (2011). The dynamic architecture of photoreceptor ribbon synapses: cytoskeletal, extracellular matrix, and intramembrane proteins. *Vis Neurosci* 28**,** 453-471.

Messenger, S.W., Falkowski, M.A., and Groblewski, G.E. (2014). Ca(2)(+)-regulated secretory granule exocytosis in pancreatic and parotid acinar cells. *Cell calcium* 55**,** 369-375.

Michalski, N., Goutman, J.D., Auclair, S.M., Boutet De Monvel, J., Tertrais, M., Emptoz, A., Parrin, A., Nouaille, S., Guillon, M., Sachse, M., Ciric, D., Bahloul, A., Hardelin, J.P., Sutton, R.B., Avan, P., Krishnakumar, S.S., Rothman, J.E., Dulon, D., Safieddine, S., and Petit, C. (2017). Otoferlin acts as a Ca(2+) sensor for vesicle fusion and vesicle pool replenishment at auditory hair cell ribbon synapses. *Elife* 6.

Miki, T. (2019). What We Can Learn From Cumulative Numbers of Vesicular Release Events. *Front Cell Neurosci* 13**,** 257.

Moore, R.Y., Speh, J.C., and Card, J.P. (1995). The retinohypothalamic tract originates from a distinct subset of retinal ganglion cells. *J Comp Neurol* 352**,** 351-366.

Morgans, C.W. (2001). Localization of the alpha(1F) calcium channel subunit in the rat retina. *Investigative ophthalmology & visual science* 42**,** 2414-2418.

Morgans, C.W., Brown, R.L., and Duvoisin, R.M. (2010). TRPM1: the endpoint of the mGluR6 signal transduction cascade in retinal ON-bipolar cells. *Bioessays* 32**,** 609-614.

Morgans, C.W., Zhang, J., Jeffrey, B.G., Nelson, S.M., Burke, N.S., Duvoisin, R.M., and Brown, R.L. (2009). TRPM1 is required for the depolarizing light response in retinal ON-bipolar cells. *Proc Natl Acad Sci U S A* 106**,** 19174-19178.

Moser, T., Grabner, C.P., and Schmitz, F. (2020). Sensory Processing at Ribbon Synapses in the Retina and the Cochlea. *Physiol Rev* 100**,** 103-144.

Mostafavi, H., Thiyagarajan, S., Stratton, B.S., Karatekin, E., Warner, J.M., Rothman, J.E., and O'shaughnessy, B. (2017). Entropic forces drive self-organization and membrane fusion by SNARE proteins. *Proc Natl Acad Sci U S A* 114**,** 5455-5460.

Motulsky, H. (2010). *Intuitive biostatistics : a nonmathematical guide to statistical thinking.* New York: Oxford University Press.

Murcia-Belmonte, V., and Erskine, L. (2019). Wiring the Binocular Visual Pathways. *Int J Mol Sci* 20.

Muresan, V., Lyass, A., and Schnapp, B.J. (1999). The kinesin motor KIF3A is a component of the presynaptic ribbon in vertebrate photoreceptors. *J Neurosci* 19**,** 1027-1037.

Nachman-Clewner, M., St Jules, R., and Townes-Anderson, E. (1999). L-type calcium channels in the photoreceptor ribbon synapse: localization and role in plasticity. *The Journal of comparative neurology* 415**,** 1-16.

Nawy, S. (2000). Regulation of the on bipolar cell mGluR6 pathway by Ca2+. *J Neurosci* 20**,** 4471-4479.

Nawy, S. (2004). Desensitization of the mGluR6 transduction current in tiger salamander On bipolar cells. *J Physiol* 558**,** 137-146.

Naylor, A., Hopkins, A., Hudson, N., and Campbell, M. (2019). Tight Junctions of the Outer Blood Retina Barrier. *Int J Mol Sci* 21.

Neher, E. (1998). Usefulness and limitations of linear approximations to the understanding of Ca++ signals. *Cell Calcium* 24**,** 345-357.

Nickell, S., Park, P.S., Baumeister, W., and Palczewski, K. (2007). Three-dimensional architecture of murine rod outer segments determined by cryoelectron tomography. *J Cell Biol* 177**,** 917-925.

Nielsen, T.A., Digregorio, D.A., and Silver, R.A. (2004). Modulation of glutamate mobility reveals the mechanism underlying slow-rising AMPAR EPSCs and the diffusion coefficient in the synaptic cleft. *Neuron* 42**,** 757-771.

Okawa, H., and Sampath, A.P. (2007). Optimization of single-photon response transmission at the rod-to-rod bipolar synapse. *Physiology (Bethesda)* 22**,** 279-286.

Okawa, H., Sampath, A.P., Laughlin, S.B., and Fain, G.L. (2008). ATP consumption by mammalian rod photoreceptors in darkness and in light. *Curr Biol* 18**,** 1917-1921.

Otis, T.S., and Jahr, C.E. (1998). Anion currents and predicted glutamate flux through a neuronal glutamate transporter. *J Neurosci* 18**,** 7099-7110.

Palmer, M.J., Taschenberger, H., Hull, C., Tremere, L., and Von Gersdorff, H. (2003). Synaptic activation of presynaptic glutamate transporter currents in nerve terminals. *J Neurosci* 23**,** 4831-4841.

Pang, J.J., Gao, F., Barrow, A., Jacoby, R.A., and Wu, S.M. (2008a). How do tonic glutamatergic synapses evade receptor desensitization? *J Physiol* 586**,** 2889-2902.

Pang, J.J., Gao, F., Barrow, A., Jacoby, R.A., and Wu, S.M. (2008b). How do tonic glutamatergic synapses evade receptor desensitization? *The Journal of physiology* 586**,** 2889-2902.

Pang, Z.P., Bacaj, T., Yang, X., Zhou, P., Xu, W., and Sudhof, T.C. (2011). Doc2 supports spontaneous synaptic transmission by a Ca(2+)-independent mechanism. *Neuron* 70**,** 244-251.

Pangrsic, T., Singer, J.H., and Koschak, A. (2018). Voltage-Gated Calcium Channels: Key Players in Sensory Coding in the Retina and the Inner Ear. *Physiol Rev* 98**,** 2063-2096.

Parsons, T.D., and Sterling, P. (2003). Synaptic ribbon. Conveyor belt or safety belt? *Neuron* 37**,** 379-382.

Peichl, L., and Gonzalez-Soriano, J. (1994). Morphological types of horizontal cell in rodent retinae: a comparison of rat, mouse, gerbil, and guinea pig. *Vis Neurosci* 11**,** 501-517.

Peloquin, J.B., Doering, C.J., Rehak, R., and Mcrory, J.E. (2008). Temperature dependence of Cav1.4 calcium channel gating. *Neuroscience* 151**,** 1066-1083.

Pelucchi, B., Grimaldi, A., and Moriondo, A. (2008). Vertebrate rod photoreceptors express both BK and IK calcium-activated potassium channels, but only BK channels are involved in receptor potential regulation. *J Neurosci Res* 86**,** 194-201.

Picaud, S.A., Larsson, H.P., Grant, G.B., Lecar, H., and Werblin, F.S. (1995). Glutamate-gated chloride channel with glutamate-transporter-like properties in cone photoreceptors of the tiger salamander. *J Neurophysiol* 74**,** 1760-1771.

Pugh, E.N., Jr. (2018). The discovery of the ability of rod photoreceptors to signal single photons. *J Gen Physiol* 150**,** 383-388.

Pugh, E.N., Jr., and Lamb, T.D. (1993). Amplification and kinetics of the activation steps in phototransduction. *Biochim Biophys Acta* 1141**,** 111-149.

Pulido, C., and Marty, A. (2017). Quantal Fluctuations in Central Mammalian Synapses: Functional Role of Vesicular Docking Sites. *Physiological Reviews* 97**,** 1403-1430.

Puller, C., Haverkamp, S., and Grunert, U. (2007). OFF midget bipolar cells in the retina of the marmoset, Callithrix jacchus, express AMPA receptors. *J Comp Neurol* 502**,** 442-454.

Puller, C., Haverkamp, S., Neitz, M., and Neitz, J. (2014). Synaptic elements for GABAergic feed-forward signaling between HII horizontal cells and blue cone bipolar cells are enriched beneath primate S-cones. *PLoS One* 9**,** e88963.

Quadros, R.M., Miura, H., Harms, D.W., Akatsuka, H., Sato, T., Aida, T., Redder, R., Richardson, G.P., Inagaki, Y., Sakai, D., Buckley, S.M., Seshacharyulu, P., Batra, S.K., Behlke, M.A., Zeiner, S.A., Jacobi, A.M., Izu, Y., Thoreson, W.B., Urness, L.D., Mansour, S.L., Ohtsuka, M., and Gurumurthy, C.B. (2017). Easi-CRISPR: a robust method for one-step generation of mice carrying conditional and insertion alleles using long ssDNA donors and CRISPR ribonucleoproteins. *Genome Biol* 18**,** 92.

Ramakrishnan, N.A., Drescher, M.J., and Drescher, D.G. (2012). The SNARE complex in neuronal and sensory cells. *Mol Cell Neurosci* 50**,** 58-69.

Ramirez, D.M.O., Crawford, D.C., Chanaday, N.L., Trauterman, B., Monteggia, L.M., and Kavalali, E.T. (2017). Loss of Doc2-Dependent Spontaneous Neurotransmission Augments Glutamatergic Synaptic Strength. *J Neurosci* 37**,** 6224-6230.

Ramirez, J.M., Trivino, A., Ramirez, A.I., Salazar, J.J., and Garcia-Sanchez, J. (1996). Structural specializations of human retinal glial cells. *Vision Res* 36**,** 2029-2036.

Rao-Mirotznik, R., Buchsbaum, G., and Sterling, P. (1998). Transmitter concentration at a three-dimensional synapse. *J Neurophysiol* 80**,** 3163-3172.

Rao-Mirotznik, R., Harkins, A.B., Buchsbaum, G., and Sterling, P. (1995). Mammalian rod terminal: architecture of a binary synapse. *Neuron* 14**,** 561-569.

Rao, R., Buchsbaum, G., and Sterling, P. (1994). Rate of quantal transmitter release at the mammalian rod synapse. *Biophys J* 67**,** 57-63.

Rea, R., Li, J., Dharia, A., Levitan, E.S., Sterling, P., and Kramer, R.H. (2004). Streamlined synaptic vesicle cycle in cone photoreceptor terminals. *Neuron* 41**,** 755-766.

Redman, S. (1990). Quantal analysis of synaptic potentials in neurons of the central nervous system. *Physiol Rev* 70**,** 165-198.

Redman, S., and Walmsley, B. (1983). Amplitude fluctuations in synaptic potentials evoked in cat spinal motoneurones at identified group Ia synapses. *J Physiol* 343**,** 135-145.

Reichenbach, A., and Bringmann, A. (2019). Glia of the human retina. *Glia*.

Reingruber, J., Holcman, D., and Fain, G.L. (2015). How rods respond to single photons: Key adaptations of a G-protein cascade that enable vision at the physical limit of perception. *Bioessays* 37**,** 1243-1252.

Rickman, C., and Davletov, B. (2003). Mechanism of calcium-independent synaptotagmin binding to target SNAREs. *J Biol Chem* 278**,** 5501-5504.

Rieke, F., and Baylor, D.A. (1998). Origin of reproducibility in the responses of retinal rods to single photons. *Biophys J* 75**,** 1836-1857.

Rieke, F., and Schwartz, E.A. (1996). Asynchronous transmitter release: control of exocytosis and endocytosis at the salamander rod synapse. *J Physiol* 493 (Pt 1)**,** 1-8.

Risselada, H.J., and Grubmuller, H. (2012). How SNARE molecules mediate membrane fusion: recent insights from molecular simulations. *Curr Opin Struct Biol* 22**,** 187-196.

Rizo, J., and Sudhof, T.C. (2002). Snares and Munc18 in synaptic vesicle fusion. *Nat Rev Neurosci* 3**,** 641-653.

Rodarte, E.M., Ramos, M.A., Davalos, A.J., Moreira, D.C., Moreno, D.S., Cardenas, E.I., Rodarte, A.I., Petrova, Y., Molina, S., Rendon, L.E., Sanchez, E., Breaux, K., Tortoriello, A., Manllo, J., Gonzalez, E.A., Tuvim, M.J., Dickey, B.F., Burns, A.R., Heidelberger, R., and Adachi, R. (2018). Munc13 proteins control regulated exocytosis in mast cells. *The Journal of biological chemistry* 293**,** 345-358.

Rossi, M.L., Martini, M., Pelucchi, B., and Fesce, R. (1994). Quantal nature of synaptic transmission at the cytoneural junction in the frog labyrinth. *The Journal of physiology* 478 (Pt 1)**,** 17-35.

Rudolph, S., Tsai, M.C., Von Gersdorff, H., and Wadiche, J.I. (2015). The ubiquitous nature of multivesicular release. *Trends in neurosciences* 38**,** 428-438.

Saari, J.C. (2016). Vitamin A and Vision. *Subcell Biochem* 81**,** 231-259.

Sabatini, B.L., and Regehr, W.G. (1996). Timing of neurotransmission at fast synapses in the mammalian brain. *Nature* 384**,** 170-172.

Saito, T., and Kaneko, A. (1983). Ionic mechanisms underlying the responses of off-center bipolar cells in the carp retina. I. Studies on responses evoked by light. *J Gen Physiol* 81**,** 589-601.

Sampath, A.P., and Rieke, F. (2004). Selective transmission of single photon responses by saturation at the rod-to-rod bipolar synapse. *Neuron* 41**,** 431-443.

Sanchez, E., Gonzalez, E.A., Moreno, D.S., Cardenas, R.A., Ramos, M.A., Davalos, A.J., Manllo, J., Rodarte, A.I., Petrova, Y., Moreira, D.C., Chavez, M.A., Tortoriello, A., Lara, A., Gutierrez, B.A., Burns, A.R., Heidelberger, R., and Adachi, R. (2018). Syntaxin 3, but not syntaxin 4, is required for mast cell-regulated exocytosis, where it plays a primary role mediating compound exocytosis. *J.Biol.Chem.* 294**,** 3012-3023.

Sanes, J.R., and Masland, R.H. (2015). The types of retinal ganglion cells: current status and implications for neuronal classification. *Annu Rev Neurosci* 38**,** 221-246.

Sara, Y., Virmani, T., Deak, F., Liu, X., and Kavalali, E.T. (2005). An isolated pool of vesicles recycles at rest and drives spontaneous neurotransmission. *Neuron* 45**,** 563-573.

Sato, S., and Kefalov, V.J. (2016). cis Retinol oxidation regulates photoreceptor access to the retina visual cycle and cone pigment regeneration. *J Physiol* 594**,** 6753-6765.

Scanziani, M., Capogna, M., Gahwiler, B.H., and Thompson, S.M. (1992). Presynaptic inhibition of miniature excitatory synaptic currents by baclofen and adenosine in the hippocampus. *Neuron* 9**,** 919-927.

Scheefhals, N., and Macgillavry, H.D. (2018). Functional organization of postsynaptic glutamate receptors. *Mol Cell Neurosci* 91**,** 82-94.

Schein, S., and Ahmad, K.M. (2005). A clockwork hypothesis: synaptic release by rod photoreceptors must be regular. *Biophys J* 89**,** 3931-3949.

Schein, S., and Ahmad, K.M. (2006). Efficiency of synaptic transmission of single-photon events from rod photoreceptor to rod bipolar dendrite. *Biophys J* 91**,** 3257-3267.

Schmitz, F. (2009). The making of synaptic ribbons: how they are built and what they do. *Neuroscientist* 15**,** 611-624.

Schmitz, F., Konigstorfer, A., and Sudhof, T.C. (2000). RIBEYE, a component of synaptic ribbons: a protein's journey through evolution provides insight into synaptic ribbon function. *Neuron* 28**,** 857-872.

Schmitz, Y., and Witkovsky, P. (1997). Dependence of photoreceptor glutamate release on a dihydropyridine-sensitive calcium channel. *Neuroscience* 78**,** 1209-1216.

Schneeweis, D.M., and Schnapf, J.L. (1995). Photovoltage of rods and cones in the macaque retina. *Science* 268**,** 1053-1056.

Schneggenburger, R., and Neher, E. (2000). Intracellular calcium dependence of transmitter release rates at a fast central synapse. *Nature* 406**,** 889-893.

Schneggenburger, R., and Neher, E. (2005). Presynaptic calcium and control of vesicle fusion. *Curr Opin Neurobiol* 15**,** 266-274.

Schneider, N., Cordeiro, S., Machtens, J.P., Braams, S., Rauen, T., and Fahlke, C. (2014). Functional properties of the retinal glutamate transporters GLT-1c and EAAT5. *The Journal of biological chemistry* 289**,** 1815-1824.

Sharpe, L.T., Stockman, A., Fach, C.C., and Markstahler, U. (1993). Temporal and spatial summation in the human rod visual system. *J Physiol* 463**,** 325-348.

Shen, Y., Rampino, M.A., Carroll, R.C., and Nawy, S. (2012). G-protein-mediated inhibition of the Trp channel TRPM1 requires the Gbetagamma dimer. *Proc Natl Acad Sci U S A* 109**,** 8752-8757.

Sheng, Z., Choi, S.Y., Dharia, A., Li, J., Sterling, P., and Kramer, R.H. (2007). Synaptic Ca2+ in darkness is lower in rods than cones, causing slower tonic release of vesicles. *J Neurosci* 27**,** 5033-5042.

Singer, J.H., Lassova, L., Vardi, N., and Diamond, J.S. (2004). Coordinated multivesicular release at a mammalian ribbon synapse. *Nature neuroscience* 7**,** 826-833.

Snellman, J., Kaur, T., Shen, Y., and Nawy, S. (2008). Regulation of ON bipolar cell activity. *Prog Retin Eye Res* 27**,** 450-463.

Snellman, J., Mehta, B., Babai, N., Bartoletti, T.M., Akmentin, W., Francis, A., Matthews, G., Thoreson, W., and Zenisek, D. (2011). Acute destruction of the synaptic ribbon reveals a role for the ribbon in vesicle priming. *Nat Neurosci* 14**,** 1135-1141.

Song, H., Ming, G., Fon, E., Bellocchio, E., Edwards, R.H., and Poo, M. (1997). Expression of a putative vesicular acetylcholine transporter facilitates quantal transmitter packaging. *Neuron* 18**,** 815-826.

Soucy, E., Wang, Y., Nirenberg, S., Nathans, J., and Meister, M. (1998). A novel signaling pathway from rod photoreceptors to ganglion cells in mammalian retina. *Neuron* 21**,** 481-493.

Specht, D., Wu, S.B., Turner, P., Dearden, P., Koentgen, F., Wolfrum, U., Maw, M., Brandstatter, J.H., and Tom Dieck, S. (2009). Effects of presynaptic mutations on a postsynaptic Cacna1s calcium channel colocalized with mGluR6 at mouse photoreceptor ribbon synapses. *Invest Ophthalmol Vis Sci* 50**,** 505-515.

Stafford, B.K., Manookin, M.B., Singer, J.H., and Demb, J.B. (2014). NMDA and AMPA receptors contribute similarly to temporal processing in mammalian retinal ganglion cells. *J Physiol* 592**,** 4877-4889.

Sterling, P., Cohen, E., Freed, M.A., and Smith, R.G. (1987). Microcircuitry of the on-beta ganglion cell in daylight, twilight, and starlight. *Neurosci Res Suppl* 6**,** S269-285.

Sterling, P., and Matthews, G. (2005). Structure and function of ribbon synapses. *Trends Neurosci* 28**,** 20-29.

Sudhof, T.C. (2002). Synaptotagmins: why so many? *J Biol Chem* 277**,** 7629-7632.

Sudhof, T.C. (2014). The molecular machinery of neurotransmitter release (Nobel lecture). *Angew Chem Int Ed Engl* 53**,** 12696-12717.

Sugita, S., Shin, O.H., Han, W., Lao, Y., and Sudhof, T.C. (2002). Synaptotagmins form a hierarchy of exocytotic Ca(2+) sensors with distinct Ca(2+) affinities. *EMBO J* 21**,** 270-280.

Sun, J., Pang, Z.P., Qin, D., Fahim, A.T., Adachi, R., and Sudhof, T.C. (2007). A dual-Ca2+-sensor model for neurotransmitter release in a central synapse. *Nature* 450**,** 676-682.

Suryanarayanan, A., and Slaughter, M.M. (2006). Synaptic transmission mediated by internal calcium stores in rod photoreceptors. *J Neurosci* 26**,** 1759-1766.

Szmajda, B.A., and Devries, S.H. (2011). Glutamate spillover between mammalian cone photoreceptors. *The Journal of neuroscience : the official journal of the Society for Neuroscience* 31**,** 13431-13441.

Takamori, S. (2016). Presynaptic Molecular Determinants of Quantal Size. *Front Synaptic Neurosci* 8**,** 2.

Takeshita, D., Smeds, L., and Ala-Laurila, P. (2017). Processing of single-photon responses in the mammalian On and Off retinal pathways at the sensitivity limit of vision. *Philos Trans R Soc Lond B Biol Sci* 372.

Tan, G.M., Yu, D., Wang, J., and Soong, T.W. (2012). Alternative splicing at C terminus of Ca(V)1.4 calcium channel modulates calcium-dependent inactivation, activation potential, and current density. *J Biol Chem* 287**,** 832-847.

Taylor, W.R., and Smith, R.G. (2004). Transmission of scotopic signals from the rod to rod-bipolar cell in the mammalian retina. *Vision Res* 44**,** 3269-3276.

Thoreson, W.B., and Burkhardt, D.A. (1990). Effects of synaptic blocking agents on the depolarizing responses of turtle cones evoked by surround illumination. *Vis Neurosci* 5**,** 571-583.

Thoreson, W.B., and Burkhardt, D.A. (1991). Ionic influences on the prolonged depolarization of turtle cones in situ. *J Neurophysiol* 65**,** 96-110.

Thoreson, W.B., and Dacey, D.M. (2019). Diverse Cell Types, Circuits, and Mechanisms for Color Vision in the Vertebrate Retina. *Physiol Rev* 99**,** 1527-1573.

Thoreson, W.B., and Mangel, S.C. (2012). Lateral interactions in the outer retina. *Prog Retin Eye Res* 31**,** 407-441.

Thoreson, W.B., Rabl, K., Townes-Anderson, E., and Heidelberger, R. (2004). A highly Ca2+-sensitive pool of vesicles contributes to linearity at the rod photoreceptor ribbon synapse. *Neuron* 42**,** 595-605.

Thorn, P., and Gaisano, H. (2012). Molecular control of compound Exocytosis: A key role for VAMP8. *Communicative & integrative biology* 5**,** 61-63.

Tinsley, J.N., Molodtsov, M.I., Prevedel, R., Wartmann, D., Espigule-Pons, J., Lauwers, M., and Vaziri, A. (2016). Direct detection of a single photon by humans. *Nat Commun* 7**,** 12172.

Tom Dieck, S., Altrock, W.D., Kessels, M.M., Qualmann, B., Regus, H., Brauner, D., Fejtova, A., Bracko, O., Gundelfinger, E.D., and Brandstatter, J.H. (2005a). Molecular dissection of the photoreceptor ribbon synapse: physical interaction of Bassoon and RIBEYE is essential for the assembly of the ribbon complex. *The Journal of cell biology* 168**,** 825-836.

Tom Dieck, S., Altrock, W.D., Kessels, M.M., Qualmann, B., Regus, H., Brauner, D., Fejtova, A., Bracko, O., Gundelfinger, E.D., and Brandstatter, J.H. (2005b). Molecular dissection of the photoreceptor ribbon synapse: physical interaction of Bassoon and RIBEYE is essential for the assembly of the ribbon complex. *J Cell Biol* 168**,** 825-836.

Townes-Anderson, E., Macleish, P.R., and Raviola, E. (1985a). Rod cells dissociated from mature salamander retina: ultrastructure and uptake of horseradish peroxidase. *J Cell Biol* 100**,** 175-188.

Townes-Anderson, E., Macleish, P.R., and Raviola, E. (1985b). Rod cells dissociated from mature salamander retina: ultrastructure and uptake of horseradish peroxidase. *The Journal of cell biology* 100**,** 175-188.

Trexler, E.B., Casti, A.R., and Zhang, Y. (2011). Nonlinearity and noise at the rod-rod bipolar cell synapse. *Vis Neurosci* 28**,** 61-68.

Trussell, L.O., Zhang, S., and Raman, I.M. (1993). Desensitization of AMPA receptors upon multiquantal neurotransmitter release. *Neuron* 10**,** 1185-1196.

Tse, D.Y., Chung, I., and Wu, S.M. (2014). Possible roles of glutamate transporter EAAT5 in mouse cone depolarizing bipolar cell light responses. *Vision Res* 103**,** 63-74.

Tsintsadze, T., Williams, C.L., Weingarten, D.J., Von Gersdorff, H., and Smith, S.M. (2017). Distinct Actions of Voltage-Activated Ca(2+) Channel Block on Spontaneous Release at Excitatory and Inhibitory Central Synapses. *J Neurosci* 37**,** 4301-4310.

Tsukamoto, Y., Morigiwa, K., Ueda, M., and Sterling, P. (2001). Microcircuits for night vision in mouse retina. *J Neurosci* 21**,** 8616-8623.

Tsukamoto, Y., and Omi, N. (2014). Some OFF bipolar cell types make contact with both rods and cones in macaque and mouse retinas. *Front Neuroanat* 8**,** 105.

Tsukamoto, Y., and Omi, N. (2015). OFF bipolar cells in macaque retina: type-specific connectivity in the outer and inner synaptic layers. *Front Neuroanat* 9**,** 122.

Tsukamoto, Y., and Omi, N. (2017). Classification of Mouse Retinal Bipolar Cells: Type-Specific Connectivity with Special Reference to Rod-Driven AII Amacrine Pathways. *Front Neuroanat* 11**,** 92.

Ubach, J., Lao, Y., Fernandez, I., Arac, D., Sudhof, T.C., and Rizo, J. (2001). The C2B domain of synaptotagmin I is a Ca2+-binding module. *Biochemistry* 40**,** 5854-5860.

Usukura, J., and Yamada, E. (1987). Ultrastructure of the synaptic ribbons in photoreceptor cells of Rana catesbeiana revealed by freeze-etching and freeze-substitution. *Cell Tissue Res* 247**,** 483-488.

Uthaiah, R.C., and Hudspeth, A.J. (2010). Molecular anatomy of the hair cell's ribbon synapse. *The Journal of neuroscience : the official journal of the Society for Neuroscience* 30**,** 12387-12399.

Vaithianathan, T., Henry, D., Akmentin, W., and Matthews, G. (2016). Nanoscale dynamics of synaptic vesicle trafficking and fusion at the presynaptic active zone. *Elife* 5.

Vakilian, M., Tahamtani, Y., and Ghaedi, K. (2019). A review on insulin trafficking and exocytosis. *Gene* 706**,** 52-61.

Van Hook, M.J., Nawy, S., and Thoreson, W.B. (2019). Voltage- and calcium-gated ion channels of neurons in the vertebrate retina. *Prog Retin Eye Res* 72**,** 100760.

Van Hook, M.J., Parmelee, C.M., Chen, M., Cork, K.M., Curto, C., and Thoreson, W.B. (2014). Calmodulin enhances ribbon replenishment and shapes filtering of synaptic transmission by cone photoreceptors. *J Gen Physiol* 144**,** 357-378.

Van Hook, M.J., and Thoreson, W.B. (2013). Simultaneous whole-cell recordings from photoreceptors and second-order neurons in an amphibian retinal slice preparation. *Journal of visualized experiments : JoVE* (76). doi**,** 10.3791/50007.

Van Hook, M.J., and Thoreson, W.B. (2015). Weak endogenous Ca2+ buffering supports sustained synaptic transmission by distinct mechanisms in rod and cone photoreceptors in salamander retina. *Physiol Rep* 3.

Van Rossum, M.C., and Smith, R.G. (1998). Noise removal at the rod synapse of mammalian retina. *Vis Neurosci* 15**,** 809-821.

Vasileva, M., Horstmann, H., Geumann, C., Gitler, D., and Kuner, T. (2012). Synapsin-dependent reserve pool of synaptic vesicles supports replenishment of the readily releasable pool under intense synaptic transmission. *Eur J Neurosci* 36**,** 3005-3020.

Verweij, J., Hornstein, E.P., and Schnapf, J.L. (2003). Surround antagonism in macaque cone photoreceptors. *J Neurosci* 23**,** 10249-10257.

Verweij, J., Kamermans, M., and Spekreijse, H. (1996). Horizontal cells feed back to cones by shifting the cone calcium-current activation range. *Vision Res* 36**,** 3943-3953.

Vielma, A.H., and Schmachtenberg, O. (2016). Electrophysiological fingerprints of OFF bipolar cells in rat retina. *Sci Rep* 6**,** 30259.

Vlasits, A.L., Euler, T., and Franke, K. (2019). Function first: classifying cell types and circuits of the retina. *Curr Opin Neurobiol* 56**,** 8-15.

Von Gersdorff, H., and Matthews, G. (1997). Depletion and replenishment of vesicle pools at a ribbon-type synaptic terminal. *J Neurosci* 17**,** 1919-1927.

Von Gersdorff, H., Vardi, E., Matthews, G., and Sterling, P. (1996). Evidence that vesicles on the synaptic ribbon of retinal bipolar neurons can be rapidly released. *Neuron* 16**,** 1221-1227.

Wadiche, J.I., Arriza, J.L., Amara, S.G., and Kavanaugh, M.P. (1995). Kinetics of a human glutamate transporter. *Neuron* 14**,** 1019-1027.

Walch-Solimena, C., Blasi, J., Edelmann, L., Chapman, E.R., Von Mollard, G.F., and Jahn, R. (1995a). The t-SNAREs syntaxin 1 and SNAP-25 are present on organelles that participate in synaptic vesicle recycling. *J Cell Biol* 128**,** 637-645.

Walch-Solimena, C., Blasi, J., Edelmann, L., Chapman, E.R., Von Mollard, G.F., and Jahn, R. (1995b). The t-SNAREs syntaxin 1 and SNAP-25 are present on organelles that participate in synaptic vesicle recycling. *The Journal of cell biology* 128**,** 637-645.

Waldner, D.M., Bech-Hansen, N.T., and Stell, W.K. (2018). Channeling Vision: CaV1.4-A Critical Link in Retinal Signal Transmission. *Biomed Res Int* 2018**,** 7272630.

Wang, T.M., Holzhausen, L.C., and Kramer, R.H. (2014). Imaging an optogenetic pH sensor reveals that protons mediate lateral inhibition in the retina. *Nat Neurosci* 17**,** 262-268.

Ward, S.M., and Kenyon, J.L. (2000). The spatial relationship between Ca2+ channels and Ca2+-activated channels and the function of Ca2+-buffering in avian sensory neurons. *Cell Calcium* 28**,** 233-246.

Warren, T.J., Van Hook, M.J., Supuran, C.T., and Thoreson, W.B. (2016a). Sources of protons and a role for bicarbonate in inhibitory feedback from horizontal cells to cones in Ambystoma tigrinum retina. *J Physiol* 594**,** 6661-6677.

Warren, T.J., Van Hook, M.J., Tranchina, D., and Thoreson, W.B. (2016b). Kinetics of Inhibitory Feedback from Horizontal Cells to Photoreceptors: Implications for an Ephaptic Mechanism. *J Neurosci* 36**,** 10075-10088.

Weber, J.P., Toft-Bertelsen, T.L., Mohrmann, R., Delgado-Martinez, I., and Sorensen, J.B. (2014). Synaptotagmin-7 is an asynchronous calcium sensor for synaptic transmission in neurons expressing SNAP-23. *PLoS One* 9**,** e114033.

Wen, X., Saltzgaber, G.W., and Thoreson, W.B. (2017). Kiss-and-Run Is a Significant Contributor to Synaptic Exocytosis and Endocytosis in Photoreceptors. *Frontiers in cellular neuroscience* 11**,** 286.

Wen, X., Van Hook, M.J., Grassmeyer, J.J., Wiesman, A.I., Rich, G.M., Cork, K.M., and Thoreson, W.B. (2018). Endocytosis sustains release at photoreceptor ribbon synapses by restoring fusion competence. *J Gen Physiol* 150**,** 591-611.

Wienbar, S., and Schwartz, G.W. (2018). The dynamic receptive fields of retinal ganglion cells. *Prog Retin Eye Res* 67**,** 102-117.

Williams, C.L., and Smith, S.M. (2018). Calcium dependence of spontaneous neurotransmitter release. *J Neurosci Res* 96**,** 335-347.

Witkovsky, P., Schmitz, Y., Akopian, A., Krizaj, D., and Tranchina, D. (1997). Gain of rod to horizontal cell synaptic transfer: relation to glutamate release and a dihydropyridine-sensitive calcium current. *J Neurosci* 17**,** 7297-7306.

Woo, S.S., James, D.J., and Martin, T.F. (2017). Munc13-4 functions as a Ca(2+) sensor for homotypic secretory granule fusion to generate endosomal exocytic vacuoles. *Molecular biology of the cell* 28**,** 792-808.

Wu, X.S., Xue, L., Mohan, R., Paradiso, K., Gillis, K.D., and Wu, L.G. (2007). The origin of quantal size variation: vesicular glutamate concentration plays a significant role. *J Neurosci* 27**,** 3046-3056.

Xu, J., Pang, Z.P., Shin, O.H., and Sudhof, T.C. (2009). Synaptotagmin-1 functions as a Ca2+ sensor for spontaneous release. *Nat Neurosci* 12**,** 759-766.

Xu, J.W., and Slaughter, M.M. (2005). Large-conductance calcium-activated potassium channels facilitate transmitter release in salamander rod synapse. *J Neurosci* 25**,** 7660-7668.

Xu, Y., Orlandi, C., Cao, Y., Yang, S., Choi, C.I., Pagadala, V., Birnbaumer, L., Martemyanov, K.A., and Vardi, N. (2016). The TRPM1 channel in ON-bipolar cells is gated by both the alpha and the betagamma subunits of the G-protein Go. *Sci Rep* 6**,** 20940.

Yagi, T., and Macleish, P.R. (1994). Ionic conductances of monkey solitary cone inner segments. *J Neurophysiol* 71**,** 656-665.

Yang, X.L., Gao, F., and Wu, S.M. (1999). Modulation of horizontal cell function by GABA(A) and GABA(C) receptors in dark- and light-adapted tiger salamander retina. *Vis Neurosci* 16**,** 967-979.

Yang, X.L., and Wu, S.M. (1991). Feedforward lateral inhibition in retinal bipolar cells: input-output relation of the horizontal cell-depolarizing bipolar cell synapse. *Proc Natl Acad Sci U S A* 88**,** 3310-3313.

Yao, J., Gaffaney, J.D., Kwon, S.E., and Chapman, E.R. (2011). Doc2 is a Ca2+ sensor required for asynchronous neurotransmitter release. *Cell* 147**,** 666-677.

Yin, P., Gandasi, N.R., Arora, S., Omar-Hmeadi, M., Saras, J., and Barg, S. (2018). Syntaxin clusters at secretory granules in a munc18-bound conformation. *Molecular biology of the cell* 29**,** 2700-2708.

Yoo, H., and Mihaila, D.M. (2020). "Neuroanatomy, Visual System, Pupillary Light Reflexes and Pathway," in *StatPearls*. (Treasure Island (FL)).

Yuan, Y., Huo, H., and Fang, T. (2018). Effects of Metabolic Energy on Synaptic Transmission and Dendritic Integration in Pyramidal Neurons. *Front Comput Neurosci* 12**,** 79.

Zampighi, G.A., Schietroma, C., Zampighi, L.M., Woodruff, M., Wright, E.M., and Brecha, N.C. (2011). Conical tomography of a ribbon synapse: structural evidence for vesicle fusion. *PLoS One* 6**,** e16944.

Zenisek, D., Horst, N.K., Merrifield, C., Sterling, P., and Matthews, G. (2004). Visualizing synaptic ribbons in the living cell. *The Journal of neuroscience : the official journal of the Society for Neuroscience* 24**,** 9752-9759.

Zenisek, D., Steyer, J.A., and Almers, W. (2000). Transport, capture and exocytosis of single synaptic vesicles at active zones. *Nature* 406**,** 849-854.

Zhang, C., and Peskin, C.S. (2015). Improved signaling as a result of randomness in synaptic vesicle release. *Proc Natl Acad Sci U S A* 112**,** 14954-14959.

Zhu, D., Koo, E., Kwan, E., Kang, Y., Park, S., Xie, H., Sugita, S., and Gaisano, H.Y. (2013). Syntaxin-3 regulates newcomer insulin granule exocytosis and compound fusion in pancreatic beta cells. *Diabetologia* 56**,** 359-369.